AFOSR-TR- 91 0659

Contr 105/90

15 April 1990 - 14 April 1991

Annual Technical Report in the subject

A STATISTICAL PHYSICS ANALYSIS OF ROCK AND CONCRETE DAMAGE RESPONSE

Grant No. AFOSR - 89 - 0374

by

R. Englman and Z. Jaeger

Soreq Nuclear Research Center, Yavne 70600, Israel

Program Manager: Dr. Spencer T. Wu
Air Force Office of Scientific Research
Bolling Air Force Base, DC 20332 - 6448

Yavne, May 1991

DISCLAIMER NOTICE

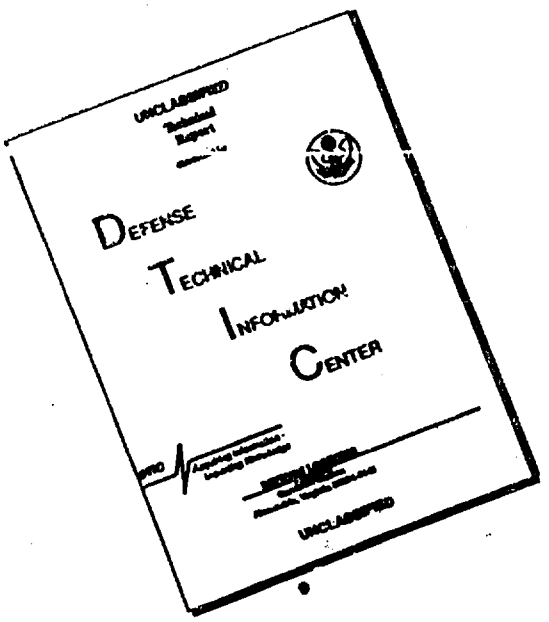

THIS DOCUMENT IS BEST QUALITY AVAILABLE. THE COPY FURNISHED TO DTIC CONTAINED A SIGNIFICANT NUMBER OF PAGES WHICH DO NOT REPRODUCE LEGIBLY.

Contr 103/90

15 April 1990 - 14 April 1991

Annual Technical Report in the subject

A STATISTICAL PHYSICS ANALYSIS OF ROCK AND CONCRETE DAMAGE RESPONSE

Grant No. AFOSR - 89 - 0374

by

R. Englman and Z. Jaeger

Soreq Nuclear Research Center, Yavne 70600, Israel

Program Manager: Dr. Spencer T. Wu
Air Force Office of Scientific Research
Bolling Air Force Base, DC 20332 - 6448

Yavne, May 1991

UNCLASSIFIED

SECURITY CLASSIFICATION OF THIS PAGE

REPORT DOCUMENTATION PAGE

1a. REPORT SECURITY CLASSIFICATION UNCLASSIFIED	1b. RESTRICTIVE MARKINGS
2a. SECURITY CLASSIFICATION AUTHORITY	3. DISTRIBUTION/AVAILABILITY OF REPORT Approved for public release; distribution unlimited.
2b. DECLASSIFICATION/DOWNGRADING SCHEDULE	
4. PERFORMING ORGANIZATION REPORT NUMBER(S)	5. MONITORING ORGANIZATION REPORT NUMBER(S)
6a. NAME OF PERFORMING ORGANIZATION SOREQ Nuclear Research Center 6b. OFFICE SYMBOL (If applicable)	7a. NAME OF MONITORING ORGANIZATION European Office of Aerospace Research and Development (EOARD)
6c. ADDRESS (City, State, and ZIP Code) Dept. of Physics and Applied Mathematics Yavne 70600 ISRAEL	7b. ADDRESS (City, State, and ZIP Code) Box 14 FPO N.Y. 09510-0200
8a. NAME OF FUNDING/SPONSORING ORGANIZATION AFOSR 8b. OFFICE SYMBOL (If applicable) NA	9. PROCUREMENT INSTRUMENT IDENTIFICATION NUMBER AFOSR-89-0374
8c. ADDRESS (City, State, and ZIP Code) Bolling AFB, DC 20332-6448	10. SOURCE OF FUNDING NUMBERS PROGRAM ELEMENT NO. 61102F; PROJECT NO. 2308; TASK NO. C2; WORK UNIT ACCESSION NO

11 TITLE (Include Security Classification)
A Statistical Physics Analysis of Rock and Concrete Response. (Unclassified)

12 PERSONAL AUTHOR(S)
R. Englman and Z. Jaeger

13a. TYPE OF REPORT	13b. TIME COVERED	14. DATE OF REPORT (Year, Month, Day)	15 PAGE COUNT
Annual Technical	FROM 15Apr.90 TO 14Apr.91	1991 May 30	163

16 SUPPLEMENTARY NOTATION

17 COSATI CODES			18. SUBJECT TERMS (Continue on reverse if necessary and identify by block number)
FIELD	GROUP	SUB-GROUP	Thermodyn amics, percolation, crack coalescence, fracture, fragmentation, crack-crack interaction, pores, finite size

19 ABSTRACT (Continue on reverse if necessary and identify by block number)

In our thermodynamic approach crack densities have been treated as a hierarchy of order parameters operating at successively smaller scales (from macroscopic down to microcrack scales). The formalism renormalizes surface energy densities due to interaction between microcracks, yields by thermodynamic self-consistency effective elastic constants (similar to those in effective medium approximations) and stress intensity factors (SIF) in cracked solids and provides thermodynamic definitions for observables (like R-curves and SIF).

The fracture behavior under fixed grip or constant stress conditions has been studied numerically. Above a critical strain the material attains an equilibrium non-zero crack-density that approaches the percolation threshold asymptotically with increasing strain. The effects of crack-crack interaction, of anisotropic crack-density and of pre-existing pores have

20. DISTRIBUTION/AVAILABILITY OF ABSTRACT	21. ABSTRACT SECURITY CLASSIFICATION
☒ UNCLASSIFIED/UNLIMITED ☐ SAME AS RPT. ☐ DTIC USERS	
22a. NAME OF RESPONSIBLE INDIVIDUAL Dr. Spencer Wu	22b. TELEPHONE (Include Area Code) 202-767-6962
22c. OFFICE SYMBOL NA	

DD FORM 1473, 84 MAR 83 APR edition may be used until exhausted. All other editions are obsolete.

SECURITY CLASSIFICATION OF THIS PAGE

UNCLASSIFIED

18. SUBJECT TERMS (continued)

scaling, Gruneisen parameters, effective elastic constants, strain rate, Voronoi-polygons, concrete, reinforced concrete, ceramics, R-curve, maximum entropy, critical exponents.

19. ABSTRACT (continued)

also been studied. Crack propagation in ceramic materials, subject to microcrack formation and coalescence, has been examined with models that differ in the relative time scale involved in the internal relaxation processes and the external loading rate. It was found that when the external loading rate is high, a rising R-curve is obtained, which is primarily due to microcrack shielding.

In a numerical calculation of the Gruneisen parameters in a cracked solid it was found that these decrease with increasing crack density, with the rate of decrease dependent on the type of effective field approximation (self-consistent or differential scheme) that is used. A Voronoi-polygon model of granular, disordered solids shows that at fracture the number of intergranular cracks varies with the line- or sample size L as $L^{-1.85}$. Experimental justification for the critical, percolation model was found in the scale independence of the fragment size distributions in explosively shattered reinforced concrete slabs.

TABLE OF CONTENTS

TABLE OF CONTENTS (Continued)

Abstract

In our thermodynamic approach, crack densities have been treated as a hierarchy of order parameters operating at successively smaller scales (from macroscopic down to microcrack scales). The formalism renormalizes surface energy densities due to interaction between microcracks, yields by thermodynamic self-consistency effective elastic constants (similar to those in effective medium approximations) and stress intensity factors (SIF) in cracked solids and provides thermodynamic definitions for observables (like R-curves and SIF).

The fracture behavior under fixed grip or constant stress conditions has been studied numerically. Above a critical strain the material attains an equilibrium non-zero crack density that approaches the percolation threshold asymptotically with increasing strain. The effects of crack/crack interactions, of anisotropic crack-density and of pre-existing pores have also been studied. Crack propagation in ceramic materials, subject to microcrack formation and coalescence, has been examined with models that differ in the relative time scale involved in the internal relaxation processes and the external loading rate. It was found that when the external loading rate is high, a rising R-curve is obtained, which is primarily due to microcrack shielding.

In a numerical calculation of the Gruneisen parameters in a cracked solid it was found that these decrease with increasing crack density, with the rate of decrease dependent on the type of effective field approximation (self-consistent or differential scheme) that is used. A Voronoi-polygon model of granular, disordered solids shows that at fracture the number of intergranular cracks varies with the line- or sample size L as $L^{-1.85}$. Experimental justification for the critical, percolation model was found in the scale independence of the fragment size distributions in explosively shattered reinforced concrete slabs.

(F)

PART 1.

ADMINISTRATIVE

Statement of Work

The purpose of this research is the application of percolation theory, information theory, molecular dynamics simulation and fractal analysis to an understanding of the basic issues in damage growth, damage dependent non-linear mechanical response and fragmentation processes in concrete and rock under transient high-stress loading. Although the starting point will be statistical, our ultimate goal is the merging of the statistical and the material-oriented dynamical approaches into a single theory. The defect statistics, hitherto regarded as homogeneous in time and space, will be biased by physical considerations so as to include either process dependent properties or specific material descriptions. The outcome of our theory will be erstwhile exemplified in a few basic, idealized cases, such as isotropic or anisotropic solids, materials with structure (e.g., concrete containing randomly oriented ingredients). We shall investigate model-independent properties, including the existence of critical points, the nature of singular behaviour, critical exponents, etc. The mechanical properties of cracked material near the fragmentation critical point will be analyzed in terms of critical exponents.

Status of Research

After having laid down a formalism for the micro-crack based theory of fracture in the previous year of research (summarized in our first Annual Technical Report), we have pressed forward in the original direction as well as in several new directions. Common to all our efforts is the statistical physics description of fracture processes based on a microdefect population.

Since most works in fracture are formulated in terms of one or other length scale, it was important to establish a consistent linkage between different hierarchical length scales (from the sample size down to the smallest relevant scale). This was done, along with other matters, in our work set out in Part 2. This formal work was supplemented by a quantitative study (Part 3) that showed how crack-clusters affected mechanical strength

and fracture under simplified but precisely defined conditions. In essence, we have explored the elastic constants (like Young's modulus) near the critical percolation region. Curves of crack resistance (R-curves) or stress intensities K_I have been calculated in Part 4 to link up the working zone concept with the halo of microcracks that form around the propagating macrocrack. The rising R-curves, that are found in our calculations and that have been a puzzle for some time, are due to the energy investment in the microcracks.

The statistical physics side of fracture has its counterpart in the probabilistic treatments of fragmentation. These are reviewed and developed in Part 5 from an information theoretical angle. Worthy of emphasis is section 5 where results of percolation theory are incorporated in a Maximum Entropy framework.

Elastic moduli and Grueneisen parameters are affected by the crack population in a stressed solid. Their calculation requires averaging to be performed. This is done in Part 6, which highlights the difference between two averaging schemes (the self-consistent and differential).

In the last couple of years the statistical, microcrack-based fracture concept has gained strong following, though not necessarily in the specific form that is used by the Soreq group. In a recent book some of the alternative approaches (we re-emphasize, each based on a multiplicity of microcracks and employing, as a rule, Monte Carlo methods and scaling laws) have been summarized. A review of this book is given in Part 7.

Part 8 is a preliminary report on how fracture develops in a random granular materials. It has a finite size scaling result and shows geometrical correlation in the pictures of the breakage pattern.

Some experimental vindications of the percolating multicrack concept appear in Part 9. The support cited is partly quantitative, statistical; namely, through showing that in different sets of experiments on concrete the fragment statistics agrees with that of a percolating structure near its criticality. Finally, microphotographs show macrocrack formation (during creep in some ceramics) as a percolative process involving microvoids.

The domain of applicability of our statistical physics picture for rupture is not yet delineated. In particular, it is not clear how it depends on structure, composition randomness, treatment, the speed of fracturing process or of other parameters of the process. Theory and cleverly designed experiments will no doubt answer these questions in the near future.

Details of Work Performed

Having found earlier an analytic law describing the decrease of fracture strength with porosity and its increase with the size of pores, we have shown that e.g. critical strains can depend markedly on such delicately tuned parameters as specific crack-surface energy and the anisotropy in the crack-crack interaction. The history of local stress near a macrocrack (namely, whether it relaxes faster or slower than the applied stress) was found to alter the computed R-curves. The statistical spread in granular structures (modeled in our work by Voronoi polygons) makes the initial breakage pattern more diffusely located than in a uniformly patterned granular system (as, e.g. a chessboard) and makes percolation theory a more realistic approximation. The dynamics of flow in a percolating or fractal framework has gained better understanding in the last few years and has not been investigated by ourselves.

Several criteria have been used in our research to describe the opening of a microcrack or the propagation of a macrocrack, leading to fracture. The Voronoi-method has employed a fixed relative elongation to open an interfacial crack. This would appear to favor the opening of cracks separating small neighboring grains; yet our computed results show only a slight preference for this (Part 8, Fig. 3). The strongly rising R-curve is a sign for the great energy penalty involved in opening new microcracks around a propagating macrocrack. Our computed results (Part 4) show that whenever this is encountered in practice, a strongly damaged working zone is indicated.

The interrelated aspects of micro-crack initiation, propagation and coalescence at various hierarchical levels of length scales have been treated in Part 2. It was shown how the mechanical parameters (like crack surface energy densities or stress intensity factors) differ at various levels and what is the theoretical framework (not yet worked out, at this stage) that links them. The theory also provides relationships between the reduction in the elastic strengths (e.g. in Young's modulus), that traditionally define "Damage", and geometrical properties of crack clusters [namely: the effective, excluded volume or the cube of end-to-end distances (Fig. 1 in Part 3)]. Plots of Young's moduli have been given as function of the crack occupation probability p (Part 3, Fig. 2); we have demonstrated that near the critical defect-concentration different ways of averaging (i.e., different effective field theories) give reductions in E_{eff} that are

markedly different. Some experimental efforts ought to be devoted to sort out the truth.

It is well known that a fractured or fragmented solid is not necessarily at its absolute thermodynamic energy minimum, whence the difficulties in the application of thermodynamics to fracture. On the other hand, Maximum Entropy Methods (MEM) are based on states of knowledge (which are at the roots of all probabilistic reasoning), which also hold good at non-equilibrium. In Part 5 we have given MEM predictions for fragment statistics both for a high-strain rate single, sudden fracture process and for (still a high strain rate) situation in which fracture develops over a spread of time. Though the statistics is for fragments, it is the proliferation of cracks that forms fragments.

Predictions of our statistical physics, micro-crack approach depend on the values of a relatively large number of parameters and on the physical conditions (experimental situations) under which theory is tested. Therefore a fully convincing validation of our approach appears possible only through the performance of a set of planned experiments under controlled conditions (and not the interpretation of published experimental results). Still, two important facts of our theories have received direct experimental support (Part 9): (1) the merging into macrocracks of smaller defect units (microvoids) has been documented under slow degradation, high temperature conditions (creep), (2) quantitative evidence has been found from medium and large scale deformation experiments on (reinforced) concrete for our prediction (in 1985) that fragmentation is a critical process due to the approach of the crack density to a critical value (P_{CII}). The observed mass-distributions of fragments in two sets of experiments follow quite closely the percolation theoretical predictions.

Finite size scaling (i.e. dependence on sample size) of the number of broken springs has been derived in Part 9 using a computer code that first generates a random structure and then follows its time development under applied stress or strain.

Participating Personnel

Robert Englman, (Prof.); B.Sc., A.R.C.S. (in Mathematics) in 1954 and Ph.D. (Theoretical Physics) in 1957 at London. Thesis title "Extension of the theory of the mean-free-path effects in metals".

Zeev Jaeger (Dr.); M.Sc. in Chemistry, Physics as major subjects and Mathematics and Applied Mathematics as subsidiary subjects in 1967 at the Hebrew University in Jerusalem, Ph.D. in Physics in 1973 at the Hebrew University, Jerusalem with the thesis title. "Charge-transfer states and their physical application in crystals of transition metals".

Raphael Ruppin (Dr.); M.Sc. in Physics at the Hebrew University of Jerusalem in 1964 and Ph.D. in Theoretical Solid State Physics from the Hebrew University in 1969 with the thesis title "Size dependent elementary excitations in solids".

Miriam Lemanska (Dr.); M.Sc. in Mathematics in 1952 at the Lodz University in Mathematics and Ph.D. in Nuclear Sciences in 1967 at the Technion, Haifa in the subject "Perturbation theory in fast reactors".

Michael Murat (Dr.); B.Sc. in Chemistry in 1977 from the Technion, Haifa, then M.Sc. in Physical Chemistry in 1978 from the Technion, Haifa with a thesis on "The triplet state of the biexciton" and Ph.D. in Physics in 1987 at the Tel Aviv University with a thesis entitled "The structure and physical properties of porous materials".

Interactions

Prof. T.J. Ahrens, Dept. of Geology and Astrophysics, California Institute of Technology, Pasadena Ca., Discussions with Z. Jaeger in July 1991.

Prof. S. Mindess, Department of Engineering, University of British Columbia, Vancouver, Canada, Discussions with Z. Jaeger in July 1991.

Dr. S.M. Wiederhorn, National Institute of Standards and Technology, Gaithersburg, Discussions with Z. Jaeger in Nov. 1991.

ASME Conference "Damage Mechanics in Engineering Materials", Dallas, Texas (November 1990). Attendance by Z. Jaeger who presented an invited paper.

NATO Workshop on "Toughening Mechanisms in Quasi-brittle Materials", Organized by Prof. S.P. Sah, Northwestern University, Evanston Ill. Attended by Z. Jaeger in July 1990.

Dr. P. Rossi, Laboratoire de Recherche des Ponts et Chaussées, Paris XIV. Discussion with R. Englman in November 1990.

Professors M. Elices and Planas, Department of Civil Engineering; Polytechnical University of Madrid 28040 Madrid, Spain, Discussions with R. Englman in November 1990.

Professors F. Flores, F. Guinea and E. Louis, Department of Physics, Autonomous University of Madrid, Madrid, Spain. Discussions with R. Englman in Nov. 1990.

List of Articles

1. R. Englman, "Fragments of Matter from a Maximum Entropy Viewpoint"; A review. J. Phys. Condensed Matter 3, 1019 (1991).

2. M. Murat, R. Englman and Z. Jaeger, "A Numerical Simulation of the R-curve Behavior in Microcracking Materials", J. Applied Phys. (in press).

3. R. Ruppin, "Grüneisen Parameters of a Cracked Solid", J. Phys. Chem. Solids (in press).

4. R. Englman, "Statistical Models for the Fracture Disordered Media, A book review". J. Statistical Physics (in press).

5. R. Englman, M. Murat and Z. Jaeger, "Crack-cluster Description of Fracture. I Thermodynamic Energy Functionals." Physical Review (submitted).

6. M. Murat, R. Englman and Z. Jaeger, "Crack-cluster-Description of Fracture. II. Numerical Study", Physical Review (submitted).

Patents and Inventions

None.

Statement to Program Manager

In the two years of research the microcrack population theory was developed to interpret fracture. The basic theory was produced, material rupture behavior was described by calculating crack resistance - (R) curves and experimental confirmation was established from fragment statistics in concrete and from micro-photographs of void coalescence in the creep of some ceramics. We have derived from our crack-cluster description a sharply rising R-curve frequently seen in experiment. Observed statistics arising from fracture (as in fragmentation) obey a power law, in accordance with the critical behavior occurring near the percolation limit.

PART 2

CRACK-CLUSTER DESCRIPTION OF FRACTURE

I THERMODYNAMICAL ENERGY FUNCTIONALS

R. Englman, M. Murat and Z. Jaeger

Soreq Nuclear Research Center

Yavne 70600, Israel

Abstract

The traditional physics approach, as exemplified by lattice dynamics, can be used to develop a thermodynamic formalism that generalizes continuum mechanics (elasticity theory) by including a hierarchy of cracks, namely microcracks that join up to form macroscopic cracks. Fracture processes are derived by minimizing thermodynamic energies that are functionals of crack densities and of strains (or stresses) that vary on successively smaller scales (from macroscopic down to microcrack scales). The formalism renormalizes surface energy densities due to interaction between microcracks, yields by thermodynamic self-consistency effective elastic constants (similar to those from effective medium approximations) and stress intensity factors (SIF) in cracked solids and provides thermodynamic definitions for observables in engineering practice (like R-curves and SIF). Crack densities can be treated in the formalism as order parameters: criteria for fracture using this approach are developed in the sequel paper.

1. Introduction

A thermodynamic theory of lattice dynamics, in which interatomic bonds are the discrete units, was complete by the 1930's[1,2]. The continuum theory of elasticity not based on atomistic units dates back to the days of Rayleigh[3,4]. To describe fracture a need has arisen for an intermediate type of theory of solid behavior in which there are both discrete entities, namely cracks of various sizes, alongside with intact pieces of the material which can still be represented by continuum mechanics. There is a good deal of experimental support for using this approach to explain fracture in either brittle or ductile solids. The argument is stated in more detail in §3.5 of this work with some basic referencing and is intended to justify the crack-cluster origin of fracture in brittle materials[5] and the microvoid coalescence theory of ductile failure[6,7].

When looked at from a broad historical viewpoint, this paper and its sequel[8] can be regarded as an example of the recent trend to give engineering practices in fracture mechanics a precise, physics oriented formulation. Characteristically, both thermodynamics and some form of statistical mechanics are brought into play: the first in the form of employing internal variables and their conjugate forces and the second by relating macroscopic properties of the material to microscopic variables. Both features were already present in Rice's treatment of metal plasticity in terms of slip kinetics[9,10].

The more recent efforts that form part of the trend are too numerous to list exhaustively. One wishes to mention Krajcinovic et al.'s derivation[11,12] of the conjugate force to the Budiansky - O'Connell damage-volume variable[13].

The present thermodynamic approach differs from previous works in several respects. First, our approach is presented as a hierarchical extension of Born-Huang's classic treatise of lattice dynamics, when applied to discrete units (cracks) of increasing sizes. Admittedly, this is only a didactic device but it facilitates the systematic derivation of results. Next, the transition between micro and macrodefects is performed smoothly by the use of crack clusters of increasing size, in a way originated by percolation theory. The energy release term, also called the mechanical energy, is defined for crack clusters in terms of the stress-free volume that is the equivalent of the Budiansky - O'Connell damage - volume for simple (e.g. penny-shaped) crack. We then show how several effective medium approximations can be derived from simple consistency requirements of the energy functionals. Further, we include crack-crack interaction in the energy-functional, formally in a manner natural to many-particle solid-state physics, but not yet met with in fracture mechanics. We indicate how the interaction leads to a renormalization of observables (like crack surface energy densities or stress intensity factors) in a way that can account for the large numerical discrepancies between quantities that correspond to micro- and macrocracks. In addition, we propose a thermodynamically acceptable definition of crack resistance - (R-) curves and of other observables on which the engineering characterization of materials rests. Finally, we introduce crak densities as order parameters in the energy and obtain fracture mechanics by minimization of the energy with respect to crack densities. This extension of the (more generally valid) theory is the basis of the numerical study in the sequel paper[8]. The defect density also appears as a free variable in the thermodynamic theory of Gelbart and coworkers[14].

The present approach is not free of uncertainties, which we try to describe as we go along. However, we feel that these have been in the subject for some time. Thus, the definition of R-curves is notoriously ambiguous[15,16]. The validity of any effective medium description has been questioned for a medium containing microcracks[17] . The demarcation between micro- and macrocracks is fuzzy[7]. Yet, we feel that the present formalism can be helpful as long as its limitations are clearly recognized.

2. The Energy Functionals

Our objective is a theory that is intermediate between continuum elasticity[3,4] and discrete lattice dynamics[1,2], in the sense that the displacement variable $\varepsilon(r)$ (r = the position in the material) is decomposed into a macroscopic strain ε_∞ and local strains $\varepsilon_i(\Delta r_i)$ around the i discontinuity (crack, or in ductile solids, void) in the damaged solid. $\Delta r = r - r_i$ where r_i is the location of the i'th crack. The distribution of the cracks in the solid $p(r)$ can be preassigned or, else, can be treated as the independent, order-parameter in the energy functional

$$U = U(\{\varepsilon(r)\}, \{p(r)\})$$

The latter approach is described in §3.5 and is developed in the sequel[8]. Following standard lattice dynamics treatments[1,2], we identify with U the internal energy, which is written as a sum of integrals over the full volume V of the material, which includes several cracks. [So as to put over our ideas with the best effect we dispense with the tensorial indices of strain (or stress), which practice is frequently followed in the schematic representations of fracture processes[12,14]. In a quantitative treatment,

with the precision of e.g. Ref. 13, our formalism should take account of tensorial properties, of non-zero Poisson ratios ν, etc.] We write

$$U(\varepsilon) = \frac{1}{2} E_o \int \varepsilon^2(r)dr - \frac{1}{2} E_\varepsilon \Sigma_i \int_{\Delta r \in \ell_i^3} d(\Delta r) + \gamma_o \Sigma_i \int dA_i + \Sigma_{ij} \int d(\Delta r_i) d(\Delta r_j)\, D(r_i - r_j) \tag{1}$$

The first term is the usual strain energy of the solid. The second term gives the reduction of the energy due to the relaxation from a strained state in a volume ℓ_i^3 around the i'th crack. (ℓ_i is a representative end-to-end distance of the crack[8].) This energy release is the familiar "mechanical energy" appearing in the fixed stress configuration in the form:

$$-\frac{1}{2} (\sigma_\infty^2 / E_\sigma) \ell_i^3 \tag{2}$$

(Ref. 4, p. 253). The exact form of the stress-free volume depends on the crack's shape and orientation and requires a more careful treatment than can be given here; but there can be no doubt about the relevance of this term to fracture. Thus this term is responsible in the Griffith theory for crack instability, that comes about when the macroscopic stress σ_∞ exceeds the (tensile) fracture stress σ_f[18,19]. The meanings of the Young moduli E_o and E_ε in (1) and of E_σ in (2) will be presently explained, in the course of the derivation of the effective elastic constant E_{eff} in the cracked medium.

The third term represents the surface energy needed to open up the discontinuities in the zeroth order (non-interacting microcracks) approximation with the basic surface energy density γ_o.

The last term is the crack-crack interaction. It is decomposed into two parts: a strain independent and a strain dependent part in the form

$$D(r_i-r_j) = \mathcal{V}(r_i-r_j) + E_\varepsilon\, \varepsilon_i(\Delta r_i)\varepsilon_j(\Delta r_j)\; K(r_i-r_j) \qquad (3)$$

There is no linear term in ε since both the macroscopic strain ε_∞ and the local strains $\varepsilon_i(\Delta r_i)$ are zero in the equilibrium, unstressed configuration. [The argument is similar to that leading to the elimination of the linear terms in the atomic displacement from the lattice potential of Born and Huang[1], III §11). Under conditions of fixed temperature the free-energy function F would be used instead of U. This differs from U by a crack-configuration entropy term that has been considered by us[20,21] and others[14]. However, it is not an essential component in the theoretical development and will be disregarded for the present. More important is the entropy change ΔS associated with the irreversible breaking of the bonds. This will be treated in §3.4.

The energy function U leads naturally to a formal treatment of a number of effects that are central to cracked crystals. We list these now and proceed to their discussion one-by-one, emphasizing that in a complete treatment all the effects enter together: we separate them for reasons of clarity.

(I) Self consistent effective elastic constants from thermodynamical considereations.

(II) The macrocrack surface energy density $\gamma(\neq \gamma_o)$.

(III) Self consistent stress intensity factors (SIF) at tips of interacting cracks.

(IV) Thermodynamic definition of R-curves, stress intensity factors

(V) Crack densities p as order parameters.

3.1 Effective elastic moduli

To treat (I) we simplify (1) as follows:

(a) Make $U[\varepsilon(r)]$ the function of one single strain variable only, ε_∞; this ignores all strains $\varepsilon_i(\Delta r_i)$ associated with cracks (or cracks tips) except as averages.

(b) Consider at the first stage only non-interacting cracks; so that in (1) the last term is ignored.

Then the strictly ε_∞ dependent part of $U(\varepsilon_\infty)$ has the form

$$U(\varepsilon_\infty) = \frac{\varepsilon_\infty^2}{2} E_o V - \frac{\varepsilon_\infty^2}{2} E_\varepsilon V^{ex} = \frac{\varepsilon_\infty^2}{2} E_o V \left[1 - \frac{E_\varepsilon}{E_o} \frac{V^{ex}}{V}\right]$$

where V is the volume of the solid and V^{ex} is the "excluded" crack volume, given by

$$V^{ex} = \sum_i \ell_i^3$$

analogous to Budiansky and O'Connell's[13] $\langle a^2 b \rangle$. We emphasize that V^{ex} is non-zero even if the cracks are perfectly flat and thin, i.e. do not occupy any volume in the solid. This being so, we can transform the constant grip internal energy in (4) to a constant-stress energy-functional $H(\sigma_\infty)$ analogous to the enthalpy[8], by a simple Legendre transformation not involving V^{ex} (since no work is done by σ_∞ to separate the flat cracks). Therefore

$$H(\sigma_\infty) = U[\varepsilon_\infty(\sigma_\infty)] - \sigma_\infty \varepsilon_\infty V \qquad (5)$$

Actually our starting point might also have been

$$H(\sigma_\infty) = -\frac{1}{2}\frac{\sigma_\infty^2}{E_o} V - \frac{1}{2}\frac{\sigma_\infty^2}{E_\sigma} V^{ex} \tag{6}$$

To relate E_ε in (4) to E_σ in (6) we use the thermodynamic definitions of conjugate variables, namely:

$$\frac{1}{V}\frac{\partial H(\sigma_\infty)}{\partial \sigma_\infty} = -\varepsilon_\infty \tag{7}$$

$$\frac{1}{V}\frac{\partial U(\sigma_\infty)}{\partial \varepsilon_\infty} = \sigma_\infty \tag{8}$$

and the definitions of the effective Young's module E_{eff} in the solid containing cracks (which for the moment regarded as non-interacting)

$$U(e_\infty) = \frac{e_\infty^2}{2} E_{eff} \tag{9}$$

$$H(\sigma_\infty) = -\frac{\sigma_\infty^2}{2E_{eff}} \tag{10}$$

The presence of the same E_{eff} in (9) and (10) amounts to the self-consistency requirement, emphasized by Hashin[23] and by other workers therein. The consequence of self-consistency can be put in the form (which is not unique)

$$E_{eff} = E_o[1 + (\theta-1)v]/(1+\theta v) \tag{11}$$

$$E_\varepsilon = E_o/(1+\theta v) \tag{12}$$

$$E_\sigma = E_o[1-(1-\theta)v] \tag{13}$$

where we introduce

$$v \equiv v^{ex}/v$$

and θ is some quantity between 0 and 1. The limiting case

$$\theta = 0;\quad E_{eff} = E_o(1 - v);\quad E_\varepsilon = E_o;\quad E_\sigma = E_{eff} \tag{14}$$

is the choice adopted by Budiansky and O'Connell[13], characterized by an effective Young's module that goes to zero at $v = 1$, equivalent to ref (13)'s 9/16 catastrophy. At the opposite extreme

$$\theta = 1;\quad E_{eff} = E_o/(1 + v);\quad E_\varepsilon = E_{eff};\quad E_\sigma = E_o \tag{15}$$

E_{eff} tends to zero only asymptotically for high crack density as also in the Differential Scheme (DS) of Hashin[23].

It is important to recognize that the class of effective moduli in (11) - (13) were obtained by thermodynamic self-consistency and not by any physical[14] or geometrical[15] argument.

Extension of these considerations to account for the tensorial character of ε and σ, including effective Poisson's ratios ν_{eff} will be given in a future publication.

3.2 Renormalized Surface Energy Density

The numerical value of the surface energy density γ varies according to whether the created discontinuity is on an atomic scale, micro or macrocrack

scale[17,18]. The breaking of atomic bonds is too energy costly (~ 10 eV) to be caused by ordinary fracture processes; γ - values for visible discontinuities are lower than these by a factor of 10^{-2} - 10^{-4} [Ref. 26]; the presence of microcrack-clouds immediately surrounding the macrocracks and creating the "plastic zone" near the crack tip reduces γ[19,27,28].

The first term in (3) is the source of these effects. It represents the mutual influence of the i'th and j'th cracks. Accordingly, the Δr integrations in the last term in (1) are to be taken over the discontinuity surfaces. Regarding γ_o as atomic quantities of the order of dissociation energies the integral in (1) is to be taken over all cut atomic bonds in the microcracks. For the i'th microcrack the last integral is then written as a correction to the atomic quantity γ_o in the form:

$$\delta\gamma_{i_1} \int dS_{i_1} = t_{i_1} \int dS_{i_1} \sum_{j_1=i_1} \int d(\Delta r_{j_1}) \, V(r_{i_1} - r_{j_1}) \qquad (16)$$

where the integrations $dS, d(\Delta r_j)$ are over atomic dimensions, t_{i_1} is the (atomic) thickness of the i_1 microcrack and r_{j_1} is the coordinate of the $j_1(=i_1)$'th atomic thickness of the i_1 microcrack. In brief, and in a schematic form, $\delta\gamma_{i_1}$ as given by (16) represents the correction to γ_o due to other broken atomic bonds in the i_1 microcrack:

$$\gamma_{i_1} = \gamma_o + \delta\gamma_{i_1}$$

For a crack cluster, consisting of a connected configuration of several microcracks, and denoted by i_2, an integral similar to (16) will further renormalize γ_{i_2}, as follows:

$$\gamma_{i_2} = \gamma_{i_1} + \delta\gamma_{i_2}$$

where $\delta\gamma_{i_1}$ represents contributions to the i_1 microcrack by other microcracks belonging to the i_2 crack cluster.

Microcracks from other crack clusters ($j_2 \neq i_2$) are unlikely to contribute to γ_{i_2} since the interaction V is of short range. However, close-by microcracks surrounding the i_2 crack cluster will alter γ_{i_2}, in the sense of the plastic zone correction to γ due to Irwin[19].

While the preceding discussion is overly qualitative, it can lead the way to a systematic prediction of surface energies observed in fracture.

3.3 Self consistent stress intensity factor (SIF) at crack tips.

We now go beyond regarding the energy functional U as depending on only one variable, the macroscopic strain ε_∞ only. Various extensions are possible. Indeed we shall not go along the whole length with Born and Huang[1] to describe $U(\varepsilon)$ as a function of all atomic displacements. Rather, we consider strains only in the vicinity of cracks. Here, too, we can have strains $\varepsilon(\Delta r_i)$ associated with the i crack as function of <u>all</u> points Δr_i near the crack, or only on the crack surface. Leaving the latter possibility aside, we shall describe more simply (and less accurately) local crack-induced strain effects in terms of a single strain ε_i associated with each crack (or crack tip). We need not make at this stage a distinction

between microcracks, crack clusters or macrocracks. This formulation will be shown to be equivalent to previous calculations of the effective SIF at crack-tips due to interacting cracks or at a macrocrack due to several microcracks, or a microcrack array. The level of approximation in Kachanov's works[29,30] is similar to the present one. There is no difficulty in refining the present simplified theory, provided it is accepted that deeper levels of approximations can be got simply by making $U(\varepsilon)$ a function of additional strain variables. Additional stress variables are obtained by the conjugate relations.

$$\frac{1}{V}\frac{\partial U(\varepsilon)}{\partial \varepsilon_i} = \sigma_i \tag{17}$$

$$\frac{1}{V}\frac{\partial H(\sigma)}{\partial \sigma_i} = -\varepsilon_i \tag{18}$$

Inserting into the first two integrals in (1) for regions near the i crack

$$\varepsilon(r) = \varepsilon_\infty + \varepsilon_i$$

where $\sum_i \varepsilon_i = 0$,

we obtain integrands in the form

$$\varepsilon_\infty^2 + 2\varepsilon_\infty \varepsilon_i + \varepsilon_i^2 \tag{19}$$

where the first term gives the macroscopic strain energy, the second term is an interaction whose physical meaning is the strain near the crack induced by the macroscopic strain and the third term is a local strain energy. In the crack interaction term the strain dependent part [shown in (3)] has the similar forms, multiplying the interaction K_{ij},

$$\varepsilon_\infty^2 + \varepsilon_\infty(\varepsilon_i + \varepsilon_j) + \varepsilon_i\varepsilon_j \tag{20}$$

In the absence of macroscopic strain the SIF can be calculated from (17), which gives

$$\sigma_i = E_o[\varepsilon_i - E_\varepsilon(v + \sum_j K_{ij}\,\varepsilon_j)] \tag{21}$$

$$= E_o[\delta_{ij} - E_\varepsilon(v\delta_{ij} + K_{ij})]\varepsilon_j \tag{22}$$

$$= E_{ij}^{*}\,\varepsilon_j \tag{23}$$

having used the summation convention for repeated crack-indices in the last two expressions and introducing the effective modulus matrix E_{ij}^{*}. Assuming the existence of the inverse E_{ij}^{*-1} we rewrite the interaction in (1), (3) as

$$\sum_{i,i',j,j'} \sigma_i\, E_{ii'}^{*-1}\, K_{i'j'}\, E_{j'j}^{*-1}\, \sigma_j \tag{24}$$

The mean stresses σ_i on each crack i being given as in (23) we can calculate the stress fields due to them at each point r_i on the i_o'th crack, following standard methods in elasticity[31]. From these then follow the SIF.

The result is equivalent to Kachanov's[29,30] (after making the necessary adjustments in the formalism, like $V^{ex} = 0$, $E_\varepsilon = E_o$). It is significant that the self consistency of the mean stresses, obtained by him in the form of a mean field assumption, again arises from the thermodynamic formulation [Eq. (17), (18)] automatically. Unfortunately, the advance in the theory is but formal since crack-crack interaction stresses have been calculated only

for a few, special geometries[32,33]. (The interpolation formula used in the sequel paper has an illustrative purpose.)

3.4 Thermodynamic observables

The macroscopic variables σ_∞, ε_∞, defined in Eqs. (7), (8), are evident observables. So are the local variables σ_i, ε_i [Eqs. (17),(18)], though σ_i, ε_i may not be externally controllable. However, our free energy contains additional parameters which should also give rise to observables, namely the crack positions or crack densities. In principle each microcrack should be associated with a (microscopic) observable. From a practical viewpoint we consider a much smaller number of variables, which will be further reduced to two: the critical stress intensity factor K_{IC} and the R-curve variable.

To obtain K_{IC} from the energy functionals U or H[(1) or (5)] we associate with the crack cluster volumes ℓ_i^3 (belonging to the i'th macrocrack) a length a_i.

$$a_i \sim \ell_i \tag{25}$$

while for a penny-shaped or wedge-like macrocrack other relationships will hold. We have already discussed at some length in earlier works[20,21] that the dependence of ℓ_i on the number of microcracks belonging to the crack-cluster is related to the fractal dimension of the macrocrack and only in very special cases, like extremely correlated crack growth, will depend on the extent of the macrocrack.

With certain assumptions about the general mechanism of crack growth, which are basically similar to those of Griffith[18] and will be elaborated on in the next section, we can regard the a_i as free parameters in the energy

functional and obtain their value $\hat{a}_i$ at equilibrium for a fixed tensile stress σ^T from

$$\frac{\partial H(\sigma)}{\partial a_j} = 0 \qquad (j=\text{all macrocrack labels}) \tag{26}$$

while for fixed strain $\hat{a}_i$ is found from

$$\frac{\partial U(\varepsilon_\infty)}{\partial a_j} = 0 \tag{27}$$

The form of U in (1) makes it plausible that for a sufficiently high stress an accessible minimum (local or absolute) value of $\hat{a}_i$ will arise which will be of the order of the sample size: the sample will then be fractured. The least stress achieving this condition is the fracture stress,

$$\sigma^T = \sigma_f \tag{28}$$

The phrase "accessible minimum (local or absolute)" will be amplified in the next section: "minimum" refers to the energy as function of the microcrack density[20]. The minimum changes depending on what conditions, e.g. fixed stress or strain, hold, the accessibility of that minimum hinges on the issue whether microcrack opening and healing occur. The critical SIF will then be given by

$$K_{IC} = \sigma_f \sqrt{\pi b/p_c} \tag{29}$$

where b is the linear dimension of the microcrack and p_c a numerical factor. (In a percolation picture[8] p_c is the critical crack occupation at percolation.)

R-curve measurements are aimed at determining the energy input rate needed to extend a stable macrocrack (not yet cutting across the sample) by unit length. Techniques of measurements have been described in detail[34-36] and involve first the application of stress leading to a small extension of a crack and subsequently the measurement of the change of the Young's module (or, of its inverse, the compliance) due to the crack extension. Important for our considerations is the circumstance that the crack-extension is an irreversible process, involving a finite entropy change ΔS, whereas the Young's module is measured (before and after the crack extension) isoentropically $\Delta S = 0$. As described lucidly by Wannier[22], in hard materials the irreversible change takes place almost without any change of stress, it is therefore permissible to write the energy functional of (1) and (4) as

$$H(\sigma) = -\frac{1}{2}(\sigma^2/E_{eff})_S + (\gamma\Sigma_j \int dA_j)_\sigma \tag{30}$$

$$U(\varepsilon) = \frac{1}{2}(\varepsilon^2/E_{eff})_S + (\gamma\Sigma_j \int dA_j)_\varepsilon \tag{31}$$

where the subscripts are the commonly used specifications of the thermodynamic quantities which are held constant in the term. γ is the renormalized surface energy density in accordance with our discussion in § 3.2, and the integrals and sums $\Sigma_j \int dA_j$ exhaust the total area of all microcracks. The dependences on the macrocrack sizes a_i enter in the first term through E_{eff} and in the second term through the total crack area which

is evidently a functional of the linear macrocrack sizes a_i. The irreversible energy change has been identified above as this second term and its derivative as the crack resistance for the i microcrack

$$\left[\frac{\partial}{\partial a_i}\left(\gamma\Sigma_j \int dA_j\right)\right]_\xi = R_i \qquad (\xi = \sigma,\ \varepsilon) \tag{32}$$

However, in equilibrium for each macro crack size, when

$$\frac{dH}{da_i} = 0$$

$$\left(\frac{\partial H}{\partial a_i}\right)_S + \left(\frac{\partial H}{\partial a_i}\right)_\sigma = 0 \tag{33}$$

and similarly for $U(\varepsilon)$.

It follows therefore from (32) and (33) that

$$\begin{aligned} R &= -\left(\frac{\partial H}{\partial a}\right)_\sigma \\ &= \frac{1}{2}\sigma^2\left(\frac{\partial}{\partial a}\ (E_{eff})^{-1}\right)_\sigma \\ &= G(\text{the stress energy release rate}) \end{aligned} \tag{34}$$

where the subscript i has been dropped since measurements are usually made upon a unique (usually, prenotched) crack. An equivalent relation holds under fixed grip (ε constant) conditions.

The staleness of the result (34) is misleading: In actuality, it establishes R as a proper thermodynamical observable whereas in all previous

approaches known to us R features as the a derivative of part of the energy, which is not a thermodynamical observable.

3.5 Crack densities p as stochastic variables

In writing out the energy functional U (Eq. (1)) the origin of the cracks was left unspecified and so was the precise nature of and distinctions between macrocracks (or crack-clusters), microcracks and broken interatomic bonds. These issues will now be addressed, against the background of considerable uncertainties.

The need for a discussion arises because of the growing realization that discontinuities in solids visible to the naked eye, ranging from fracture to spall planes to pores, arise from the merging or coalescence of microcracks (not of visible size)[7,37-39]. Moreover, there is clear evidence for the role of microcracks that surround a fracture crack in toughening and in the enhancement of the surface energy through the presence of a plastic zone (we refer to our discussion of the renormalized γ and to References 19,27,37).

In their discussion of crack initiation Curran et al.[7] define microcracks as those having sizes comparable to "graininess" that defines the continuum limit of the material and supply a list of them to which we refer for factual details. The definition assigns to microcracks a measure of stability, at least as regards to their tendency only to grow not to closeup. Opposing this viewpoint is the suggestion that physical processes of a given type (such as having a given loading rate) result in microcracks of a definite average size, implying the possibility that crack-sizes fluctuate also in time until converging upon an average[40]. Thus, in

essence, crack- growth arises only through a proliferation of cracks, through merging, as already noted with respect to macrocracks[20].

For clarity, let us remark that in this work, and presumably in many other modern papers, macrocrack is taken as synonomous to (micro-) crack cluster. The reluctance of macrocracks to disappear by closing up under normal laboratory conditions is apparent.

There might well be sub-microcrack entitities which could represent sites of nucleation for microcracks and which open and close until they reach microcrack dimensions. This hypothesis is physically sensible since extremely high stresses can concentrate upon tiny surfaces, and these are capable of changing the atomic configurations one way or the other.

In summary, in addition to the picture of a given microcrack population which can increase by further application of stress, there are other possibilities of fluctuating populations (of microcracks or of sub-microcracks) which will adjust to the global criteria of thermodynamics. In other words, one may venture to hypothesize ergodicity among the different realizations of crack populations in a solid that is (or is not) subject to applied stresses. This situation is amenable to a Monte Carlo simulation of crack populations, e.g. by percolation techniques.

To include a stochastic crack population, the needed concepts are a density $\rho(r)$ of potential crack sites, that is a function of the coarse-grained position r (so that $\rho(r)$ varies slowly over ranges of several microcrack sizes), and the variables $p(r)$ (taking values between 0 and 1) which gives the probability of occupation of potential crack sites. Though not absolutely necessary, $p(r)$ is regarded as a free variable of the energy functionals U or H, such that these are minimal for the actual occupation probabilities $\hat{p}(r)$;

$$\frac{\delta U}{\delta p(r)} \text{ or } \frac{\delta H}{\delta p(r)} = 0 \qquad \text{at } p = \hat{p}. \tag{35}$$

The structure of the energy as function of $p(r)$ and of $\rho(r)$ is given in the following:

$$U(\{\varepsilon(r)\},\{p(r)\}) = \frac{1}{2} E_o \int \varepsilon^2(r)dr - \frac{1}{2} E_\varepsilon \int dr\rho(r) \int d(\Delta r)p(r)\varepsilon^2(r)$$

$$+ \gamma_o b^2 \int_{\Delta r \in b(r)} dr\rho(r)[p(r) + cb^2|\nabla p|^2]$$

$$+ \int drdr'\rho(r)\rho(r')p(r)p(r')D(r-r') \tag{36}$$

Here b is the linear size of the basic crack unit (plaquette) and a gradient term (with a positive phenomenological coefficient c) has been included in the third term to discourage spatial fluctuations in $p(r)$.

4. Discussion

Some arguable assumptions of the theory have already been discussed in the article. One might also cavil at the use of flat cracks, while in other approaches central place is given to the crack width[41] or to crack opening displacements[42]. It is possible to replace in our formalism [e.g., Eq. (36)] the probability field $p(r)$ by a width distribution without much modification. We also note that the macro-cracks or crack clusters possess widths due to their geometrical structure.

Among possible, experimental verifications of the theory one would name determination of the microcrack distribution near a macrocrack, as a function of distance and orientation. This is technically feasible now[39].

Independent measurements of E_{eff} and V^{ex} (the excluded volume due to crack-clusters) would test the relations proposed in §3.1. R-curve measurements under controlled conditions (fixed grip or stress) would dissolve some uncertainties.

Acknowledgements

Work was sponsored in part by the U.S. Air Force Office of Scientific Research, Air Force Systems Command, USAF under Grant No. 89 - 0374. The U.S. Government is authorized to reproduce and distribute reprints for Government purposes nothwithstanding any copyright notation therein.

We thank D.J. Bergman and D. Krajcinovic for useful discussions.

References

1. M. Born and K. Huang, The Dynamical Theory of Crystal Lattices, (Clarendon, Oxford 1954).

2. A.A. Maradudin, E.W. Montroll and G.H. Weiss, Theory of Lattice Dynamics in the Harmonic Approximation (Academic, New York, 1960).

3. P.W.S. Rayleigh, The Theory of Sound, Vols. 1 and 2 (Dover, New York 1945).

4. S.P. Timoshenko and J.N. Goodier, Theory of Elasticity (McGraw-Hill, New York, 1970) 3rd edition.

5. F.A. McClintock and F. Zaverl, Intern. J. Fracture 15, 107 (1979).

6. R. Thomson, Solid St. Phys. 39, 2 (1986).

7. D.R. Curran, L. Seaman and D.A. Shockey, Physics Reports 147, 253 (1987).

8. M. Murat, R. Englman and Z. Jaeger. (following paper)

9. J.R. Rice, J. Mech. Phys. Solids 19, 61 (1971).

10. J.R. Rice, "Continuum Mechanics and Thermodynamics of Plasticity in Relation to Microscale Deformation Mechanisms" in Constitutive Equations in Plasticity, Ed. Ali S. Argon (MIT press, Boston, 1975) p. 23-80.

11. D. Krajcinovic, M. Basista and D. Sumarac, J. Appl. Mechanics (to be published).

12. D. Krajcinovic in Proceedings of the NATO Advanced Research Workshop "Toughening Mechanisms in Quasi-Brittle Materials" (July 1990), Ed. S.P. Shah, p. 415 - 436. (Contributions) in the same workshop volume by K.T. Faber et al. (p. 3), D. Francois (p. 55), P.G. Meredith (p. 73), Z.P. Bazant (p. 143), S. Mindess (p.335), M. Kachanov (p. 439) and

others attest to the spread of the microcrack - based characterization of fracture in brittle solids).

13. B. Budiansky and R.J. O'Connell, Int. J. Solids Structures 12, 81 (1976).

14. R.L. Blumberg-Selinger, Z.-G. Wang, W.M. Gelbart and A. Ben-Shaul, Phys. Rev. A 43, 4396 (1991)

15. L.R.F. Rose and M.V. Swain, J. Am. Ceram. Soc. 69, 203 (1986).

16. O. Schmenkel and R.W. Steinbrech, J. Am. Ceram. Soc. 71, C271(1988). Also R.W. Steinbrech, et. al. in Ref. 12 p. 353-375.

17. M. Kachanov in Ref. 12 p. 439-443.

18. A.A. Griffith, Phil. Trans. R. Soc. A221, 163 (1921).

19. G.R. Irwin "Fracture" Encyclopedia of Physics, Ed. S. Flügge (Springer, Berlin, 1958) 551-589.

20. R. Englman and Z. Jaeger, Physics A. (to appear)

21. Z. Jaeger and R. Englman, ASME Journal (1990-1).

22. G.H. Wannier, Statistical Physics (Wiley, New York, 1966).

23. Z. Hashin, J. Mech. Phys. Solids 36, 719 (1988).

24. D.A.G. Bruggeman, Ann. Physik (Leipzig) 24, 636 (1935).

25. Y. Kantor and D.J. Bergman, J. Phys. C15 2033 (1982); J. Mech. Phys. Solids 30, 355 (1982).

26. G.C. Sih, Canadian Fracture Conferences 10, 65 (1983).

27. D.G. Holloway, The Physical Properties of Glass (Wykeham, London, 1973).

28. R.F. Cook, J. Mater. Res. 1, 852 (1986).

29. M. Kachanov, Ann. Israel Phys. Soc. 8, 205 (1986).

30. M. Kachanov, Intern. J. Solids Structures 23, 23 (1987).

31. I.N. Sneddon and M. Lowengrub, Crack Problems in the Classical Theory of Elasticity (Wiley, New York, 1960).

32. J.M. Kennedy and N.G.W. Cook, Proc. II. Intern. Conf. Constitutive Laws for Eng. Materials 2, 879 (1987).

33. D.P. Rooke and D.J. Cartwright, Compendium of Stress Intensity Factors (Hillingdon Press, Middx. 1976).

34. A.G. Atkins and Y.W. Mai, Elastic and Plastic Fracture (Ellis Horwood, Chichester U.K., 1985).

35. H.L. Ewalds and R.J.H. Wanhill, Fracture Mechanics (Edward Arnold, London, 1980).

36. ASTM Standard Practice E561-81, Standard Practice for R-curve Determination 1982 Annual Book of ASTM Standards, Part 10, pp. 680-692 (ASTM, Philadelphia, 1980).

37. K.T. Faber, T. Iwagoshi and A. Ghosh, J. Am. Ceram. Soc. 71, C-399 (1988); (Also K.T. Faber et al. on p. 3 in Ref. 12.)

38. A.G. Evans and Y. Fu, Acta Metall. 33, 1525 (1985).

39. S.M. Wiederhorn (private communication, 1989).

40. D.E. Grady, J. Appl. Phys. 53, 322 (1982).

41. J.B. Rundle and W. Klein, Phys. Rev. Letters 63, 171 (1989).

42. J. Planas and M. Elices, Eng. Fracture Mech. 35, 87 (1990).

This page is left intentionally blank.

PART 3

Crack-Cluster Description of Fracture
II. Numerical Study

Michael Murat, Robert Englman and Zeev Jaeger

Soreq Nuclear Research Center
Yavne 70600, Israel

ABSTRACT: A thermodynamic description of fracture based on percolation theory is studied numerically. The fracture behavior under fixed-grip and constant stress conditions are found to be different. Above a critical fixed strain the material attains an equilibrium non-zero crack density which approaches the percolation threshold assymptotically with increasing strain. This equilibrium may or may not be readily accessible depending upon the applied strain. The corresponding fracture stress is calculated using the free energy appropriate to constant stress conditions. Effects of the crack-crack interaction, anisotropic crack density and pre-existing pores on the fracture behavior are also studied.

I. Introduction

Recently, an attempt has been made [1,2,3] to reformulate the Griffith criterion for crack growth [4] for a granular medium using ideas from the percolation theory [5]. In this formulation it is proposed that the fundamental thermodynamic variable which serves as the order parameter is the crack concentration p, and not the length of the single or the dominant crack as in the original Griffith theory. A basic crack has a typical size b, which may vary between interatomic distances to macroscopic scales ($\sim 10^{-3}$ m) depending upon the material. A free energy, which is a function of the crack density only, is then minimized to determine the equilibrium crack density in the material. When a material of volume V is held at an average strain ϵ, (fixed grip conditions) this free energy, $F_\epsilon(p)$ can be written in the form

$$F_\epsilon(p) = \frac{E_0 \epsilon^2 V}{2} + U_{\epsilon M} + U_S - TS. \tag{1}$$

Here the first term is the elastic strain energy of the uncracked material whose Young's modulus is E_0, $U_{\epsilon M}$ is the mechanical energy released under fixed grip conditions due to the reduction of the stress in the vicinity of the crack, U_S is the excess energy in the system due to the opening of new crack surfaces and S is the configurational entropy of the cracks. If on the other hand, the external stress σ is specified, (constant stress conditions) the appropriate [6] free energy that should be minimized is the Legendre transformed free energy

$$\begin{aligned} F_\sigma(p) &= F_\epsilon(p) - \epsilon\sigma V \\ &= -\frac{\sigma^2 V}{2E_0} + U_{\sigma M} + U_S - TS, \end{aligned} \tag{2}$$

with $\sigma = \partial F_\epsilon / \partial \epsilon$. When evaluated on a lattice representation of the material, with a lattice constant b, the terms appearing in the free energy have rather simple forms. Denoting the linear size of the material by L, (in units of b), we get for the surface energy

$$U_S = 2N\gamma b^2 p. \tag{3}$$

Here N is the number of faces in the 3 dimensional lattice, which is proportional to L^3 and γ is the surface energy density of the material. In a 2 dimensional version of the theory, N would be the number of bonds, which is proportional to L^2 and the factor b^2 would be replaced by b. For the case of externally specified stress, the mechanical energy released is given by [7,8]

$$U_{\sigma M} = -\frac{\sigma^2}{2E_\sigma} \sum_i l_{i\perp}^3, \tag{4}$$

while for a system with specified strain,

$$U_{\epsilon M} = -\frac{E_\epsilon \epsilon^2}{2} \sum_i l_{i\perp}^3, \tag{5}$$

The moduli E_ϵ and E_σ will be defined later. This form assumes a uniform stress σ (or strain ϵ) throughout the material, which is assumed to be originating from uniaxial tension. $l_{i\perp}$ is the component of the end-to-end distance of cluster i of cracks in the direction perpendicular to the tension. For the 2 dimensional case the exponent 3 has to be replaced by 2. The magnitude of U_M is a monotonicly increasing function of p up to the percolation threshold, in the vicinity of which it peaks strongly. This peak is bounded by the total volume (area in 2 dimensions) of the lattice as the total volume within which stress is relieved cannot be greater than the sample volume.

The use of different moduli E_ϵ and E_σ in the expressions for the mechanical energy released is essential for obtaining the same *effective* modulus E_{eff} under both conditions. As one can define E_{eff} through either

$$\frac{E_{eff}\epsilon^2 V}{2} = \frac{E_0 \epsilon^2 V}{2} + U_{\epsilon M} \tag{6}$$

or

$$-\frac{\sigma^2 V}{2E_{eff}} = -\frac{\sigma^2 V}{2E_0} + U_{\sigma M}, \tag{7}$$

the equivalence of both definitions prescribes two relations between the three moduli, E_σ, E_ϵ and E_{eff}. We are thus free to use a certain physical model or approximation to fix

one of those. The self consistent field (SCF) approximation of Budiansky and O'Connell [8] results in the choice

$$E_\sigma = E_0(1-v)\,, \tag{8}$$

where $v = (1/V)\sum_i l_{i\perp}^3$ (*cf.* Eq. (4)). It then follows that $E_\epsilon = E_0$ and $E_{eff} = E_\sigma$. Another choice, which can be shown [3] to be related to the differential scheme (DS) of Hashin [9] corresponds to

$$E_\epsilon = \frac{E_0}{1+v}, \tag{9}$$

together with $E_{eff} = E_\epsilon$ and $E_\sigma = E_0$.

A parameterization (which is not unique) that includes the two preceeding results as limiting cases is to write down the three moduli in terms of a free parameter θ such that

$$E_\epsilon = \frac{E_0}{1+\theta v}\,,$$

$$E_\sigma = E_0[1-(1-\theta)v] \tag{10}$$

and

$$E_{eff} = E_0\frac{1-(1-\theta)v}{1+\theta v}\,.$$

The SCF approximation, Eq. (8) corresponds to $\theta = 0$, while the expression resembling the DS approximation, Eq. (9) is equivalent to the limiting case $\theta = 1$.

The entropy term is a simple combinatorical contribution resulting from the number of ways of placing Np cracks on N faces. It is given by

$$S = -Nk_B[p\log p + (1-p)\log(1-p)]\,. \tag{11}$$

However, since $k_BT \ll \gamma b^2$ except for atomic scale cracks, the entropy term can be neglected for all practical purposes.

In an earlier version of the theory [1], an estimate for the fracture stress was obtained using some simple arguments. Although not stated explicitely in that work, the form of

the free energy used corresponds to that of DS under constant stress conditions. This estimate amounts to approximating the mechanical energy (Eq. (4)) by the contribution from the largest cluster of cracks for $p \simeq p_c$. When one plots the total free energy as a function of the crack density, one obtains two minima. One is near $p = 0$ (for $k_B T \ll \gamma b^2$) while the other one is at the percolation threshold, p_c. At low values of the stress, the former is the more stable one. When the stress is larger than a critical 'fracture' stress, σ_f, the second minima becomes more stable. Neglegting the contributions to U_M from the finite clusters of cracks, one finds that $\sigma_f = \sqrt{6\gamma E_0 p_c/b}$. This resembles the Griffith formula ($\sigma_c \propto \sqrt{\gamma E_0/a}$) relating the critical stress, σ_c to the crack length, a; however the percolation result is for an assembly of random cracks while the Griffith theory applies to a single crack.

There are several points in this theory that need to be further investigated. First, approximating U_M by the contribution from the percolating cluster only is unfounded. It may be the case that the stable crack density is obtained at a value of p different from the percolation threshold, in which case one needs to evaluate the sum in Eqs. (4) and (5) rather than replacing it by V, its upper limit. A further important point is the introduction of crack-crack interactions into the theory. This point has been answered in the later version of the theory [2] in a formal manner. However, the effects of the interactions can be obtained only by adetailed calculation involving a numerical simulation. Another important generalization, which again is addressed formally in Ref. 2 is the minimization of the free energy with respect to a position and orientation dependen. crack density.

In this work we address these points using numerical simulations of a two dimensional version of the model. We calculate the free energies defined in Eqs. (1) and (2) using definitions of the moduli E_ϵ and E_σ corresponding to both SCF and DS approximations. We also study the effects of interaction between cracks by adding a heuristic term to the free energy to represent the crack-crack interaction. We also partially address the point raised

in the preceeding paragraph about the anisotropic crack density by minimizing the free energy with respect to an orientation dependent crack probability, which assumes different values in the directions parallel and perpendicular to that of the uniaxial tensile stress. In the next section we give details of the calculations, including the form of the interaction assumed. Section III presents the results for the cases with and without interaction. Also presented are the results for the lattices into which pre-existing pores have been introduced to study the effect of pore concentration and size on the fracture properties. In Section IV, we discuss the physical relevance of these results and compare them with theory where applicable. The results are summarized briefly in Section V.

II. Model and Method

We represent the material in two dimensions by a square lattice of size $L \times L$. The cracks can form only on the bonds of the lattice. The probability that a given bond represents a crack is independent of the status of other bonds and is given by p. For the sake of generality, we differentiate between bonds that are parallel to the direction of the stress and those that are perpendicular to it and assign them crack probabilities $p_{\parallel}$ and $p_{\perp}$ respectively.

There is a huge number of realizations of the lattice consistent with a given $(p_{\parallel}, p_{\perp})$. Each such realization corresponds to a different value of the energy. Since the only order parameter in our theory is the pair $(p_{\parallel}, p_{\perp})$, each realization is equally allowed in the evaluation of the average free energy. (This corresponds to an infinite temperature since realizations with different energies have equal probabilities.) To calculate this average energy, we simulate the lattice with a given $(p_{\parallel}, p_{\perp})$ several times and calculate the average free energy and other required averages.

The simulations are performed in the following manner: We assign to each bond a random number between 0 and 1 and place a crack on it if that random number is smaller

than $p_{\parallel}$ or $p_{\perp}$, depending upon its orientation. We then identify the connected cracks that form a 'cluster' of cracks. Several quantities are calculated for each cluster; these are the length of the cluster in both directions, denoted by $l_{\parallel}$ and $l_{\perp}$, coordinates of its center of mass, its radius of gyration R_g and the total number of lattice sites it covers. These are needed to calculate the different terms appearing in the expression for the free energy corresponding to a particular crack cluster. Fig. 1 shows several of these quantities for a typical cluster.

The term representing the excess surface energy due to the opening of cracks is calculated trivially. It is given by the total number of open bonds (cracks) in the lattice, which averages to $L^2(p_{\parallel} + p_{\perp})$. The term that gives the amount of mechanical energy released needs some consideration, since some of the cracks fall entirely or partly inside the region from which stress is relieved due to the presence of another crack. Therefore simply summing over $l_{\perp}^2$ of each cluster of cracks will overestimate this contribution. To avoid this problem, we place on each cluster an imaginary square of side $l_{\perp}$ centered on the center of mass of the cluster. A counter assigned to each lattice site is incremented by 1 if the site is inside the square, by 0.5 if it is exactly on an edge and by 0.25 if it is on a corner of the square. A site may be included in more than one such square. Any counter that reaches the value 1 is not changed any further. We then sum over the values of the counters on each lattice site and identify this sum (after multiplication by the stress or strain dependent factor) as the strain energy released.

The elimination of the overlap of the stress-free areas around each crack amounts to a certain interaction between the cracks; it is a short-range, excluded volume type of interaction. However, we know that the existence of a crack at a finite distance from another one changes the stress intensity at the tip of the latter, in a manner dependent upon their length and relative orientation [10]. To account for this additional long-range interaction, we assume an interaction energy between any pair of 'crack clusters' in the

lattice with a magnitude proportional to

$$E_I(i,j) = \{\left|\vec{l_i}\cdot\vec{l_j}\right| - \frac{l_i l_j}{2}\}e^{-r_{ij}^2/a_{ij}^2}. \tag{12}$$

Here $\vec{l_i}$ is a vector with components $l_\parallel$ and $l_\perp$, of the crack cluster i, l_i its length, r_{ij} is the distance between the centers of mass of the two clusters and $a_{ij}^2 = R_{gi}^2 + R_{gj}^2$. The form of this interaction energy is rather heuristic, and is certainly an extreme oversimplification of the reality. Analytical forms for crack-crack interaction are known only for some very simple crack configurations [10,11]. For the composite cracks that appear in our percolation formalism, evaluation of an interaction energy for an arbitrary crack configuration is beyond the scope of any realistic calculation. Another important effect that this simple form does not exhibit is the screening of the interaction between a pair of cracks by a third that lies on the line connecting the centers of the two. We have, however, chosen to use this simple form with the following considerations in mind: The magnitude of the interaction should decrease rapidly with the distance between the cracks, while the length scale characterizing this decay should depend on the sizes of the cracks. The interaction is also orientation-dependent in such a way that cracks perpendicular to each other are favored (negative interaction energy) rather than cracks with parallel orientation. We hope that despite its obvious drawbacks, the introduction of such an interaction energy will capture the basic physics of interacting crack systems.

In a given configuration of the lattice, the contributions from all pairs are summed over and the result is averaged over several configurations. The resulting average, which we denote by E_I, is now a function of $(p_\parallel, p_\perp)$ only and it modifies the 'unperturbed' free energy, F_0 as

$$F = F_0 + A\gamma E_I + B\frac{\sigma^2}{2E}E_I; \tag{13}$$

that is, both the stress dependent and stress independent terms of the free energy are modified. Here F and F_0 may be for fixed-grip or constant stress conditions.. The assumption

of the same form of the interaction for the stress-dependent and the stress-free interaction is another simplification since the stress-free interaction may be shorter ranged than the stress-dependent one. A and B are arbitrary parameters giving the relative strength of the interaction energy compared to the 'unperturbed' free energy. We expect that this kind of long range and size dependent interaction will not contribute significantly to the stress-independent part of the energy, since any local distortion should not propagate for more than several atomic distances [12]. Thus we expect $A \ll B$. However, we keep both contributions and calculate the interaction energy for several values of the pair A and B.

III. Results

We simulated lattices of linear size $L = 20$ and 50. The facts that the the number of crack pairs that need to be considered in the evaluation of the interaction term grows as the square of the number of clusters in the lattice and that the whole simulation has to be repeated for several values of $(p_{\|}, p_{\perp})$ prevented us from carrying out the calculation on larger lattices. It seems, however, that the results from the two cases do not indicate an appreciable finite size effect, and that the conclusions can be safely extrapolated to larger lattices.

First, let us present the results for the case in which $p_{\|} = p_{\perp} = p$; that is, bonds are cracked with the same probability regardless of their orientation with respect to the direction of the tensile stress acting on the material. Fig. 2 shows the effective Young's modulus (scaled by E_0) as a function of p for the two approximations corresponding to $\theta = 0$ and $\theta = 1$. We will refer to the two cases as the SCF approximation and DS approximation respectively, although these names refer only to the qualitative resemblence between our two limiting cases and the SCF results of Budiansky and O'Connell [8] and the DS results of Hashin [9]. The SCF effective modulus decays linearly for $p \ll 1$ and practically vanishes around $p = 0.5$. A quadratic fit in the range $0 \leq p \leq 0.2$ yields

$Eeff/E_0 = 1 - 0.98p - 2.31p^2$, which if extrapolated vanishes at $p = 0.48$, very close to the (bond) percolation threshold of the lattice, $p_c = 0.5$. (In the simulations, the effective modulus saturates at a very low value for $p > 0.5$ due to the way the sum in Eqs. (4) and (5) is calculated. As the center of the spanning cluster of cracks does not always coincide with the center of the lattice, the imaginary square placed on the cluster to calculate the stress-free area does not cover the whole lattice. Thus even for $p \geq p_c$ we may obtain $v \leq 1$, leading to a small but non-zero effective modulus.) The DS modulus starts to decay linearly as well, but saturates at $E_0/2$ for $p > 0.5$. This is due to the fact that v will never be larger than 1, while the analogous crack density parameter of Hashin [9] can grow indefinitely.

From here on we will use the SCF approximation to evaluate the free energies, unless otherwise stated. The energies are measured in units of γb (cf. Eq. (3)). Fig. 3 shows the dependence of the fixed-grip free energy on the crack concentration for several values of the dimensionless strain variable $e \equiv \frac{\epsilon^2 E_0 b}{4\gamma}$ without crack-crack interactions: $A = B = 0$. The data shown are for $L = 50$. For $e = 0$, the free energy consists only of the excess surface energy, which increases linearly with the crack density. As e is increased, a local minimum appears, which for $e = e_1 \simeq 1.0$ (equivalent to $\epsilon = \epsilon_1 \simeq \sqrt{4\gamma/E_0 b}$) attains the energy value of 0 at $p = p_1 \simeq 0.40$, the same as the energy value in the intact material with $p = 0$. At even higher values of the strain, this local minimum becomes the absolute minimum, which gets deeper with increasing strain. At strains for which $e > e_2 \simeq 2$ ($\epsilon > \epsilon_2 \simeq \sqrt{2}\epsilon_1$), the initial slope of the free energy becomes negative. With increasing e the value of p for which F_ϵ is minimum moves slightly toward higher values of p, approaching the critical value of $p_c = 1/2$ for much higher values of the external strain. The local fluctuation of the curves is due to the fact that only 20 realizations of the lattice were simulated for each p. A similar behavior was obtained for $L = 20$, where 400 lattices were used for the averaging. The results for e_1 and p_1 were slightly different from the ones observed for $L = 50$. They

are shown in Table I together with the numerical results for other cases analyzed.

In Fig. 4 we show the average constant-stress free energy of 20 $L = 50$ systems as a function of the crack concentration at several values of the applied stress. This function exhibits a very different behavior compared to that of the fixed-grip free energy. At any finite value of the stress the free energy assumes an extremely large negative value as p approaches p_c. This is due to the fact that within the SCF approximation the effective modulus vanishes approaching p_c. For low values of the stress the energy increases at low crack concentrations before decreasing rapidly close to p_c. However for $s \equiv \frac{\sigma^2 b}{4\gamma E_0} \simeq 2$ $(\sigma \simeq \sqrt{8E_0\gamma/b})$ this positive slope vanishes and becomes negative for higher stresses.

When we allow the crack clusters to interact, a somewhat different picture emerges. Fig. 5 shows the average fixed grip free energies for the same lattices used for Fig. 3 with interaction parameters $A = B = 1$. For $e = 0$, the energy again rises linearly for small values of p, but the rise becomes much steeper when the interaction between the cracks become significant at larger p. It seems that no minimum is formed now at a non-zero value of p before $e \simeq 1.5$; rather we find an energy that increases with a small slope with increasing p, before it shoots up at around $p \simeq 0.3$. At a strain that corresponds to $e \simeq 1.5$, a global minimum is observed at $p \simeq 0.25$. It seems that e_1 and e_2 (corresponding to strains at which a minimum occurs and at which the initial slope becomes negative respectively) coincide in this case.

We calculated the free energy as a function of the crack concentration for several values of the interaction parameters and identified e_1 and p_1 for each case as described above. An increase in either of the two parameters causes e_1 (and consequently the corresponding strain) to increase and p_1 to decrease. Table I summarizes the resulting e_1 and p_1 for both $L = 20$ and $L = 50$ as a function of the interaction parameters.

The restriction of $p_{\parallel} = p_{\perp}$ turns out an unfavorable one for our system. When we allow the two kinds of bonds to have different probabilities to represent cracks, the energy of the

system is lowered by decreasing the number of cracks parallel to the tensile stress. In fact, when crack-crack interaction is not taken into account, the minimum of the fixed-grip free energy at any given stress σ is attained on the $p_{\|} = 0$ line. Fig. 6 shows this behavior for several values of e on the line $p_{\|} = 0$. One can see from the figure that the local minimum near $p_{\perp 1} \simeq 0.5$ becomes stable at $e = e_1 \simeq 0.58$, which is lower than the one obtained when all the bonds are restricted to have the same probability of cracking. This means that the condition represented by the minimum on the $p_{\|} = 0$ line will be achieved before any other local minimum, including the one on the isotropic line, reaches the energy value of zero. It will thus be the relevant one whenever the condition of isotropicity is removed. As in the isotropic case, at even higher strains the initial slope becomes negative. Here we find this to occur for $e > e_2 \simeq 0.8$.

One would expect that introduction of interactions that favor cluster pairs that are perpendicular to each other will move this minimum away from the $p_{\|} = 0$ line. We find, however, that even though the location of the minimum and the stress level at which it becomes the absolute minimum change, it still remains on the $p_{\|} = 0$ line. The reason, apparently is that when we introduce a small number of cracks parallel to the axis of the tensile stress at random, some of them go to regions in which reduction in energy due to interactions is ineffective. They are either attached to already existing clusters of 'perpendicular' cracks, or are located far from them, so that the magnitude of the interaction is small. All these 'parallel' cracks, however, cost additional surface energy and the overall balance is unfavorable to the system. Only for values of $p_{\perp}$ significantly larger than $p_{\perp 1}$ do we see a favorable effect of addition of 'parallel' bonds. Using $A = B = 1$ for the $L = 50$ system, we find that an absolute minimum is obtained at $p_{\perp} \simeq 0.2$ for $e = 0.81$, while addition of 'parallel' bonds starts to be favorable at $p_{\perp} \simeq 0.5$.

In order to study the effects of porosity on the fracture behavior within our model, we repeated our simulations with lattices on which pores are initially placed. A pore for our

purpose is a square of side g lattice units within which all the bonds are removed (including those on its perimeter). Any two crack clusters that touch the same pore are assumed to be connected for the purpose of calculating the strain energy released and the interaction energy. Any crack placed at random inside or on the perimeter of the pore does not cause any surface energy. In accordance with Ref. 1 we studied the cases with $g = 1$ (pore size $\simeq$ basic crack length) and $g = 5$ (pore size $>$ basic crack length). When the pore size is equal to the crack length, we find that for pore concentration $\phi = 0.1$, the absolute minimum of the fixed-grip free energy is first obtained at $p = p_1 \simeq 0.3$ for $e_1 \simeq 0.8$ (with isotropy restriction and in the absence of interactions). p_1 turns out to be smaller than the one observed for the $\phi = 0$ system since the crack coalescence is assisted by the pores. e_2 is also considerably reduced to $e_2 \simeq 1.1$. The introduction of interactions again changes p_1 and e_1 in a manner similar to the pore free system. Under constant stress conditions, we find that the initial slope first turns negative at $s \simeq 0.8$. Increasing the concentration of the pores to 0.2, we obtain $e_1 \simeq e_2 \simeq 0.8$, $p_1 \simeq 0.25$ and $s \simeq 0.5$. When the pore density of 0.1 is achieved with pores larger than the basic crack size, we find that these numbers approach their values in the absence of any pores. For pores of linear size of 5 lattice units, we find that $e_1 \simeq 1.0$, $p_1 \simeq 0.4$, $e_2 \simeq 1.5$ and $s \simeq 1.2$, approaching the corresponding values for the pore-free lattice. Thus our data confirm the prediction made in Ref. 1.

IV. Discussion

One interesting result of the simulations is the appearance of the minimum of the fixed-grip free energy at a crack concentration significantly below the critical concentration for percolation when a self consistent field approximation is used. This is true both with and without the interaction terms and remains such when the isotropic restriction is removed, since with $p_{\|} = 0$, the critical value for $p_{\perp}$ is 1. The implication is that at strains ϵ that correspond to the dimensionless strain variable $e_1 < e < e_2$, there exists a stable crack concentration for the material. However, if one starts with initially crack-free material, this minimum is inaccessible since the free energy is an increasing function of the crack concentration at that strain range. Only when $e > e_2$ can this minimum be reached spontaneously. Fracture, that corresponds to an equilibrium crack density of p_c can then occur only at an infinite strain since the minimum approaches p_c only asymptotically with increasing e.

This result is in fact not surprising since in our model fracture is due to the coalescence of random crack clusters, which can occur only at $p = p_c$. Because within the self-consistent field approximation the effective Young's modulus vanishes at that concentration, any finite fracture stress would correspond to infinite strain. In order to know the fracture stress, one needs to analyze the system under constant-stress conditions. From Fig. 4 we find that indeed such a finite fracture stress exists. In our model system, at stresses that correspond to the dimensionless stress variable $s > 2.0$ the material would spontaneously break. Thus the fracture stress in our model is given by $\sigma_f \simeq \sqrt{8\gamma E_0/b}$. At this stress, the intact material has an elongation that corresponds to $e_2 = \sigma_f/E_0$ since the effective Young's modulus for the intact material is E_0. If kept at this constant stress, the equilibrium state of the material, which is at $p = p_c$ would be reached at a strain that increases without bound. Thus in a sense our model describes a perfectly plastic fracture.

Within the SCF approximation, the Young's modulus vanishes linearly at the percola-

tion threshold. The approximation that resembles the DS approach gives a finite value for the elastic constant at the geometric percolation threshold. In fact, Hashin's treatment for a cracked material [9] does not take into consideration a finite percolation threshold for cracks of negligible volume and predicts moduli that vanish only at an infinite concentration of such cracks. Treatments that go beyond the effective medium approximation (which both approaches utilize) give a soft decay of the modulus at the percolation threshold p_c of the material as $E_{eff} \propto (p - p_c)^T$, with the best estimate [13,14] for T being $T \simeq 4$ both in 2 and 3 dimensions. (In terms of the crack concentration, the material fragmentation threshold p_c [15,16] corresponds to what has been termed [17] p_c^f or p_{cII} of the cracks, in contrast to their percolation threshold termed for the present purposes p_{cI} ($< p_{cII}$, in three dimensions)

It is interesting to note that a recent study by Blumberg-Selinger *et al* [18] that utilized a thermodynamic approach to fracture also resulted in an equilibrium state with a finite density of defects. That study involved the relaxation of an elastic network in which equilibrium defects are thermally formed or destroyed until an equilibrium configuration is reached. At a certain range of the applied stress or strain, the equilibrium configuration is one in which a finite fraction of the lattice bonds are broken. This equilibrium may be stable or metastable. In that study, however, the fracture is essentially a brittle one, unlike our model in which it results from the coalescence of random crack clusters

The introduction of a long range interaction between cracks changes the fracture behavior qualitatively. It seems that under fixed-grip conditions, the distinction between e_1 and e_2 vanishes. This means that the there is no local minimum of the free energy at non-zero values of the crack concentration. We also find that irrespective of the parameters of the interaction strength, the introduction of crack-crack interactions increases the value of e_1. Even though the interaction between any two cracks can have a positive or negative effect on the energy of the system, the averaging process seems always to result in the

same trend for e_1 or for the fracture stress.

An interesting result of the model is the instability with respect to the assymetry in the probabilities of crack formation in the directions parallel and perpendicular to the direction of the external stress. The fact that in all cases studied fracture occurs when the density of cracks in the direction parallel to the stress is zero means that these cracks cost energy to form and do not relieve considerable stress energy, even when interactions are taken into account. This behavior is the closest that one can approach brittle fracture within our model, which, due to its probabilistic nature, does not account for the growth of a single crack. In reality we would expect that the microscopic structure of the material will allow for some relation or restriction between the densities in different directions in space (probably as a continous function of the direction). In our discrete model, this would correspond to looking for the minimum of the free energy along some line intermediate between the isotropic line and the $p_{\parallel} = 0$ line.

The dependence of the fracture stress on the pore density and pore size is a feature predicted by the theoretical analysis of the model [1]. The behavior found in this work is in qualitative agreement with that prediction, although the present study relies on the SCF approximation while Ref. 1 used the DS approximation. According to the theory, when the pore size is of the same order of magnitude as the basic crack size, the fracture stress should decrease as $\sigma_f \propto \sqrt{(1-\phi)p_c(\phi)}$. ϕ is the density of pores and $p_c(\phi)$ is the percolation threshold of the cracks in a lattice with a density ϕ of pores. In our simulations we found the fracture stress to decrease from what corresponds to $s = 2$ for a pore free system to $s = 0.8$ and 0.5 for systems with $\phi = 0.1$ and 0.2 respectively. We also verify numerically the prediction that as the pore size increases, the fracture stress increases towards its value in pore-free material. For $\phi = 0.1$ increasing the pore size to 5 lattice units was found to increase the fracture stress to 1.2. This behavior is also experimentally observed in several ceramic materials [19].

V. Summary

A thermodynamic description of fracture due to the coalescence of cracks and pores seems to show several interesting features when investigated using percolation techniques. We find that one obtains different results if the fracture is attained under fixed-grip or constant-stress conditions. When the material is held at a fixed strain a stable configuration with a crack density $p_1 \simeq 0.4$ is formed for strains above ϵ_1, which in a pore free material with no crack-crack interaction is given by $\epsilon_1 = \sqrt{4\gamma/E_0 b}$. This state becomes spontaneously accessible at a strain $\epsilon_2 = \sqrt{2}\epsilon_1$. The corresponding crack density increases from p_1 to p_c asymptotically with increasing strain. Fracture occurs only at infinite strain. The fracture stress is finite, however, since the effective Young's modulus vanishes linearly approaching the percolation threshold. This stress, σ_f, can be found using the free energy appropriate for the constant stress conditions. We find that it is given by $\sigma_f = \sqrt{8\gamma E_0/b} = E_0\epsilon_2$. Crack-crack interaction as introduced using a heuristic form causes the distiction between ϵ_1 and ϵ_2 to disappear, thereby rendering the equilibrium crack concentration spontaneously accessible.

When crack densities parallel to the direction of the tensile strain and perpendicular to it are allowed to be different, the system achieves its minimum free energy by having all the cracks in the direction perpendicular to the direction of the strain. Furthermore, this minimum is attained at a smaller applied strain than the one needed to achieve the metastable state with isotropic crack densities. Introduction of the crack-crack interaction does not alter this situation either.

For systems that contain pores, the fracture energy is considerably reduced. The fracture stress is also found to be an increasing function of the ratio of the pore size to the basic crack length, in agreement with the situation observed in certain ceramic materials.

Acknowledgements

This work is sponsored in part by US Air Force Office of Scientific Research, Air Force System Command, USAF under Grant No. 89-0374. The US Government is authorized to reproduce and distribute reprints for Governmental purposes notwithstanding any copyright notation therein. We thank A. Aharony, D. Bergman and R. Ruppin for helpful discussions.

REFERENCES

1. R. Englman and Z. Jaeger, to appear in *Physica*, 1990.
2. Z. Jaeger and R. Englman, preprint (1990).
3. R. Englman, M. Murat and Z. Jaeger, preceding paper
4. A. A. Griffith, *Phil. Trans. R. Soc. A* **221**, 163 (1921).
5. D. Stauffer, *Introduction to Percolation Theory*, Taylor and Francis, London, (1985).
6. L. D. Landau and E. M. Lifshitz, *Theory of Elasticity*, Pergamon Press, London, 1959, p9.
7. S. P. Timoshenko and J. N. Goodier, *Theory of Elasticity*, McGraw-Hill, Tokyo (1970).
8. B. Budiansky and R. J. O'Connell, *Int. J. Solids Structures* **12**, 81 (1976).
9. Z. Hashin, *J. Mech. Phys. Solids* **36**, 719 (1988).
10. M. Kachanov, *Int. J. Solids Structures* **23**, 23 (1987).
11. P. T. Antone, thesis, California Institute of Technology, Pasadena, California, 1972.
12. D. J. Bergman, private communication (1989).
13. J. G. Zabolitzky, D. J. Bergman and D. Stauffer, *J. Stat. Phys.* **44**, 211 (1986).
14. S. Arbabi and M. Sahimi, *Phys. Rev. B* **38**, 7173 (1988).
15. A. Aharony, A. Levi, R. Englman and Z. Jaeger, *Ann. Israel Phys. Soc.* **8**, 112 (1986).
16. J. S. Kuszmaul, Proc. XXVIII US Symposium on Rock Mechanics (Tuscon, Arizona, 1987); also SANDIA report SAND 86-2427C.

Table I

ϵ_1 and p_1 as a function of the crack-crack interaction parameters A and B for lattices of size $L = 20$ and 50. The dimensionless strain variable $e_1 = \frac{\epsilon_1^2 E_0 b}{4\gamma}$ gives the strain ϵ_1 at which the local minimum in the fixed-grip free energy at a nonzero p becomes the absolute minimum. p_1 is the corresponding crack concentration.

		$L = 20$		$L = 50$	
A	B	e_1	p_1	e_1	p_1
0.0	0.0	1.13	0.41	1.00	0.40
0.0	0.5	1.32	0.35	1.20	0.34
0.0	2.0	1.68	0.22–0.24	1.57	0.22
0.0	5.0	1.96	0.01–0.10	1.82	0.11
0.5	0.0	1.29	0.37	1.17	0.34
2.0	0.0	1.54	0.26–0.28	1.44	0.28
5.0	0.0	1.80	0.16–0.19	1.70	0.14
0.5	0.5	1.43	0.28–0.31	1.31	0.28
1.0	1.0	1.61	0.22–0.26	1.50	0.22-0.28
2.0	2.0	1.83	0.13–0.20	1.72	0.12-0.14

FIGURE CAPTIONS

Figure 1. Definition of several of the quantities calculated for a typical crack cluster with 11 bonds(cracks). $\times$ shows the position of the center of mass of the cluster. The radius of gyration of this cluster is 1.87 lattice units. σ is the external tensile stress.

Figure 2. The effective Young's modulus at crack concentration p within (a) self consistent field approximation and (b) differential scheme.

Figure 3. Average fixed-grip free energy of 20 lattices of linear size $L = 50$ as a function of the crack density for several values of the dimensionless strain variable $e \equiv \frac{\epsilon^2 b E_0}{4\gamma}$ indicated next to each curve. The interaction parameters $A = B = 0$.

Figure 4. Average constant-stress free energy of 20 lattices of linear size $L = 50$ as a function of the crack density for several values of the dimensionless stress variable $s \equiv \frac{\sigma^2 b}{4E_0\gamma}$ indicated next to each curve. The interaction parameters $A = B = 0$.

Figure 5. Average fixed-grip free energy of a lattice of linear size $L = 50$ as a function of the crack density for several values of the dimensionless strain variable $e \equiv \frac{\epsilon^2 E_0 b}{4\gamma}$ indicated next to each curve. The interaction parameters $A = B = 1$.

Figure 6. Average fixed-grip free energy *versus* density of cracks in the direction perpendicular to the axis of the tensile stress. The density of cracks in the other direction is zero. The value of the dimensionless strain variable $e \equiv \frac{\epsilon^2 E_0 b}{4\gamma}$ is shown next to each curve.

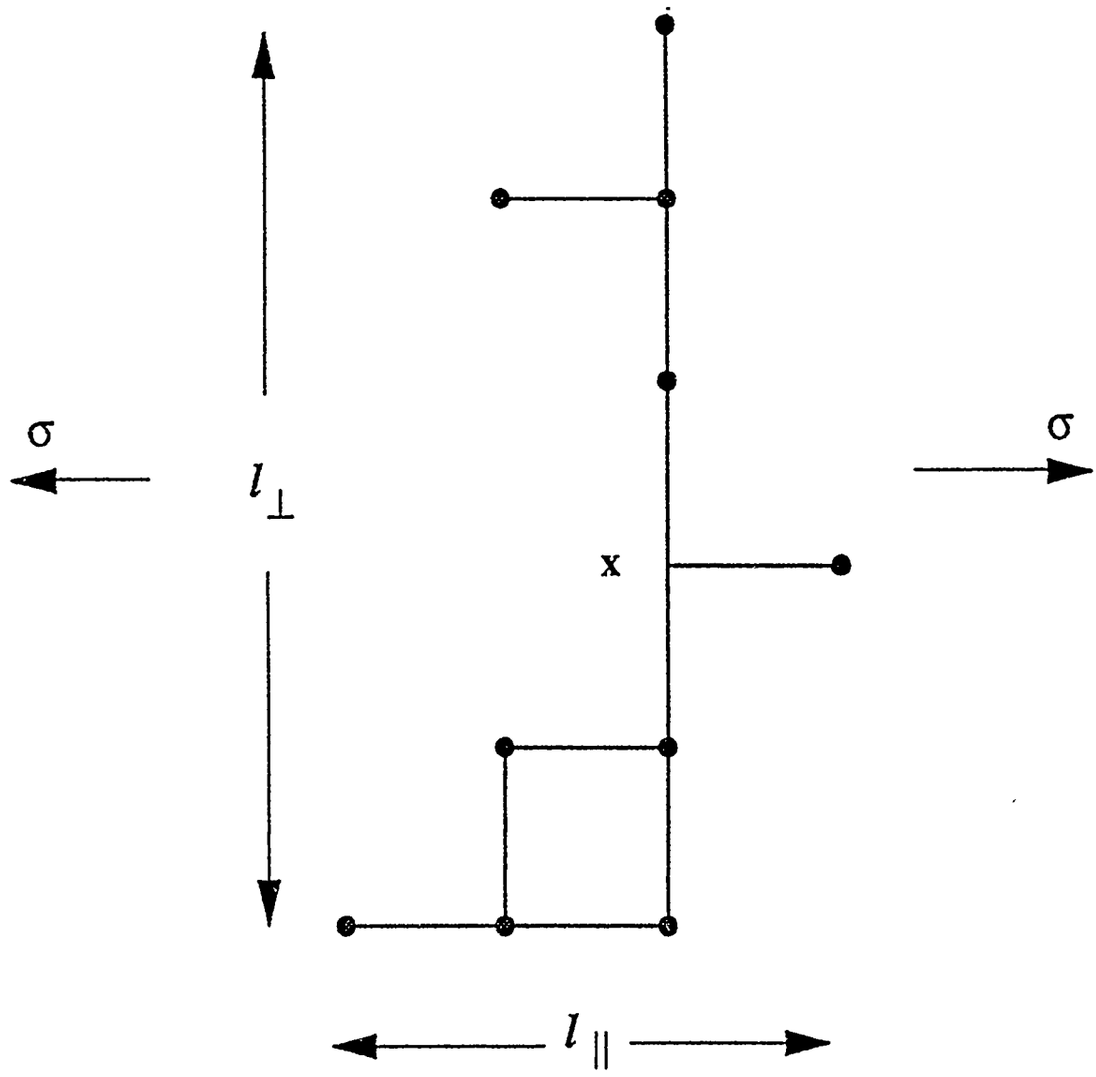

Fig. 1

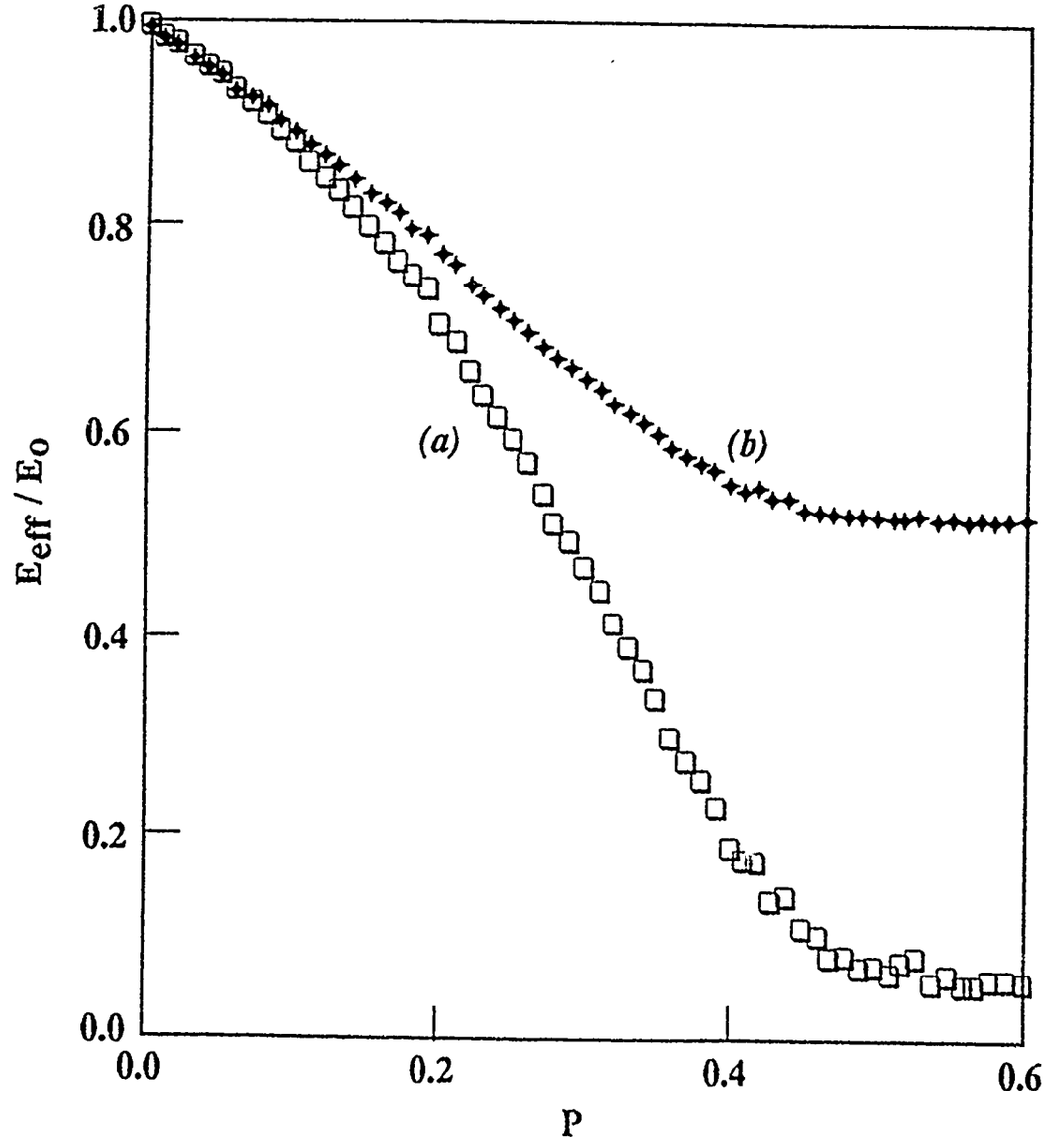

Fig. 2

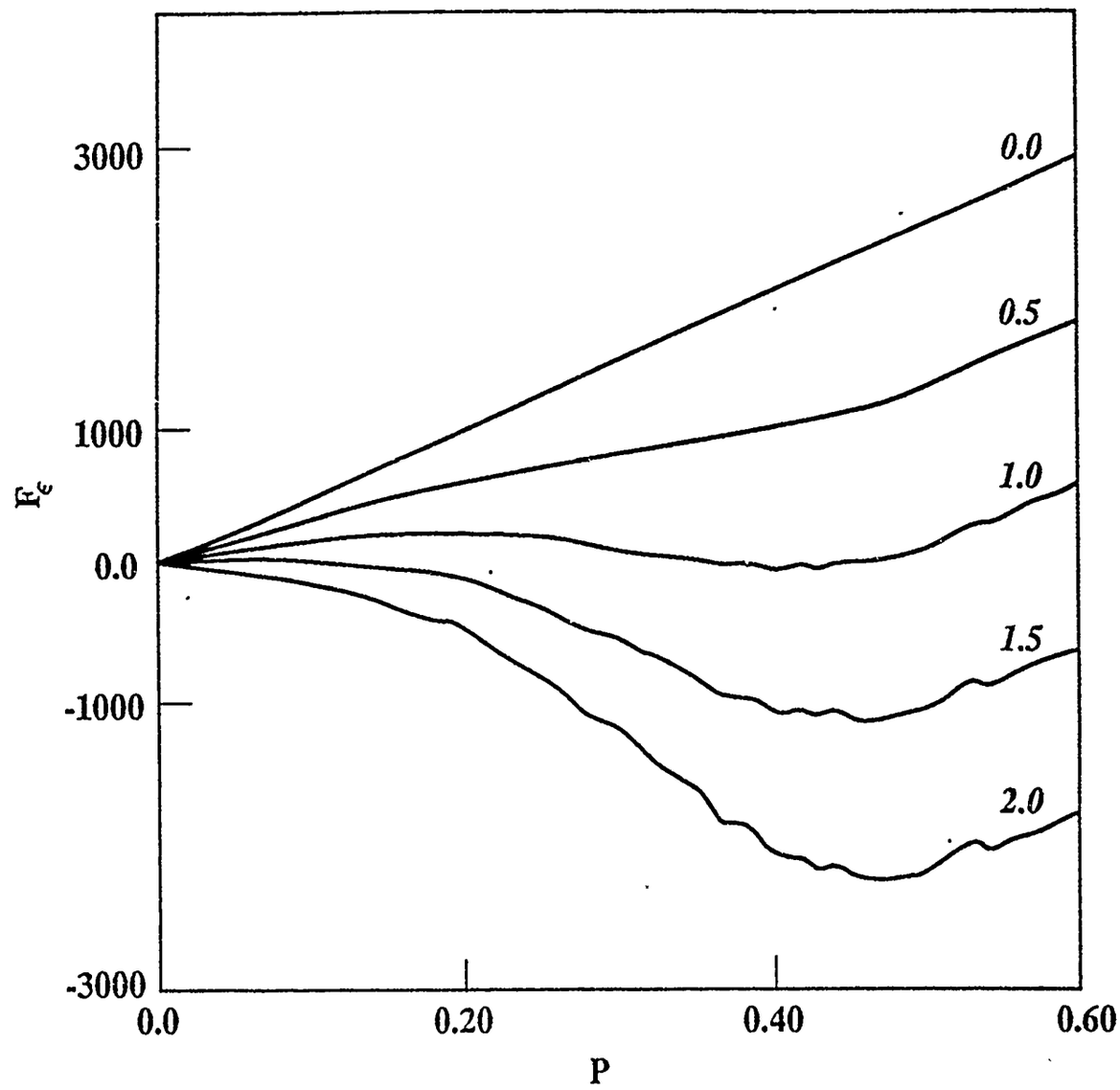

Fig. 3

17. H. Yatom and R. Ruppin, *J. Appl. Phys.* 65, 112 (1989).

18. R. L. Blumberg-Selinger, Z.-G. Wang, W. M. Gelbart and A. Ben-Shaul, Phys. Rev. A 43, 4396 (1991).

19. R. W. Rice, S. W. Freiman, R. C. Pohanka, J. J. Mecholsky and C. C. Wu, in *Fracture Mechanics of Ceramics*, R. C. Bradt, D. P. H. Hasselman and F. F. Lange, Eds., Plenum, New York, 1978, p849.

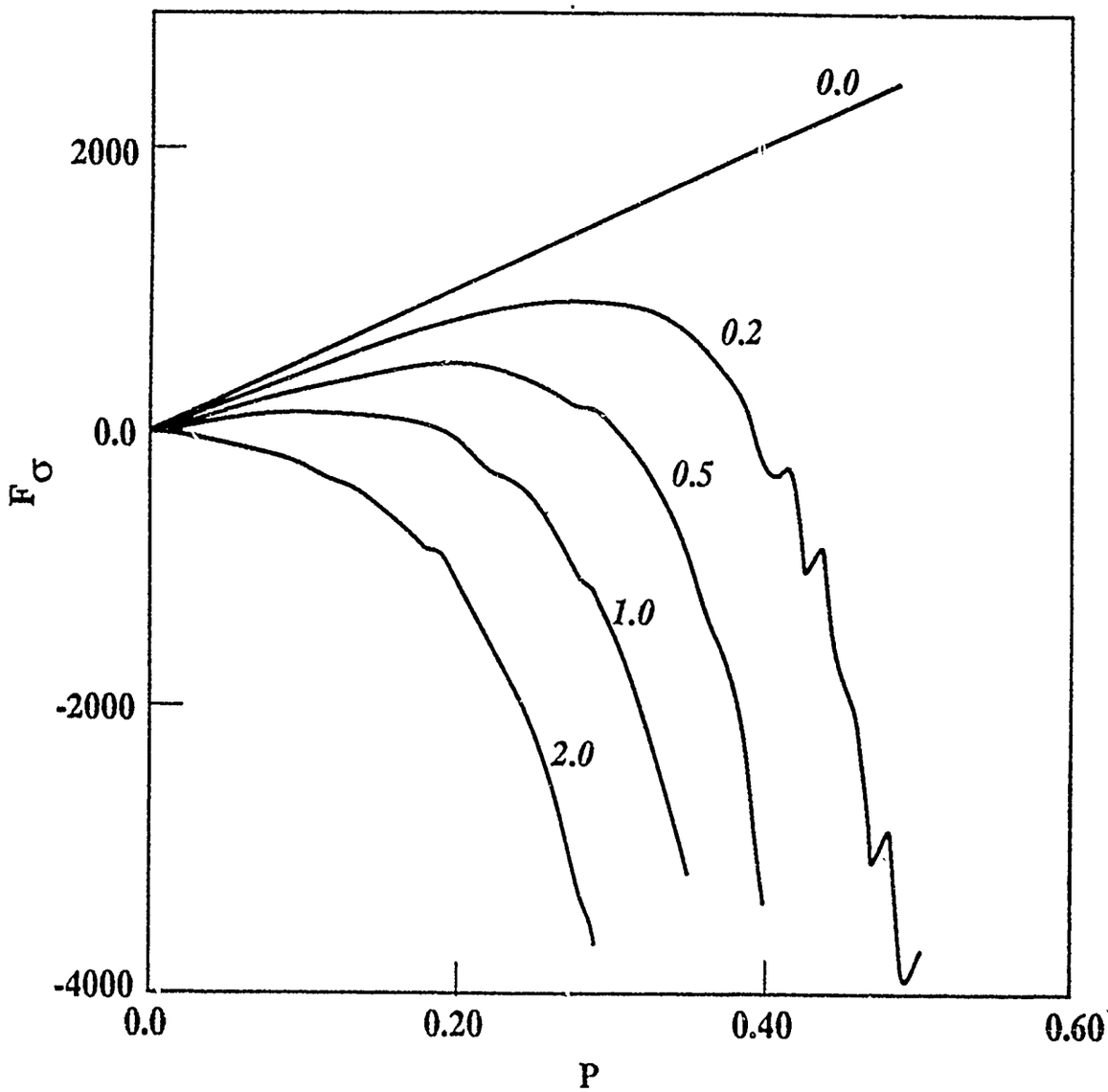

Fig. 4

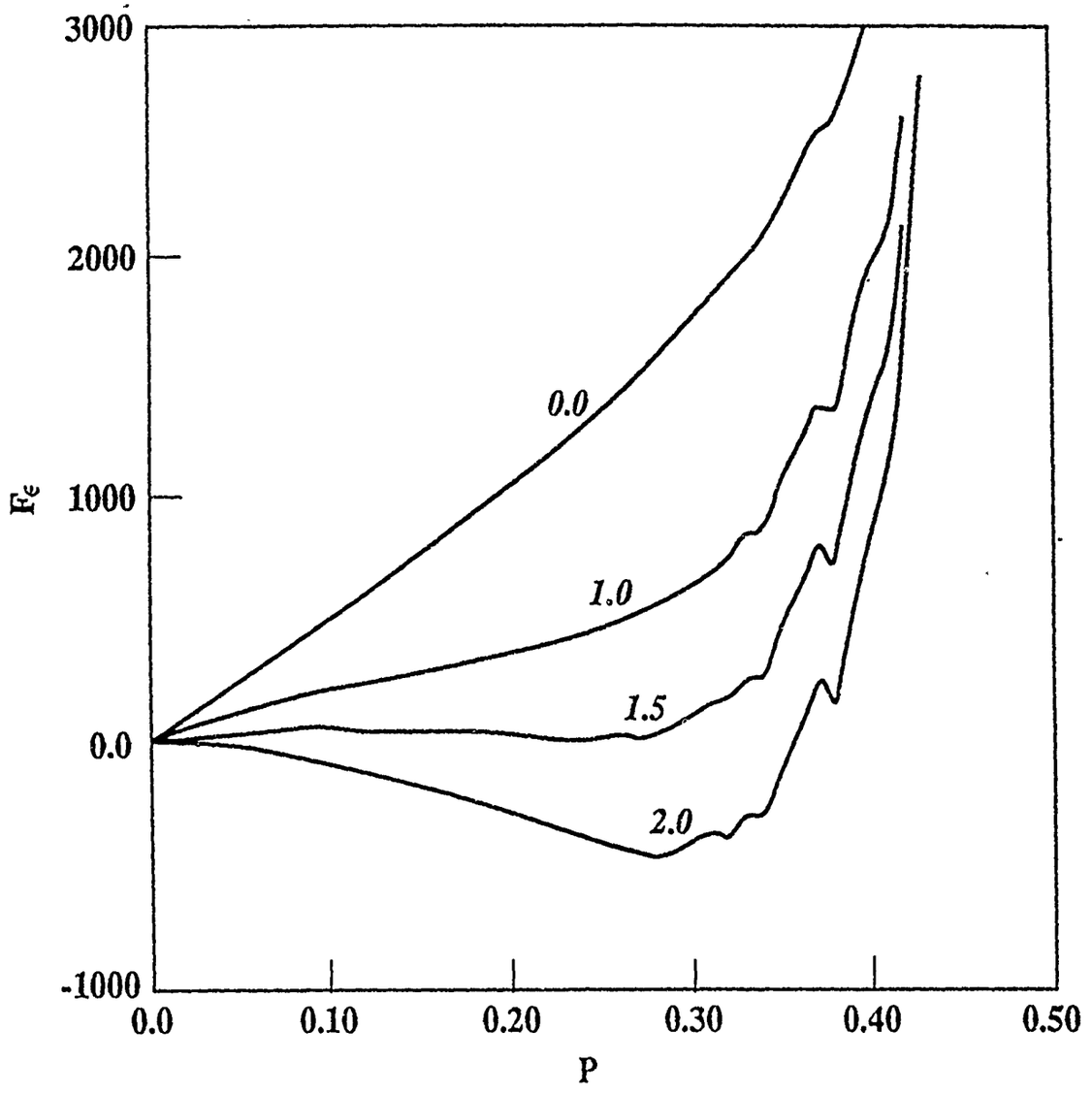

Fig. 5

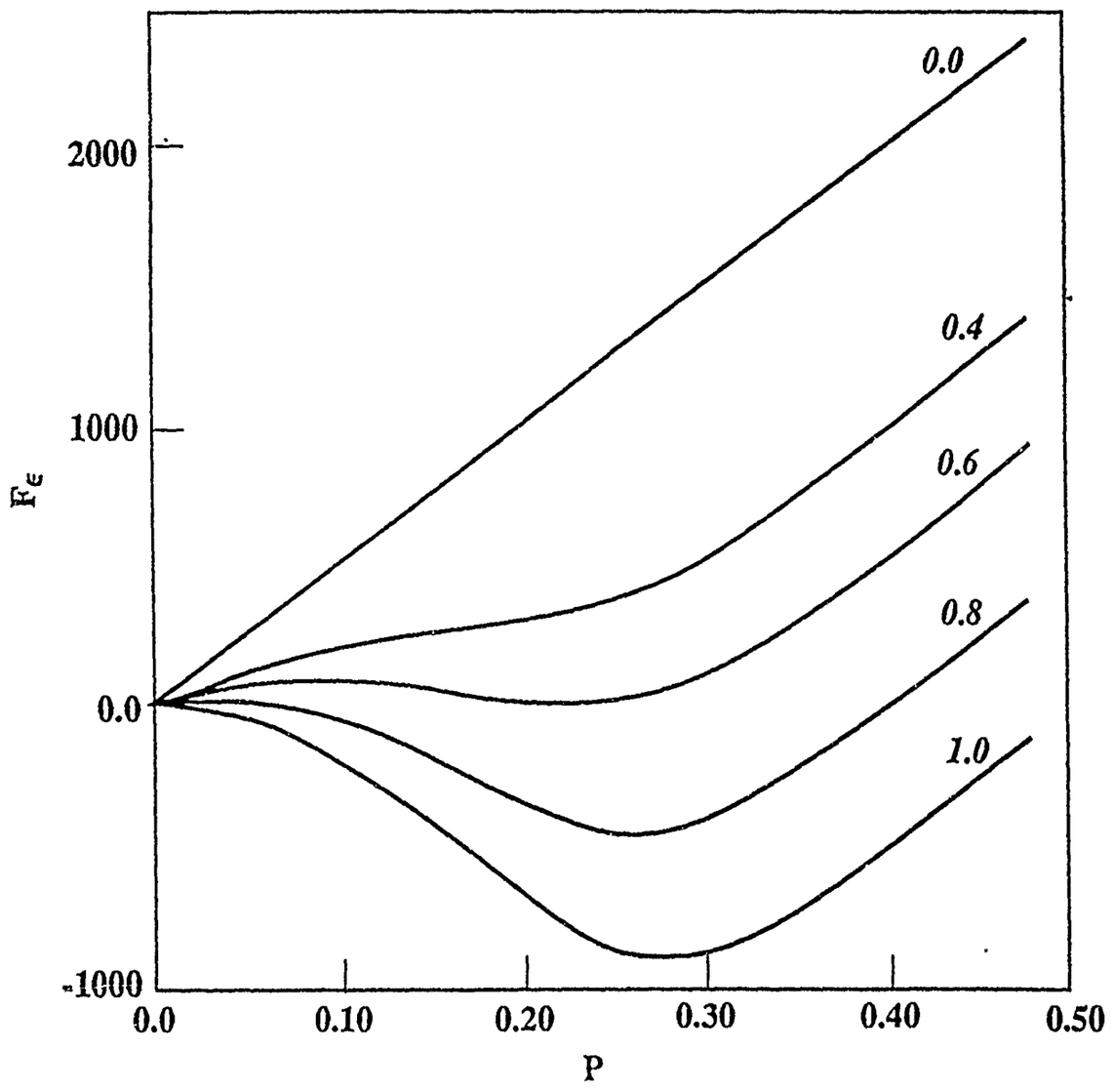
0.0
0.4
0.6
0.8
1.0
2000
1000
0.0
-1000
F_ϵ
0.0
0.10
0.20
0.30
0.40
0.50
P

Fig. 6

This page is left intentionally blank.

PART 4

A NUMERICAL SIMULATION OF THE R-CURVE BEHAVIOR IN MICROCRACKING MATERIALS

Michael Murat, Robert Englman and Zeev Jaeger

Soreq Nuclear Research Center
Yavne 70600, Israel

ABSTRACT:

We propose several models for crack propagation in ceramic materials with microcrack formation and coalescence. The models differ in the relative time scales involved in the internal relaxation processes and the external loading rate. We find that when the external loading rate is very high, a rising R-curve is obtained. For slow external loading, the results depend upon the relative rate of the different internal relaxation processes and upon the distribution of the critical stresses needed to form the microcracks. In this regime, the existence of a rising R-curve behavior is found to be primarily due to microcrack shielding.

I. INTRODUCTION

The strength of brittle materials is limited by the existence of inherent flaws within the materials. A quantitative statement of this observation was first given by Griffith[1], who considered an infinite plate of uniform thickness in which a thin crack of length $2a$ is inserted. Using a stress analysis due to Inglis[2], Griffith showed that when the material is under a tensile stress σ applied at infinity, an increase of Δa in the crack length will reduce the strain energy of the material by $2\pi b\sigma^2 a\Delta a/E$, where E is Young's modulus and b the thickness. However, the increase in the crack length will cost a surface energy of $2b\Delta a\gamma$. Here γ is the surface energy density of the solid and the factor 2 comes from the formation of two new surfaces. The crack length will spontaneously increase when the reduction in the strain energy becomes larger than the increase in the surface energy. This gives the famous Griffith criterion for the fracture stress, σ_f:

$$\sigma_f = \sqrt{2E\gamma/a\pi} \ . \tag{1}$$

One can interpret $R = 2\gamma$ as the material's resistance to further fracture. Experimental test of this prediction, performed by Griffith himself on glass, verified the dependence on the flaw size, but the critical stresses turned out to be several times higher than the predicted value. The deviation was found to be larger for metals[3]. The discrepancy implies that there is another sink for energy in addition to the new crack surfaces. Irwin[3] suggested that this sink, at least for metals, is a plastically strained zone around the crack tip within which energy is dissipated. For such cases, the resistance to fracture, R is composed of the sum of the surface energy and the plastic energy. In ceramic materials and some multiphase materials, like concrete, in which plasticity is not significant, there are additional mechanisms that dissipate energy during fracture. A prominent toughening mechanism, observed in zirconia and alumina ceramics, is the so-called 'transformation toughening'[4]. Here energy is dissipated in the transformation of the tetragonal ZrO_2 particles dispersed in the matrix into a monoclinic structure. Another mechanism suggested

for non-transforming ceramics is due to a restraining force across the newly formed crack interface caused by grain bridging[5,6]. Quoting some earlier works[7,8,9], the authors suggest that the same mechanism may be relevant to other materials like steel, concrete and rocks. A third important mechanism, on which we will base our study, is the microcrack toughening. Here a cloud of microcracks that form in front and at the sides of the main crack absorb some of the energy that would otherwise be used in increasing the length of the macrocrack in a brittle fracture. They may also act as shields that screen the macrocrack tip, thereby reducing the stress intensity there. Substantial experimental evidence to the relevance of microcracking mechanism was provided by the works of Knehens and Steinbrech[10] and Rühle *et al* [11].

These mechanisms have also been used to explain an interesting feature observed in ceramic materials, the so-called R-curve behavior. It is found in these materials, that when one evaluates the resistance to fracture R defined above as a function of the crack length increment by some standard procedures[12,13], one obtains a resistance that increases with increasing crack length. Such a behavior has immense engineering significance, as the implication of this increase is that unstable propagation of the crack is delayed until the crack reaches larger sizes, rendering the detection of the crack before a catastrophic failure possible. Theoretical models based upon the previously mentioned mechanisms[6,14,15] have concluded that a rising R-curve is possible through these mechanisms. A model treating the formation of individual microcracks was proposed by Hoagland and Embury[16] who simulated the microcracking process around a long crack by solving for the stresses in the material in a self-consistent manner. They found the number of microcracks formed for several possible distributions of microcrack formation stresses and orientations as a function of external stress intensity. R-curves for these distributions were also calculated under the assumption that the material still exhibits linear elastic behavior. With this assumption, the fracture resistance is proportional to K_I^2, where K_I is the stress intensity

factor[6]. The R-curves turn out to be continously increasing. However, due to the intensive calculations involved in the determination of the stress distribution, only crack increments of about 12 microcrack length units could be realized. The model was later extended[17] to cases where both microcracking and stable crack extension occur simultaneously.

In this work we suggest three models similar to the Hoagland-Embury model. We believe that each of these models is applicable to cases with different relative rates of the internal relaxation processes of the material and of loading. To our knowledge, earlier studies of fracture or other breakdown phenomena do not take these different rates into account[18]. We calculate the stresses in a very simplified manner, allowing for the cancellation of the crack-microcrack interaction. This makes it possible to separate the contribution to the R-curve behavior from different sources: energy dissipation due to microcrack formation and microcrack shielding. The R-curve is also evaluated using two different methods as these may lead to slightly different R-curve behavior[19,20]. In the next section we define the different models, stating the rate regimes for which we believe they are relevant. In section III, the results for the different models with several random distributions for the microcrack formation stresses are presented. We discuss the significance of the results in section IV, and identify the conditions under which a rising R-curve should be expected. We then give a brief summary of the study in the final section.

II. MODEL

We begin with a two dimensional intact material lying in the xy-plane in which a semi-infinite crack on the negative x-axis is initially inserted. The material contains regions in which a microcrack may potentially be formed. For simplicity, we assume that these potential microcracks are located in a regular manner as the bonds of a square lattice. The length of a bond defines the length scale, which is equivalent to the typical microcrack size. Our simplification amounts to neglecting the variations in the length of the microcracks that may be formed and to assuming only two possible directions for the microcracks. Furthermore, since two neighboring microcracks are in contact, the model allows for coalescence of individual microcracks among themselves or with the main crack.

We model the evolution of the cracking process in the material in the following manner: The material is placed under a uniaxial tension in the y-direction applied at infinity. The stress distribution in the material is then mainly governed by the singularity at the tip of the long crack. For this so-called Mode I, the stresses at any point in the vicinity of the crack is given by[21]

$$\sigma_{yy}(r,\theta) = \frac{K_I}{\sqrt{2\pi r}} \cos\frac{\theta}{2}\left(1+\sin\frac{\theta}{2}\sin\frac{3\theta}{2}\right)$$

$$\sigma_{xx}(r,\theta) = \frac{K_I}{\sqrt{2\pi r}} \cos\frac{\theta}{2}\left(1-\sin\frac{\theta}{2}\sin\frac{3\theta}{2}\right) \qquad (2)$$

$$\sigma_{xy}(r,\theta) = \frac{K_I}{\sqrt{2\pi r}} \cos\frac{\theta}{2}\sin\frac{\theta}{2}\cos\frac{3\theta}{2} \ .$$

Here (r,θ) are the polar coordinates of a point in a coordinate system centered on the crack tip. The stress intensity K_I is related to the external stress σ^∞ and to the crack length a as $K_I = \sigma^\infty\sqrt{a}$. If microcracking has already occurred, the stress intensity may be modified due to the screening by the microcracks, as will be explained below. Each bond in the lattice has a critical stress such that when the stress on the bond exceeds

that critical stress, a microcrack is irreversibly formed. The critical stresses are chosen randomly from a given distribution. Initially we start with a small external stress and increase it until microcracking starts to occur. The exact rules by which the microcracks form will be given below. During the course of the simulation, some of the microcracks join the main crack, causing it to extend to positions with positive x. We monitor the instantaneous position of the crack tip, given by the point with the largest value of the x-coordinate. That point is used as the origin of the coordinate system in the calculation of the new stress distribution. However, even when that tip position is not on the x-axis, the overall direction of the crack is still taken to be horizontal, since the initial crack was assumed to be semi-infinite in that direction. This assumption results in the crack growing roughly in the horizontal direction, with slight fluctuations in the vertical.

At a given stage of the simulation, the material contains several isolated microcracks and clusters of microcracks that are not linked to the main crack. Their presence alters the stress distribution in the material. In particular, the stress intensity at the tip of the main crack is changed. Kachanov[22] has found that the interaction between a macrocrack and one or more microcracks is extremely dependent, both qualitatively and quantitatively, on their relative configuration. The stress intensity at the crack tip may be enhanced or reduced depending upon the configuration. However, it is found that reduction is more dominant, due to the shielding of the external stress by the microcracks. He found that with a pair of microcracks that have the same orientation as the main crack and are symetrically located above and below the tip of the horizontal crack (with the direction of the uniaxial stress being vertical) the stress intensity at the crack tip is shielded. The stress intensity vanishes rapidly with decreasing distance between the main crack and the microcracks (Fig. 3b in Ref. 22). We take crack-microcrack interaction into account only for this type of configuration. In our lattice representation, this includes all the horizontal microcracks whose either tip has the same x-coordinate as the macrocrack. Since no closed

form for the dependence of this interaction on the crack-microcrack separation is known, we assume that the reduction in the stress intensity factor at the tip of the macrocrack is given by

$$\frac{K_I(\alpha)}{K_I(0)} = 1 - \frac{3\alpha}{\pi^2} \sum_{\mu c}' \frac{1}{(y_{\mu c} - y_{tip})^2}. \tag{3}$$

$y_{\mu c}$ and y_{tip} are the y-coordinates of the microcrack labeled as μc and of the crack tip respectively. The sum is only on those microcracks that are in the configuration described above. α is a parameter that can be varied between 0 and 1 to control the relative importance of the shielding. The factor $3/\pi^2$ assures that for $\alpha = 1$ the stress intensity at the tip is completely shielded when an infinite stack of microcracks are formed above and below the tip. The additive property of Eq. (3) is certainly an oversimplification, but we hope that this simple form will capture the essential physics involved in the crack-microcrack interaction regarding the process of microcrack toughening.

Several models differening in the exact breaking rules of the potential microcracks are studied. Physically, these models differ in the relative magnitudes of the time scales involved in the three processes taking place simultaneously in the system: time of formation of microcracks in the overstressed regions ($\tau_{\mu c}$), relaxation time of the local stress distribution when the external stress is changed or when the crack tip moves (τ_l) and the inverse rate of increase of the external stress (τ_e).

MODEL A: For a given external stress, σ^∞, calculate the stresses on all the bonds on a lattice of linear size L. If σ_{yy} on a horizontal bond, or σ_{xx} on a vertical one is above the critical stress assigned to that bond, the bond is broken (a microcrack is formed there). The connectivities of the microcracks are established and the new crack tip is identified. The tip is the point on the main crack with the highest value of x-coordinate. The stress level is increased by a prespecified amount and the stress distribution in the material is calculated again with the new tip position. The process is continued until the crack tip reaches a boundary of the lattice. We think that this model is appropriate for the case of

very fast loading rates in which $\tau_e < \tau_{\mu c} < \tau_l$. Although for most brittle elastic materials at room temperature these conditions are not satisfied, viscoelastic materials such as polymeric materials or metals and ceramics at high temperatures are possible candidates for this model[12].

MODEL B: This is similar to Model A except that if the tip position changes beacuse of microcrack coalescence, stress distribution is calculated again without raising the external stress level. This is repeated until the position of the crack tip does not change any further. Only then is the external stress level increased. This model is therefore appropriate when the local stresses relax more rapidly than the rate of increase of the external stress but more slowly than the formation of a microcrack ($\tau_{\mu c} < \tau_l < \tau_e$).

MODEL C: After identifying the bonds on which the stress is above the critical stress (as in Models A and B) only the bond with the largest excess stress is broken. If this does not change the crack tip position, the bond with the next largest excess stress is broken. If a microcrack formed changes the position of the tip, the new stress distribution is calculated and the bond with the largest excess stress is broken. This model is relevant when the relaxation time of the local stresses is shorter than the time of formation of a microcrack, which in turn is shorter than inverse rate of increase of the external stress, $\tau_l < \tau_{\mu c} < \tau_e$.

III. RESULTS

During the course of the simulations, we monitor the number of microcracks formed (N) and the increase in the length of the macrocrack (Δa) as a function of the external stress (or equivalently of the nominal stress intensity factor, K_I). Using these data, we estimate the resistance to fracture using two different commonly accepted[12,23] measures of that property. The first measure is the rate of change of the excess surface energy of the system with increasing crack length. In our system, the excess surface energy is due to the microcracks formed, so that the resistance, R is given by $R = 2\gamma dN/da$. Here γ is the surface energy density. For ideally brittle materials, the new surfaces formed are those at the tip of the crack and this definition leads to a constant value of $R = 2\gamma$, independent of crack length. The other measure of R is based upon the assumption of linear elastic behavior in the material. In this case, $R \propto K_I^2$, with the proportionality constant being a geometry dependent combination of the Young's modulus and Poisson's ratio[12]. These two measures are equivalent for brittle fracture; however, some toughening mechanisms are found to lead to qualitatively different behavior for these two definitions[19]. We expect similar discrepancies with the microcracking mechanism and thus plot both measures of resistance.

Fig. 1 shows examples of the crack structures generated by the three models when the macrocrack traversed a square lattice of linear size 60 lattice units. The initial tip of the macrocrack is on the leftmost bond of the lattice. In all the three examples shown, the effects of the microcrack shielding is ignored ($\alpha = 0$). The critical stresses are taken from a Weibull distribution[24],

$$\Pr(\sigma_c < \sigma) = 1 - \exp\left[-(\sigma/\sigma_0)^m\right], \tag{4}$$

where the left hand side denotes the probability that the critical stress of a potential microcrack will be less than σ. σ_0 and m are called the scale and shape factors respectively.

This distribution has widely been used in analyzing breakdown phenomena[25,26]. In the simulations, we have used $\sigma_0 = 1.0$ (thereby measuring all stresses in units of σ_0) and $m = 5$. One observes qualitatively different pictures in the three cases shown. In the picture corresponding to model A, we find a highly branched macrocrack (the cluster of cracks that connects the two opposite sides of the lattice). The macrocrack is surrounded by a cloud of microcracks, whose width seems to increase in the direction of the propagation of the macrocrack. The model B macrocrack is less branched and the microcrack cloud around it seems to be narrower and of constant thickness. The macrocrack resulting from model C simulation is topologically almost linear, with practically no branching. There are very few isolated microcracks around the main crack.

We show in Fig. 2 the nominal stress intensity as a function of the crack length for the three simulations pictured in Fig. 1. The stress intensity, K_I, is measured in units of $\sigma_0\sqrt{a}$, a being the original crack length. (We assume that during the whole simulation the condition $\Delta a \ll a$ prevails.) The curve for the model A simulation exhibits a monotonic increase, with no tendency to stabilize. In the other two models, the nominal stress intensity needed to propagate the cracks seems to saturate at a stress intensity of order unity. The final stress intensity needed in the model A simulation is about 1.7 (in units of $\sigma_0\sqrt{a}$), considerably larger than this asymptotic stress intensity. The different behavior is rooted in the make of the models: in model A each stress level operates only once while in models B and C the same stress keeps forming new microcracks. In all three models, there is practically no crack growth below a stress intensity of about 0.6, since the probability of having a potential microcrack whose critical stress is below $0.6\sigma_0$ (cf. Eq. (2)) is very small.

We show in Fig. 3 the total number of microcracks formed as a function of the increase in the length of the macrocrack. Again, the result for model A is qualitatively different from the other two models. While for models B and C, N increases roughly linearly (constant

fracture resistance), the increase in model A seems to be with a power larger than 1, corresponding to an increasing R-curve. We shall make a more quantitative comparison of this feature later on.

Since the results shown in Figs. 2 and 3 seem to have some noise, reflecting the stochastic nature of the lattice (random distribution of critical stresses), it is appealing to simulate a large number of lattices, each corresponding to a different realization of the distribution of the critical stresses, in order to obtain smooth results which can be better analyzed. We simulated 200 different realizations of the three models described above with the same parameters of the Weibull distribution. For each value of the crack length, we averaged the corresponding values of N and nominal stress intensity, K_I. Fig. 4 shows the average K_I as a function of Δa of the main crack. The stress intensity needed to sustain crack growth is found to grow rather significantly for model A, but is almost saturated for models B and C. In Fig. 5 we show N as a function of the crack length increment. The inserts in Fig. 5 show the same dependence on a double logarithmic plot. For model A, the average slope in the range $5 < \Delta a < 60$ is about 1.4, while for the other two models, the slope is about 1. This corresponds to a flat R-curve for models B and C and to an R-curve that is approximated as $R \propto \Delta a^{0.4}$ for model A.

So far the results have been for the case in which the screening, as defined in Eq. (3), is ignored. Would they be qualitatively different for non-zero values of the screening parameter α? In order to answer this question, we again simulated the three models with the same Weibull distribution, using $\alpha = 0.6$. For model A, the same qualitative behavior is found, with slightly more microcracks around the main crack. Also a slightly higher stress intensity was needed to cause the same crack elongation. This indicates additional toughening due to microcrack shielding, although the same $R \propto \Delta a^{0.4}$ is maintained. For model B, however, a qualitative change of behavior is observed. Fig. 6a shows N as a function of Δa. Using a double logarithmic plot, we find that the behavior is consistent

with $N \propto \Delta a^{1.2}$. Therefore, introduction of microcrack shielding changes the R-curve behavior of the material from a crack-length independent fracture resistance to one that increases with crack elongation. Furthermore, when α is increased to 0.9, we find an even steeper increase of the resistance to fracture; for this value of α, the exponent increases from 1.2 to about 1.4. For model C, the situation is qualitatively similar to the case with no microcrack shielding. Fig. 6b shows N as a function of Δa, while in the insert we present the local derivative of N. We see that the derivative is a slightly decreasing function of Δa. Note that this decrease should stop as $dN/d(\Delta a)$ reaches the value of 1 as at least one microcrack is needed to propagate the crack by one lattice unit.

Another interesting question is how the R-curve behavior is affected by the distribution of the critical stresses. The results presented so far have been for a Weibull distribution of critical stresses. We have repeated the simulations for models B and C for different distributions. In the extreme case in which all the potential microcracks have the same σ_c, we obtain in both models the result that the fracture is purely brittle; that is, the only microcrack formed is the one immediately ahead of the macrocrack and the crack propagates at the critical stress level. (In this case there is no randomness in the system and no averaging is needed.) This result is not surprising since the most stressed bond is always the one immediately in front of the crack. We also tried a uniform distribution in the range $\sigma_{c,min} < \sigma_c < \sigma_{c,max}$. We used $\sigma_{c,min} = 0.3$ and $\sigma_{c,max} = \sigma_{c,min} + 1$. In this case the results are similar to the ones obtained with Weibull distribution; an increasing R-curve behavior is observed in model B only when microcrack shielding is significant. Otherwise a constant resistance to fracture as a function of crack length is found. For model C, the resistance to fracture remained constant (or even decreased slightly for the quantity defined through $dN/d(\Delta a)$) with or without the microcrack shielding effect taken into account. For this model we also tried reducing $\sigma_{c,min}$ to 0. This presumably unrealistic limit allows for the formation of microcracks at arbitrarily large distances from the crack

tip. Probability distributions that have a non-zero value for vanishing strengths (or the analogous distribution variable in a different problem) are known to lead to significantly different critical behavior[27,28]. Even for this limiting distribution, we find no increasing R-curve behavior with model C, although both the number of microcracks formed and the nominal stress intensity at any crack length increment are larger than those observed with other distributions of the critical stresses.

IV. DISCUSSION

An important result of our simulation is the sensitivity of the R-curve behavior to the rate of loading relative to the internal relaxation processes taking place. When the loading rate is higher than the rate of stress redistibution in the material or the inverse time of formation of a single microcrack, we find an R-curve which exhibits a significant increase of the resistance with increasing crack length (Figs. 4a and 5a). The typical values of the work of fracture (or of the nominal stress intensity) observed in this case (Model A) are appreciably higher than those found in other models corresponding to slower rates of loading. Such high rates of external loading are hard to achieve unless viscoelastic effects that slow down the internal relaxations are present. Indeed, the work of fracture in a typical polymeric material, PMMA, which exhibits viscoelastic behavior, is found to increase linearly with the crack velocity[29]. However, the fracture mechanism in this case is through craze growth governed by secondary molecular processes and not by microcracking, so that the present model is not appropriate for such materials. To our knowledge, the strain rate dependence of the R-curve in a material with an established microcrack toughening mechanism has not been investigated in the high strain rate limit. As our model indicates an enhanced resistance to fracture at high rates of loading, it would be interesting to perform an experiment to check this prediction.

The other two models that we have defined, models B and C, which correspond to the

case in which the external loading is slower than the internal processes, seem to be more relevant to microcracking materials, which are predominantly elastic rather than viscoelastic. The main difference between the two models is the relative rates of the two internal relaxation processes: namely, the relaxation of the local stresses and the formation of a single microcrack. Model B is appropriate when the formation of microcracks takes place on a shorter time scale than the local stress relaxation. It is interesting to note that the model suggested by Hoagland and Embury[16] also corresponds to the time regime implicit in model B, although no mention of time scales is made in their work. The reason for this observation is that in their model, as in our model B, all potential microcrack sites on which the (self-consistently determined) stress exceeds the critical stress are allowed to become microcracks. This implicitly assumes that the local stresses do not react fast enough to the formation of microcracks, since otherwise the formation of a single microcrack (the one with the largest excess stress, as in our model C) would change the stress field in the sample.

We should note that of the three models only model C is really quasi-static since the order in which microcracks are formed is independent of the increment of the external stress. In the simulations we performed we increased the nominal stress intensity in steps of 0.05. For some cases we repeated the simulations with half the step size and obtained identical R-curves for model C. As one can expect, model A was especially sensitive to this step size. Both measures of the crack resistance exhibited a decrease with decreasing step size; the qualitative behavior, however, did not change. The nominal stress needed to sustain crack growth increased as previously. The number of microcracks formed at crack length Δa grew also proportionally to $\Delta a^{0.4}$ as with the larger step size. Although not inherently quasi-static, model B exhibited no detectable difference between the R-curves obtained with both step sizes. This shows that by allowing the stresses to relax after the formation of microcracks and before increasing the nominal stress intensity, we compensate

for the formation of more than one microcrack simultaneously and the model exhibits a quasi-static behavior.

Results for our model B show that an increasing R-curve is observed only when the critical stresses of the potential microcracks has some random distribution (Figs. 4b and 5b). When all the critical stresses have the same value with no dispersion, we obtain a constant fracture energy, given by the energy of formation of a single microcrack. If we use the alternative definition of the fracture resistance which is related to the nominal stress intensity, this case corresponds to an unstable crack propogation at a constant stress intensity, after a transient rise. When the critical stresses have some distribution, then the results depend upon the intensity of interaction between the macrocrack and the microcracks. If we ignore the crack-microcrack interactions, the number of microcracks formed to increase the crack length by an amount Δa is found to grow linearly with Δa, indicating a constant resistance to fracture. The nominal stress intensity to sustain that crack propagation, on the other hand, shows a mild increase with crack length. This discrepancy between the two definitions of the resistance to fracture has already been found[19] in ceramic materials undergoing what is termed 'transformation toughening'[4]. This is a toughening mechanism due to the transformation of zirconia particles dispersed in some ceramic materials like Al_2O_3 or Si_3N_4 from a tetragonal symmetry to monoclinic symmetry under the stress field of the macrocrack. The transformation process acts as an additional dissipative energy sink, thus increasing the energy input needed to propagate the main crack. Rose and Swain[19] found that the two definitions of the resistance show a *qualitatively* different transient behavior. the quantity defined through energy decreases to a steady state value, while the stress intensity based definition increases to the same value. In our simulations, the discrepancy is less dramatic but still noticeble. When the crack-microcrack interaction is taken into account, the number of microcracks formed increases more rapidly than the crack length increment, giving an increasing resistance to fracture.

The increase in the resistance is found to be higher the stronger microcrack the shielding defined in Eq. (3).

In the regime of time scales for which model C is appropriate, we find that microcracking does not result in a rising R-curve behavior, even when microcrack shielding is taken into account and a wide distribution of critical stresses are present in the material (although the stress intensity as a function of the crack length exhibits a slight increase, as in model B.). This is a significant result as we think that model C is relevant to some realistic cases, since we expect the microcrack formation time to be comparable to or larger than the relaxation time of the local stress distribution around the macrocrack for elastic materials. To obtain a qualitiative estimate for these two time scales, let us note that in an elastic material, the local stress relaxation will propagate with the material sound velocity, which is of order $10^3\,\mathrm{m\,sec^{-1}}$. The stresses in a region of order, say, 1 cm will relax within a time of order $\tau_l \sim 10^{-5}\,\mathrm{sec}$. Using acoustic emission data on fracture in concrete[30,31], the duration of the microcrack formation process can be estimated to be $10^{-5}\,\mathrm{sec}$ or longer. This is the same order of magnitude as τ_l and model C may be relevant in some materials. Furthermore, several models proposed for some breakdown phenonema (electrical[26,32] as well as mechanical[33,34]) also assume this time regime. Our results indicate that in such cases, the resistance to fracture will be constant as a function of the crack length increment.

V. CONCLUSIONS

We have described three simple models of crack propagation through microcrack coalescence under uniaxial tensile loading. The models differ in the relative time scales of the physical processes that occur in the system. We find that when the rate of loading is faster than the internal relaxations in the system (microcrack formation and local stress relaxation following any change in the system), the microcracking material exhibits an increasing resistance to fracture with increasing crack length. We do not, however, expect this model to be relevant for microcracking elastic materials like ceramics since it is difficult to realize such high loading rates. When the time scale involved in local stress relaxation is shorter than the inverse rate of loading, but longer than the time of formation of a single microcrack, increasing fracture resistance behavior is observed only if the material has a distribution of critical stresses of potential microcracks and if there is substantial microcrack shielding. When the interaction between the crack and the microcracks are such that they tend to cancel[22], a brittle behavior with a constant resistance to fracture is observed. When the local stress relaxation is the fastest process, we find that microcracking does not lead to any toughening; that is, the resistance to fracture does not increase with increasing crack length.

In summary, this work has shown the importance of microcrack shielding to a rising R-curve. More and better data on shielding (both experimental and theoretical) will justify further computations along the lines proposed in this study.

Acknowledgements

Work sponsered in part by US Air Force Office of Scientific Research, Air Force System Command, USAF under Grant No. 89–0374. The US Government is authorized to reproduce and distribute reprints for Governmental purposes notwithstanding any copyright notation therein.

REFERENCES

1. A. A. Griffith, *Phil. Trans. R. Soc. A* 221, 163 (1920).

2. C. E. Inglis, *Trans. Insti. Naval Archit.* 55, 219 (1913).

3. G. R. Irwin, *Fracturing of Metals*, ASM, Cleveland, Ohio, 1948.

4. A. G. Evans and A. H. Heuer, *J. Am. Ceram. Soc.* 63, 241 (1980).

5. P. L. Swanson, C. J. Fairbanks, B. R. Lawn, Y.-W. Mai and B. J. Hockey, *J. Am. Ceram. Soc.* 70, 279 (1987).

6. Y.-W. Mai and B. R. Lawn, *J. Am. Ceram. Soc.* 70, 289 (1987).

7. R. G. Hoagland, A. R. Rosenfeld and G. T. Hahn, *Metall. Trans.* 3, 123 (1972).

8. A. Hillerborg, M. Madeer and P. E. Peterson, *Cem. Concr. Res.* 6, 773 (1976).

9. P. L. Swanson, in *Fracture Mechanics of Concrete*, Vol. 8, Eds. R. C. Bradt, A. G. Evans, D. P. H. Hasselman and F. F. Lange, Plenum, New York, 1986, p299.

10. R. Knehens and R. Steinbrech, *J. Mater. Sci. Lett.* 1, 327 (1982).

11. M. Rühle, N. Claussen and A. H. Heuer, *J. Am. Ceram. Soc.* 69, 195 (1986).

12. A. G. Atkins and Y.-W. Mai, *Elastic and Plastic Fracture*, Ellis Horwood Limited, Chichester, 1985.

13. H. L. Ewalds and R. J. H. Wanhill, *Fracture Mechanics*, Delftse U. M., London, 1984.

14. B. Budiansky, J. W. Hutchinson and J. C. Lambropoulos, *Int. J. Solids Structures* 19, 337 (1983).

15. A. G. Evans and K. T. Faber, *J. Am. Ceram. Soc.* 67, 255 (1984).

16. R. G. Hoagland and J. D. Embury, *J. Am. Ceram. Soc.* 63, 404 (1980).

17. G. D. Bowling, K. T. Faber and R. G. Hoagland, *J. Am. Ceram. Soc.* 70, 849 (1987).

18. An exception is the study by Khang *et al* [26] who perform their simulations on electrical breakdown of a random fuse system in a certain rate regime, but mention that the results can be different if a different rate regime is assumed.

19. L. R. F. Rose and M. V. Swain, *J. Am. Ceram. Soc.* 69, 203-207 (1986).

20. K. K. O. Bär, G. Kleist, H. Nickel and R. Spelthan, in *Euro-Ceramics*, Vol.3, Eds., G. de With, R. A. Terpstra, and R. Metselaar, Elsevier Applied Science, London, 1989, p242.

21. B. R. Lawn and T. R. Wilshaw, *Fracture of Brittle Solids*, Cambridge University Press, Cambridge, 1975.

22. M. Kachanov, *Int. J. Fracture*, 30, R65, 1986.

23. R. F. Cook, *Phys. Rev. B* 39, 2811 (1989).

24. W. Weibull, *Fatigue Testing and Analysis of Results*, Pergamon, New York, 1961.

25. R. F. Smalley, D. L. Turcotte and S. A. Solla, *J. Geophys. Res.* 90, 1894 (1985).

26. B. Khang, G. G. Batrouni, S. Redner, L. de Arcangelis and H. Herrmann, *Phys. Rev. B* 37, 7625 (1988).

27. P. M. Kogut and J. P. Straley, *J. Phys. C: Solid State Phys.* 12, 2151 (1979).

28. B. I. Halperin, S. Feng and P. N. Sen, *Phys. Rev. Lett.* 54, 2391 (1985).

29. A. G. Atkins, C. S. Lee and R. M. Caddell, *J. Mater. Sci.* 10, 1381 (1975).

30. U. Diederichs, U. Schneider and M. Terrien, in *Fracture Mechanics of Concrete*, F. H. Wittmann, Ed., Elsevier, Amsterdam, 1983, p157.

31. A. K. Maji, C. Ouyang and S. P. Shah, *J. Mater. Res.* 5, 206 (1990).

32. P. M. Duxbury, P. L. Leath and P. D. Beale, *Phys. Rev. B* 36, 367 (1987).

33. P. D. Beale and D. J. Srolovitz, *Phys. Rev. B* 37, 5500 (1988).

34. H. J. Herrmann, A. Hansen and S. Roux, *Phys. Rev. B* 39, 637 (1989).

FIGURE CAPTIONS

Figure 1. The macrocrack and the array of microcracks formed in the system when the macrocrack has traversed the lattice of linear size $L = 60$. (a) Model A, (b) Model B and (c) Model C. In all the cases a Weibull distribution of critical stresses with $\sigma_0 = 1.0$ and $m = 5$ was used. Crack-microcrack intéraction parameter is set to 0.

Figure 2. The nominal stress intensity, K_I, needed to increase the macrocrack length by Δa for the three structures shown in Fig. 1.

Figure 3. The total number of microcracks formed (including those that have joined the microcrack) in the three structures shown in Fig. 1, when the macrocrack length increased by Δa.

Figure 4. The average K_I as a function of crack length increment for (a) Model A, (b) Model B and (c) Model C. The average is over 200 realizations of a 60×60 lattice with a Weibull distribution of critical stresses, with $\sigma_0 = 1.0$ and $m = 5$. Crack-microcrack interaction parameter is set to 0.

Figure 5. The average number of microcracks formed as a function of crack length increment for (a) Model A, (b) Model B and (c) Model C. The average is over 200 realizations of a 60×60 lattice with a Weibull distribution of critical stresses, with $\sigma_0 = 1.0$ and $m = 5$. Crack-microcrack interaction parameter is set to 0. The inserts show the same dependence on a double logarithmic plot.

Figure 6. The average number of microcracks formed as a function of crack length increment for (a) Model B and (b) Model C. The average is over 200 realizations of a 60×60 lattice with a Weibull distribution of critical stresses, with $\sigma_0 = 1.0$ and $m = 5$. Crack-microcrack interaction parameter is set to 0.6. The insert in (b) is the local derivative.

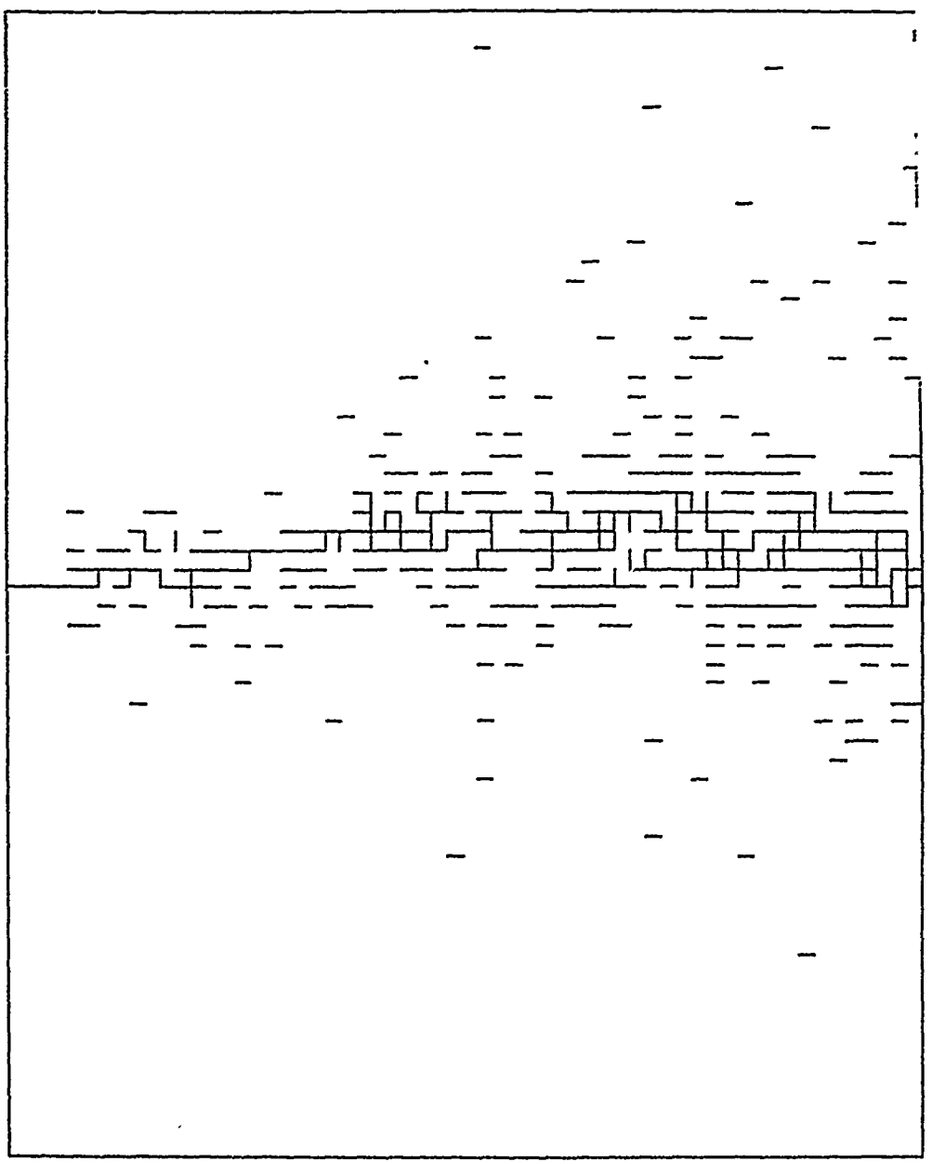

Fig 1a

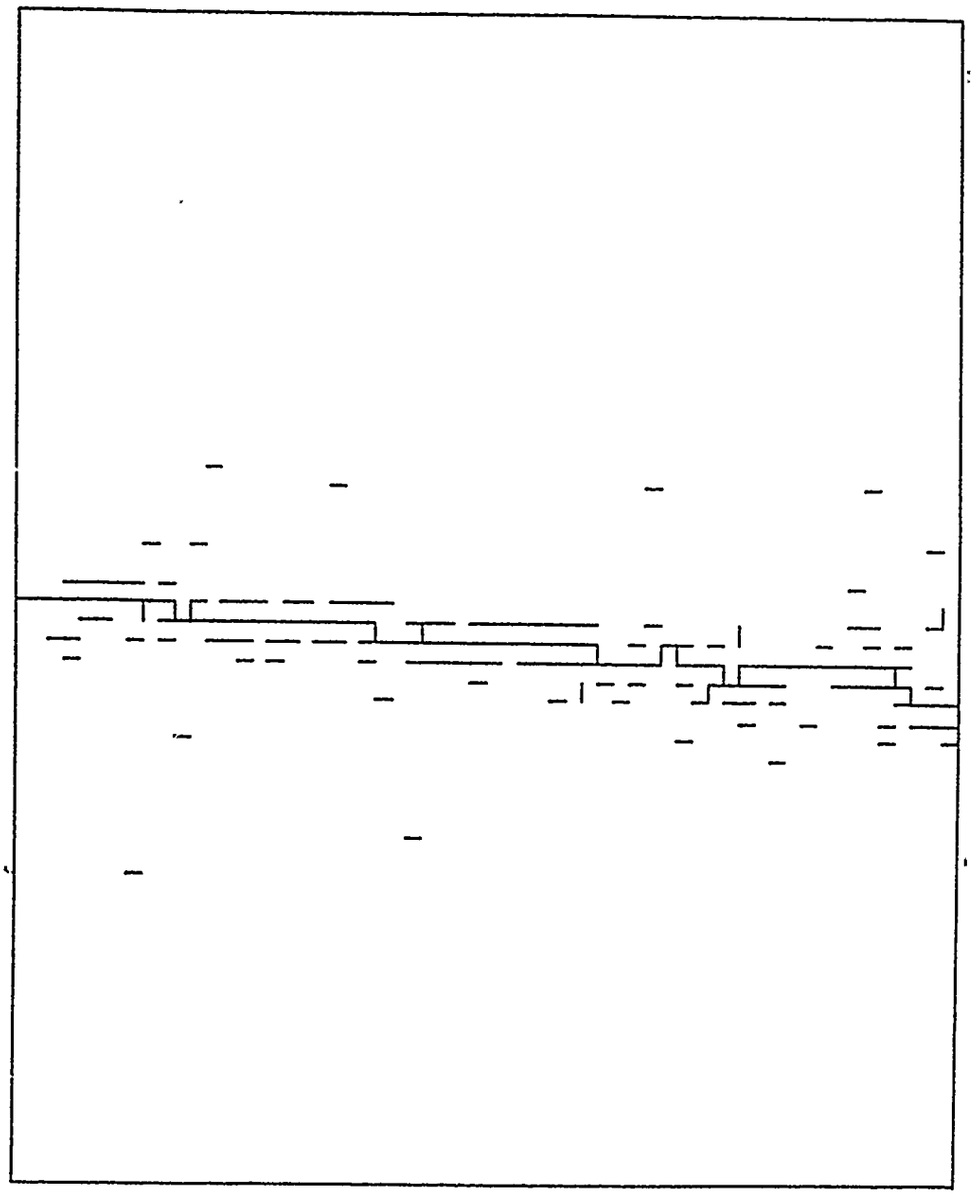

Fig. 15

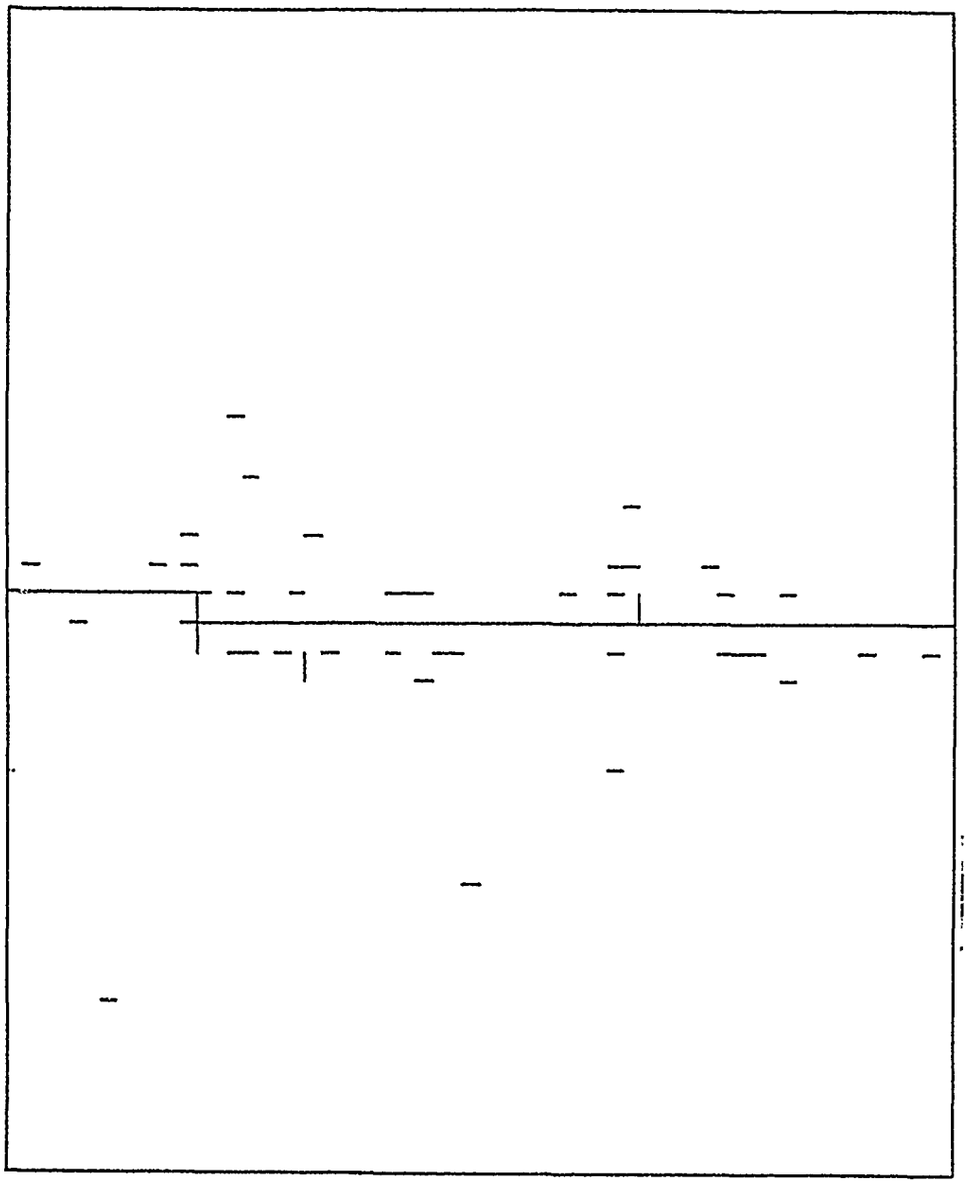

Fig. 1c

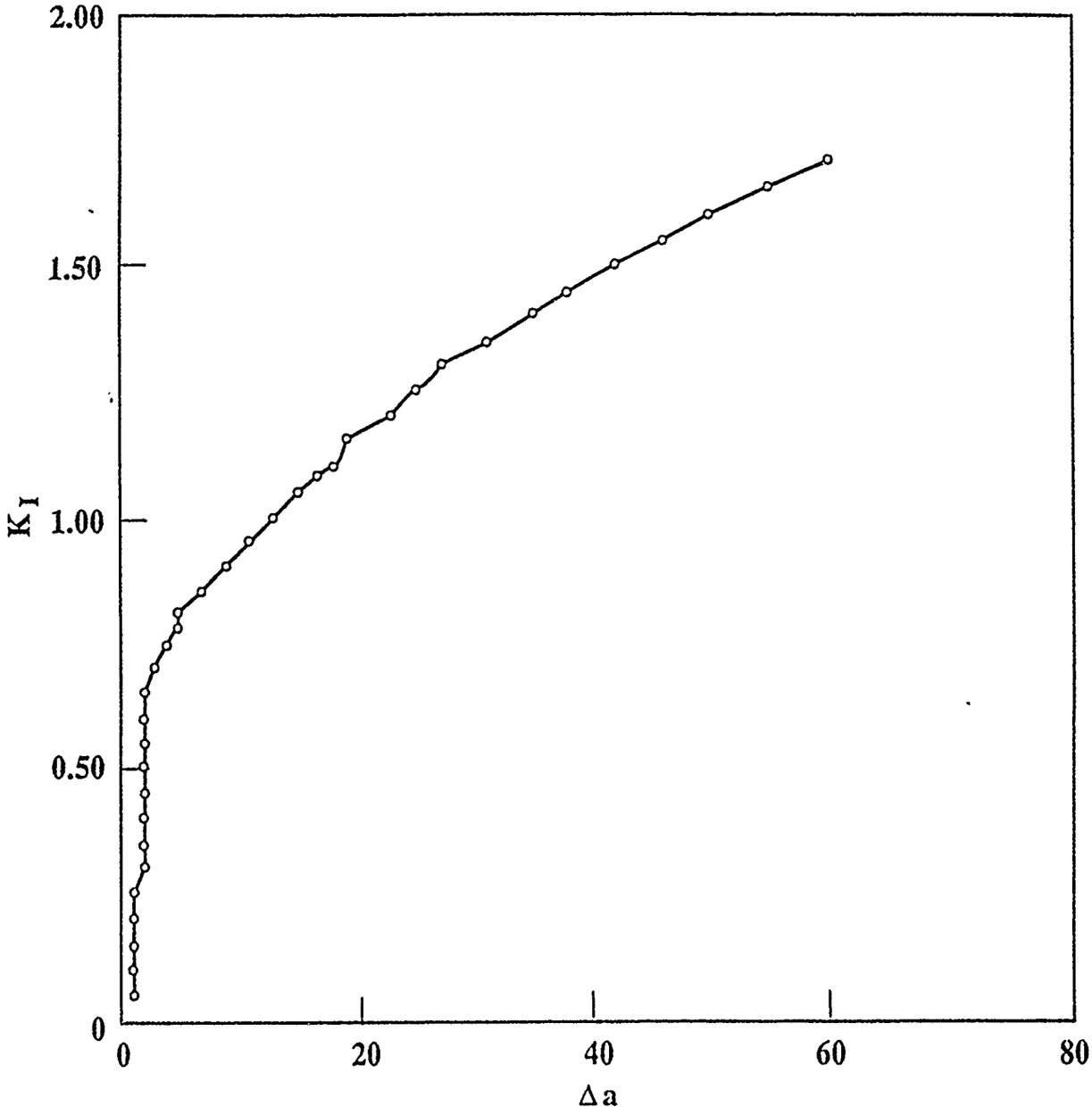

Fig. 2a

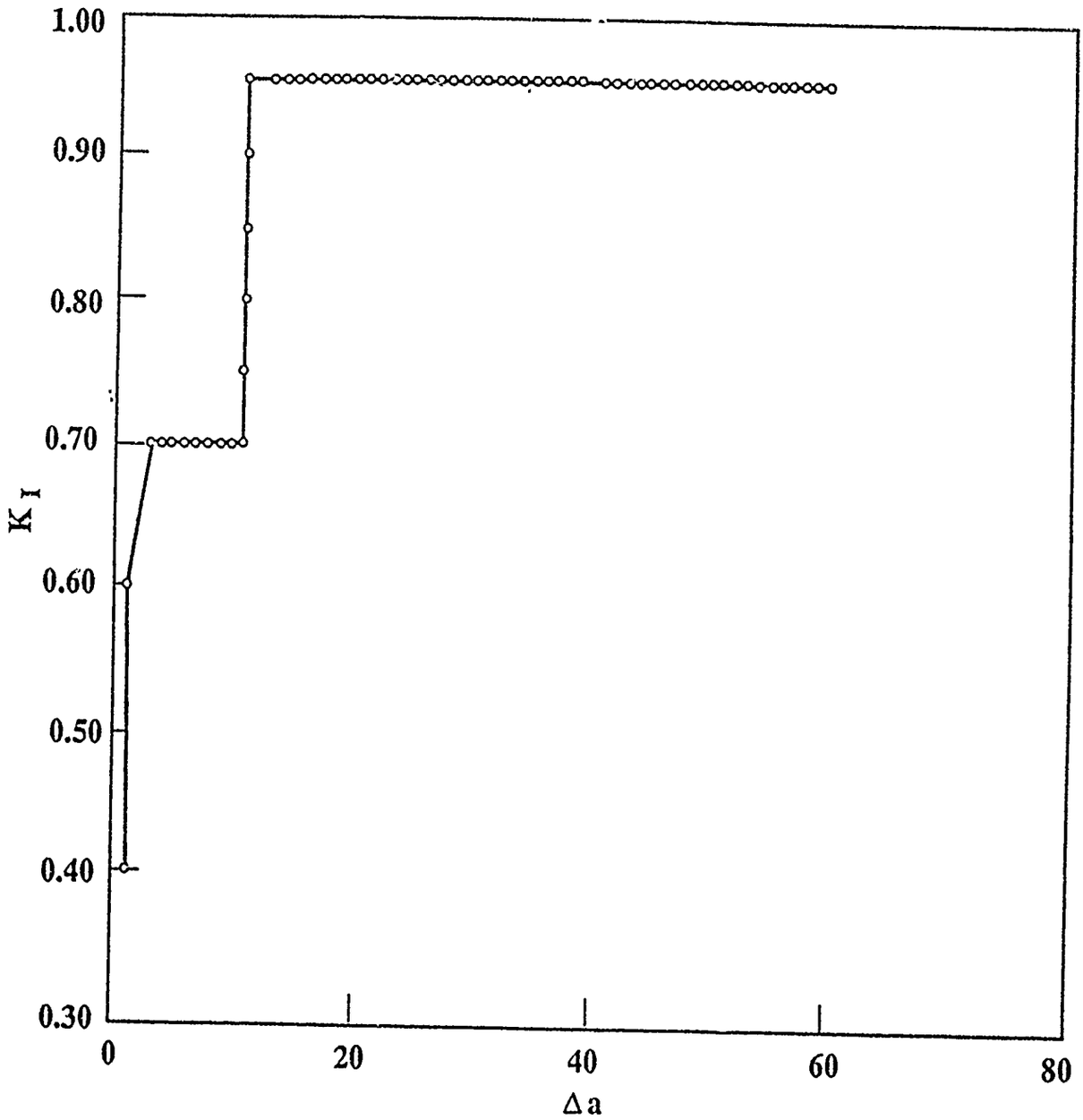

Fig. 2c

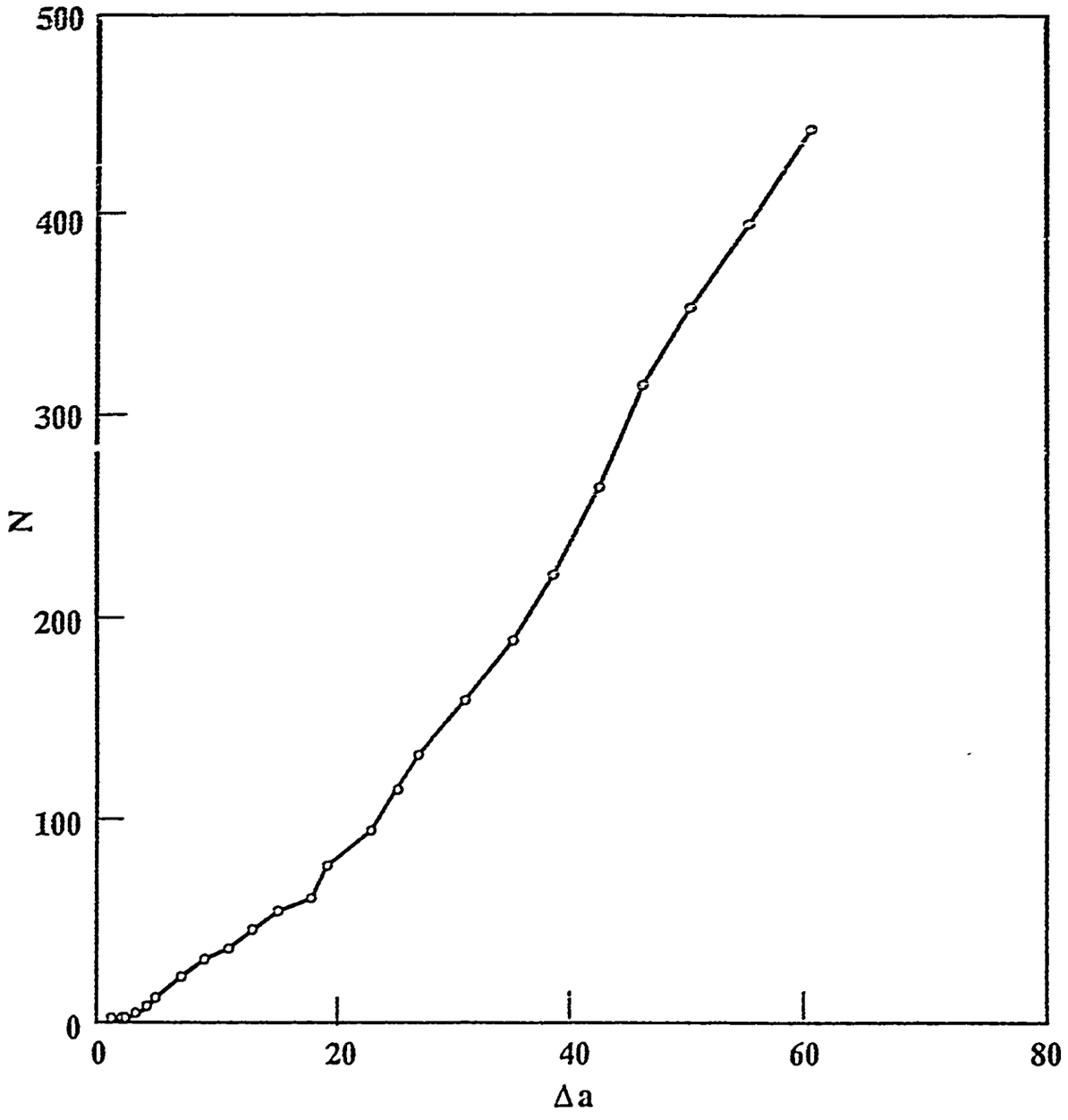

Fig. 3a

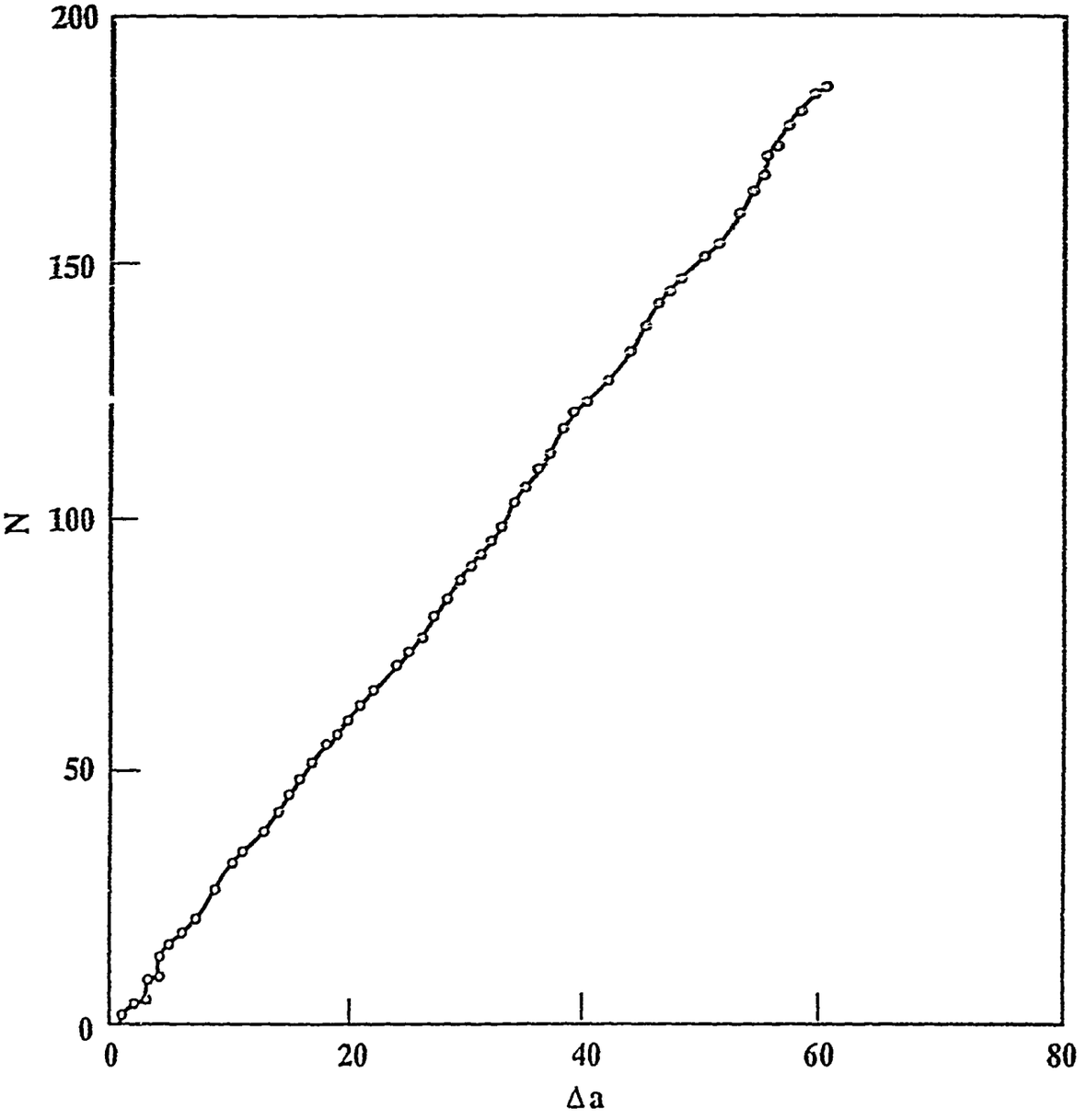

Fig. 3b

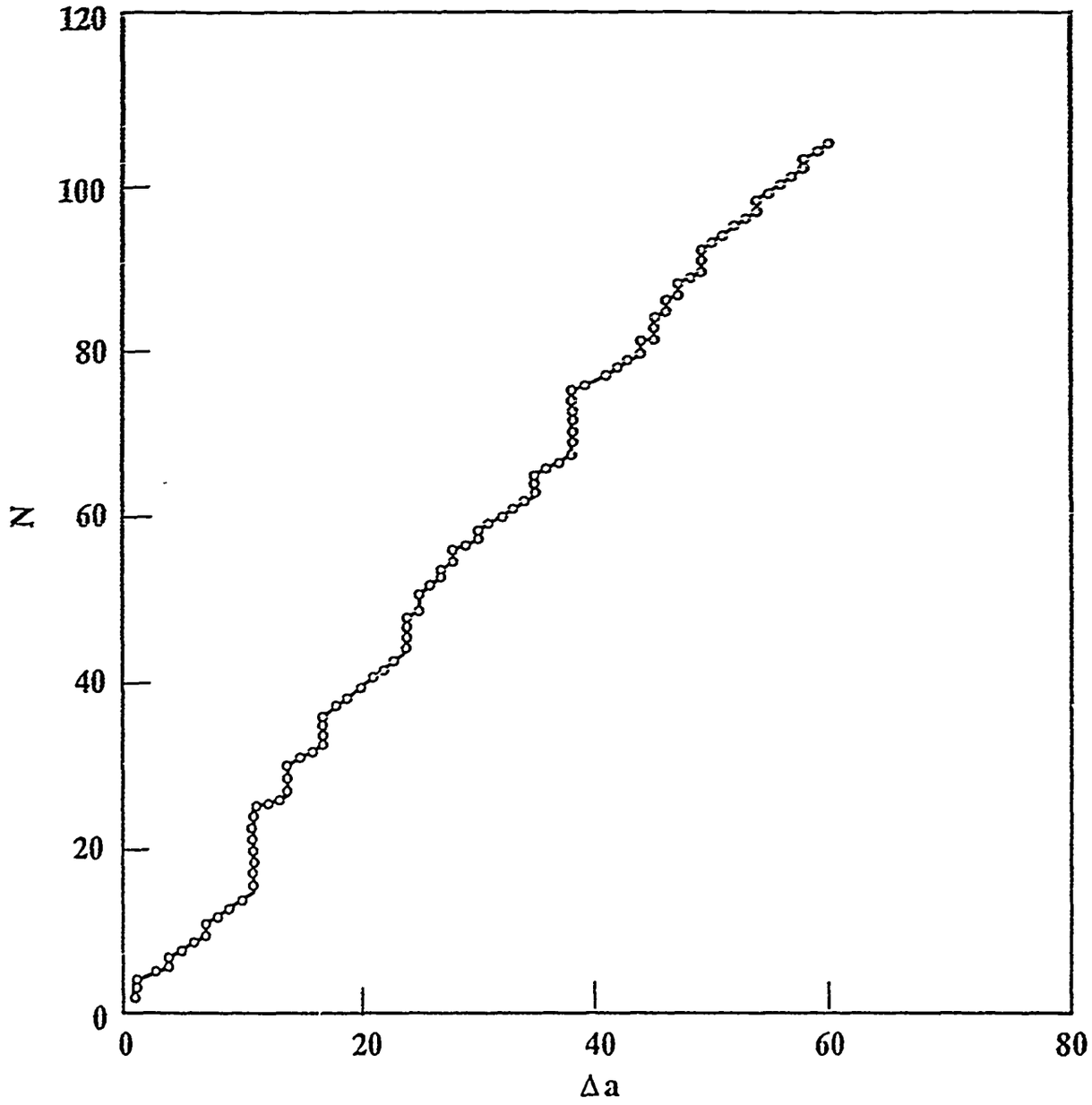

Fig. 3c

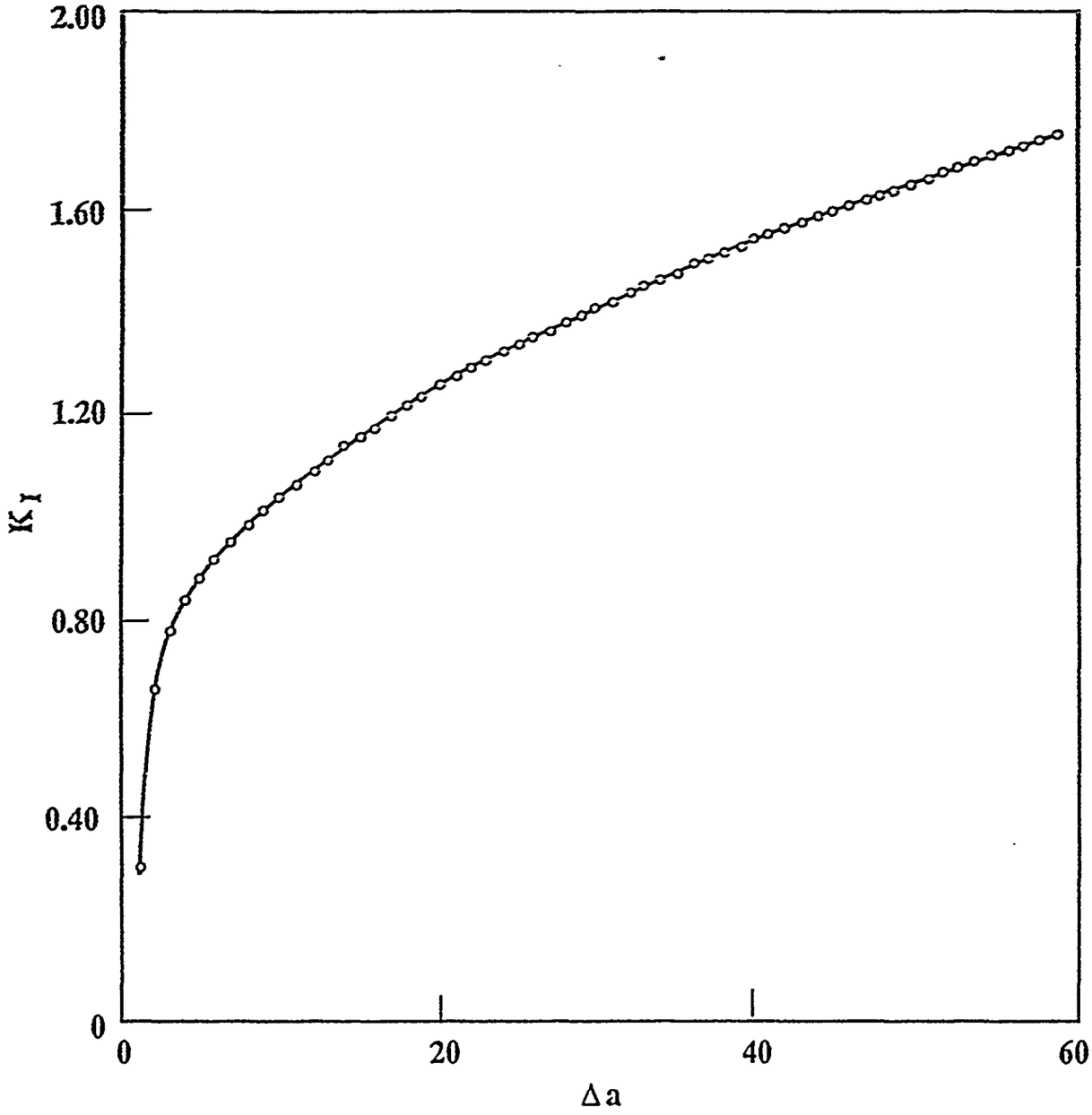

Fig. 4a

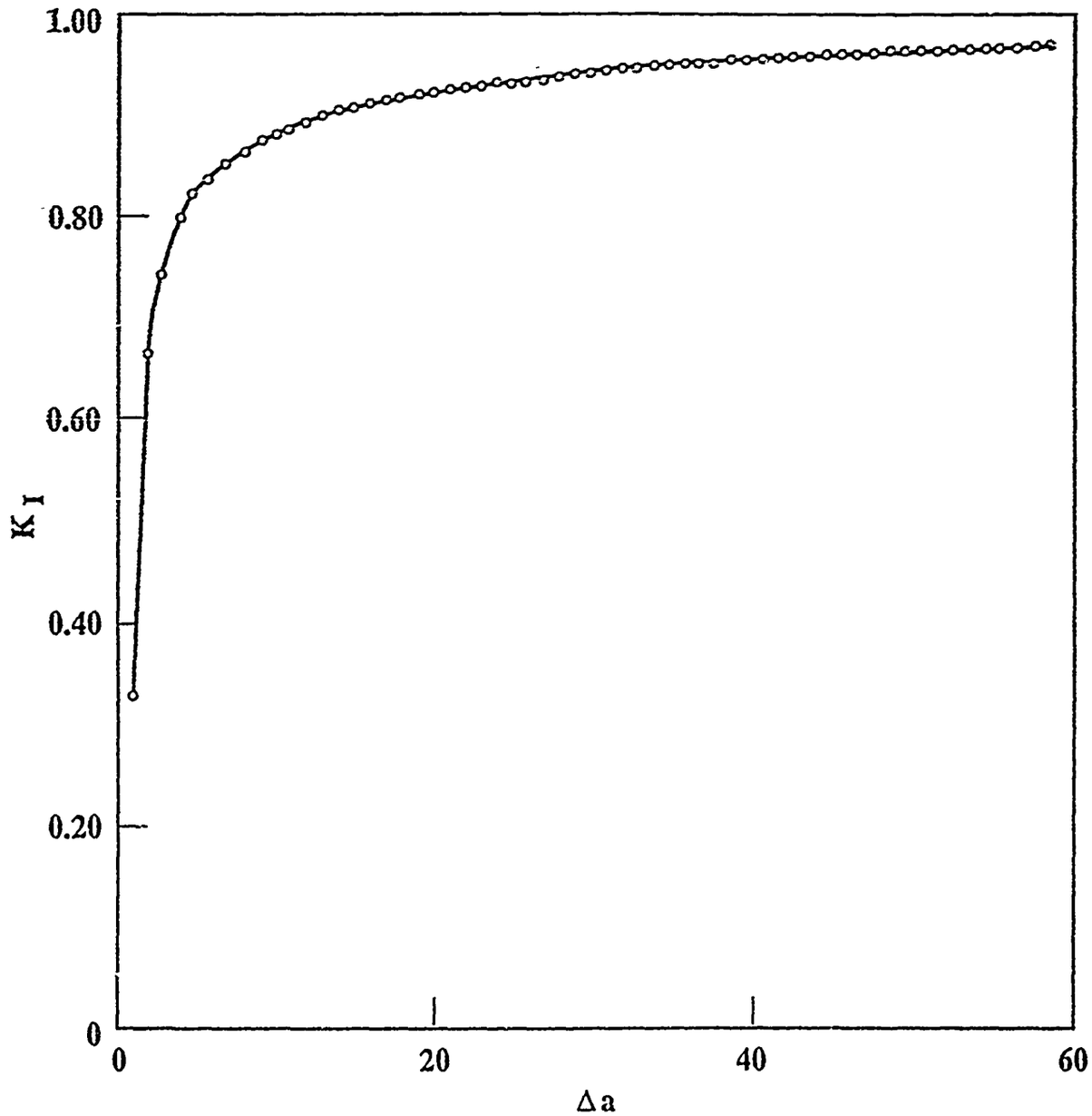

Fig. 46

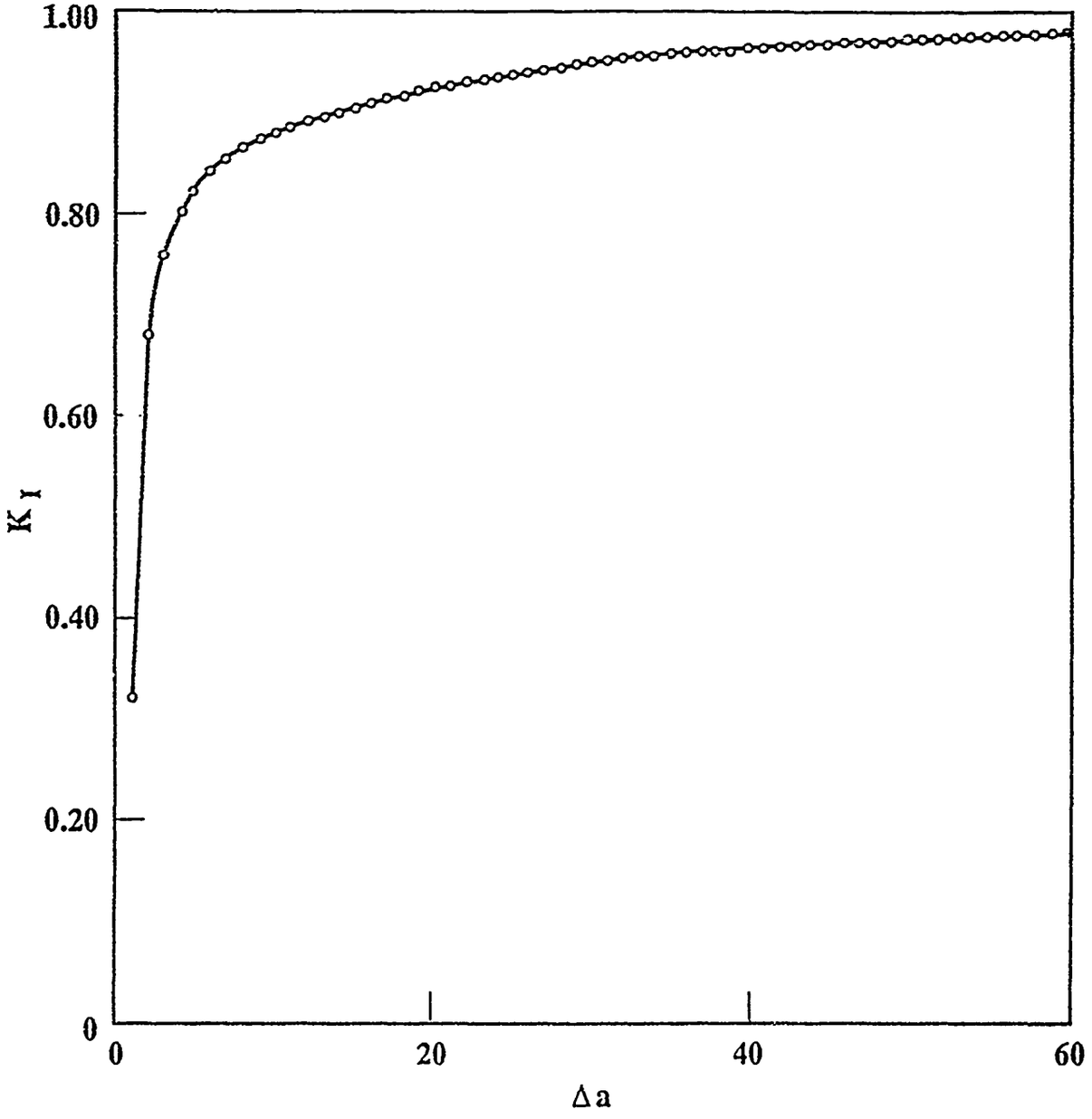

Fig: 4c

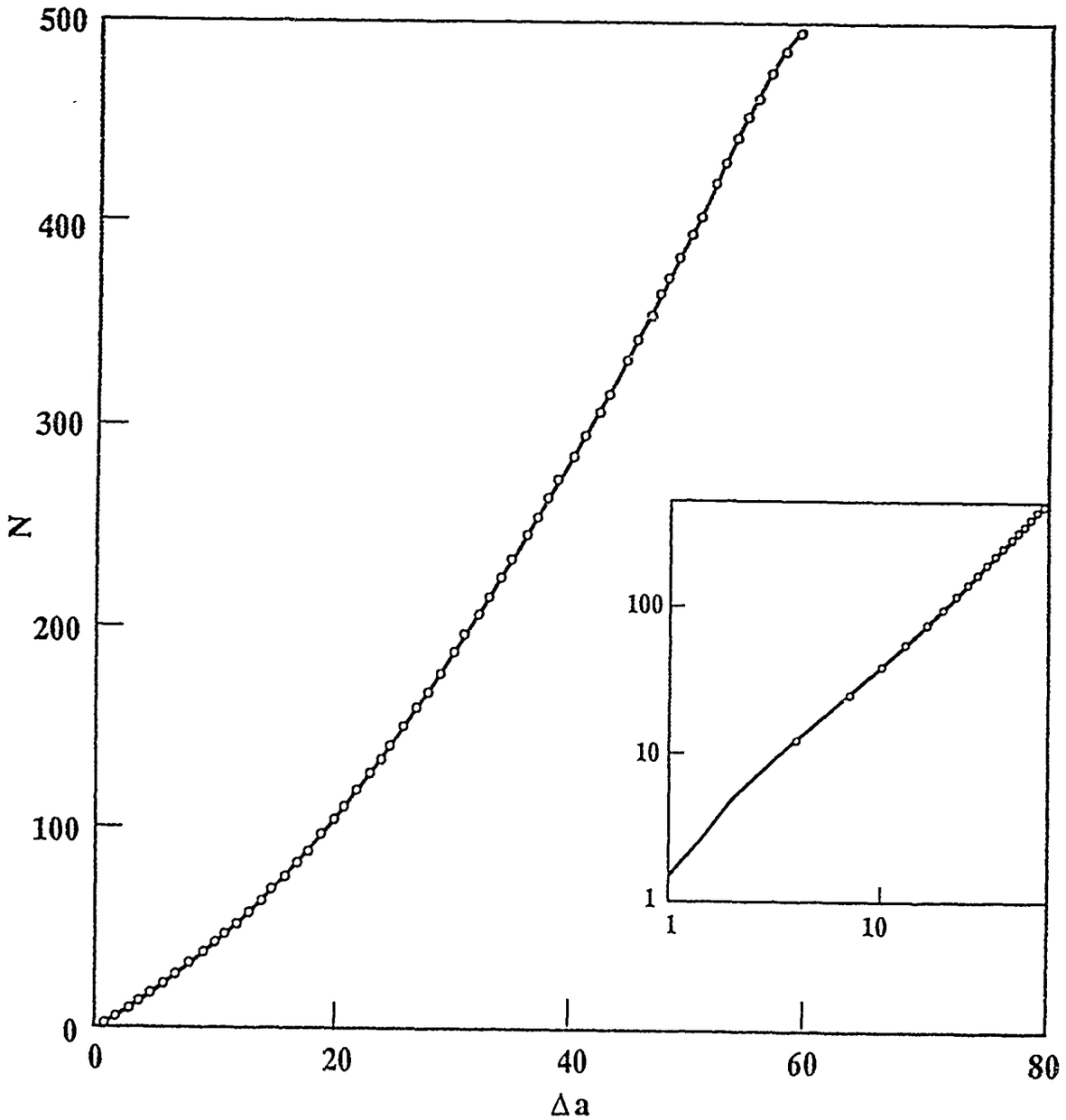

Fig. 5a

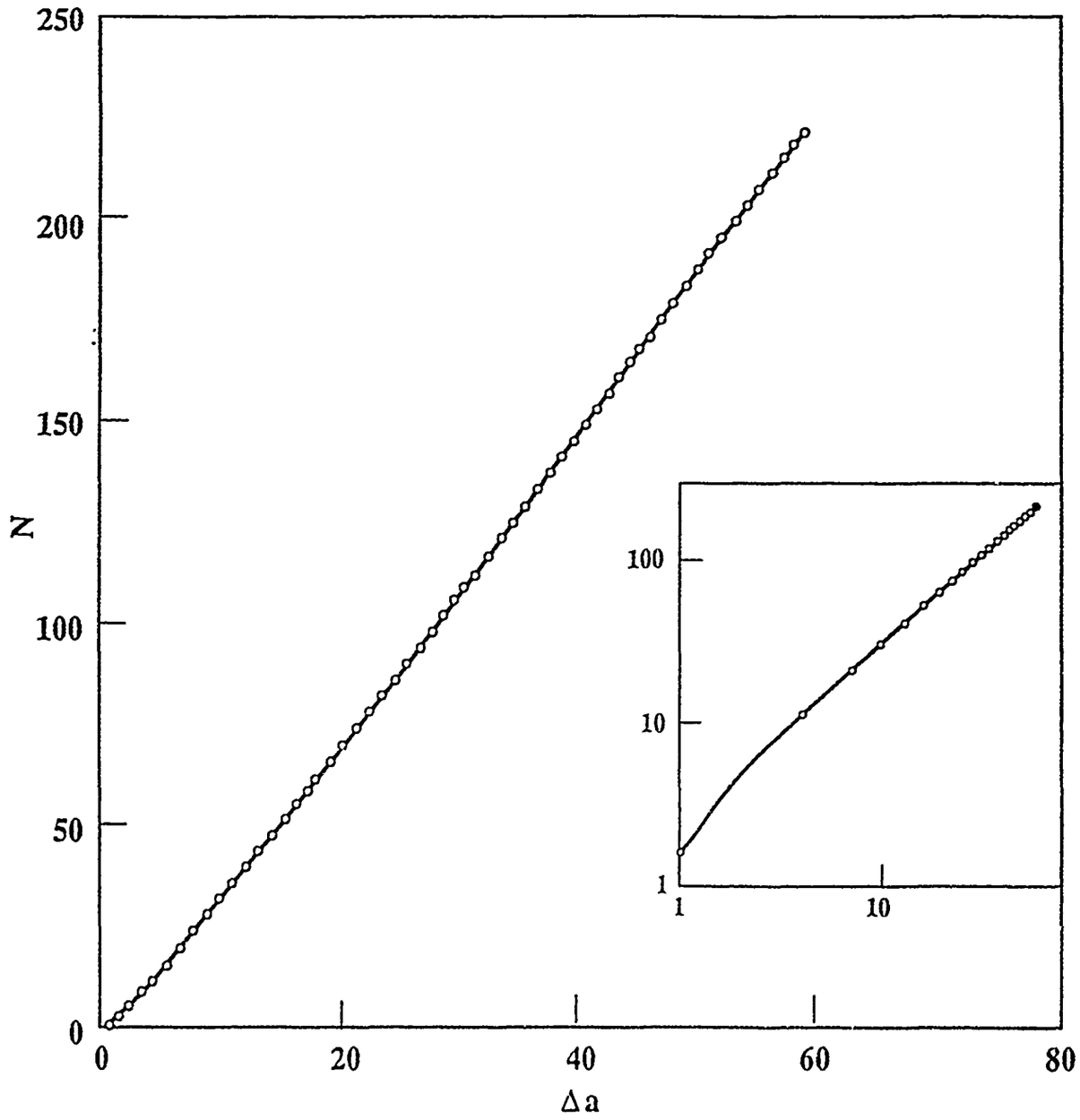

Fig. 5b

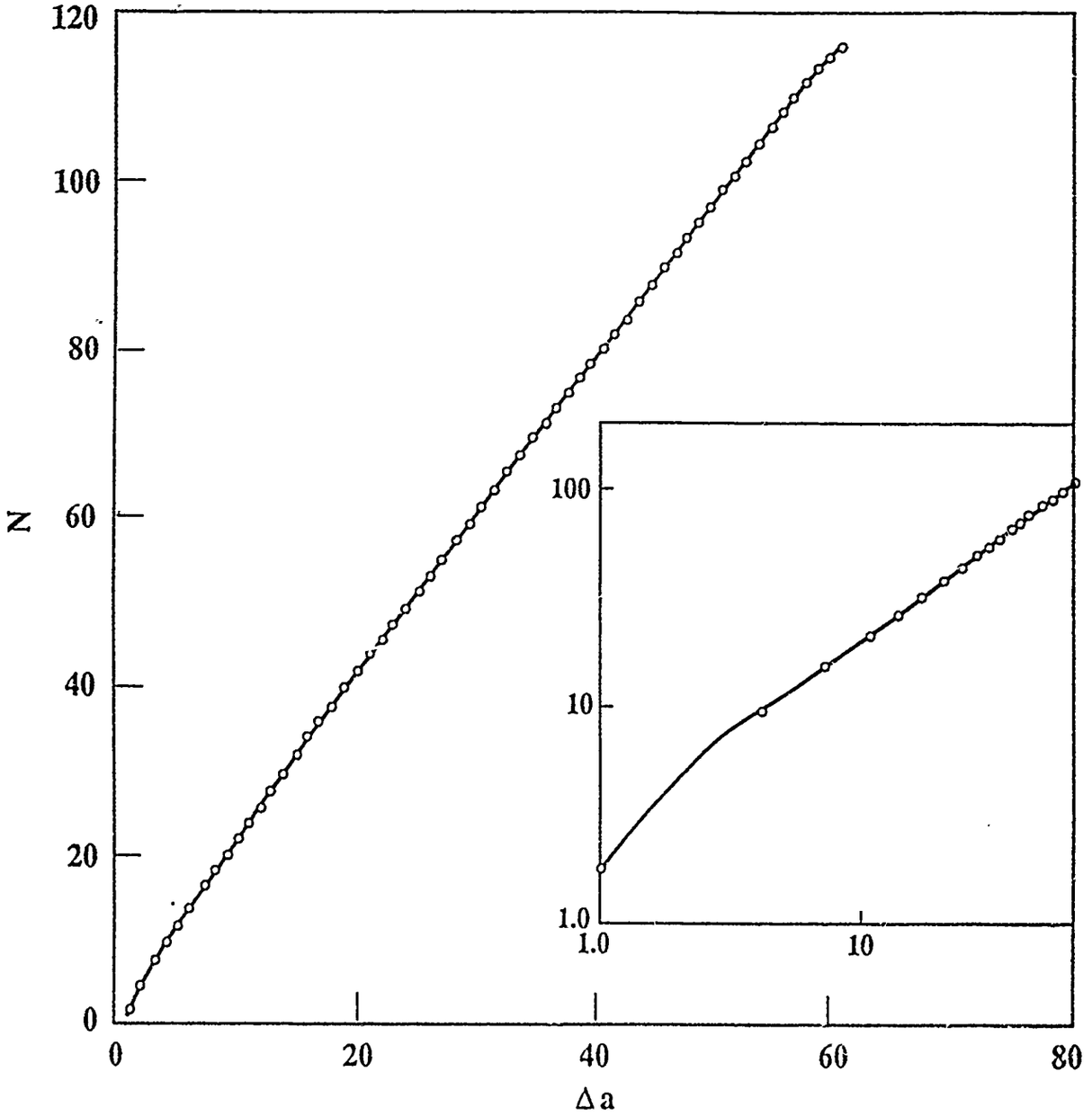

Fig. 5a

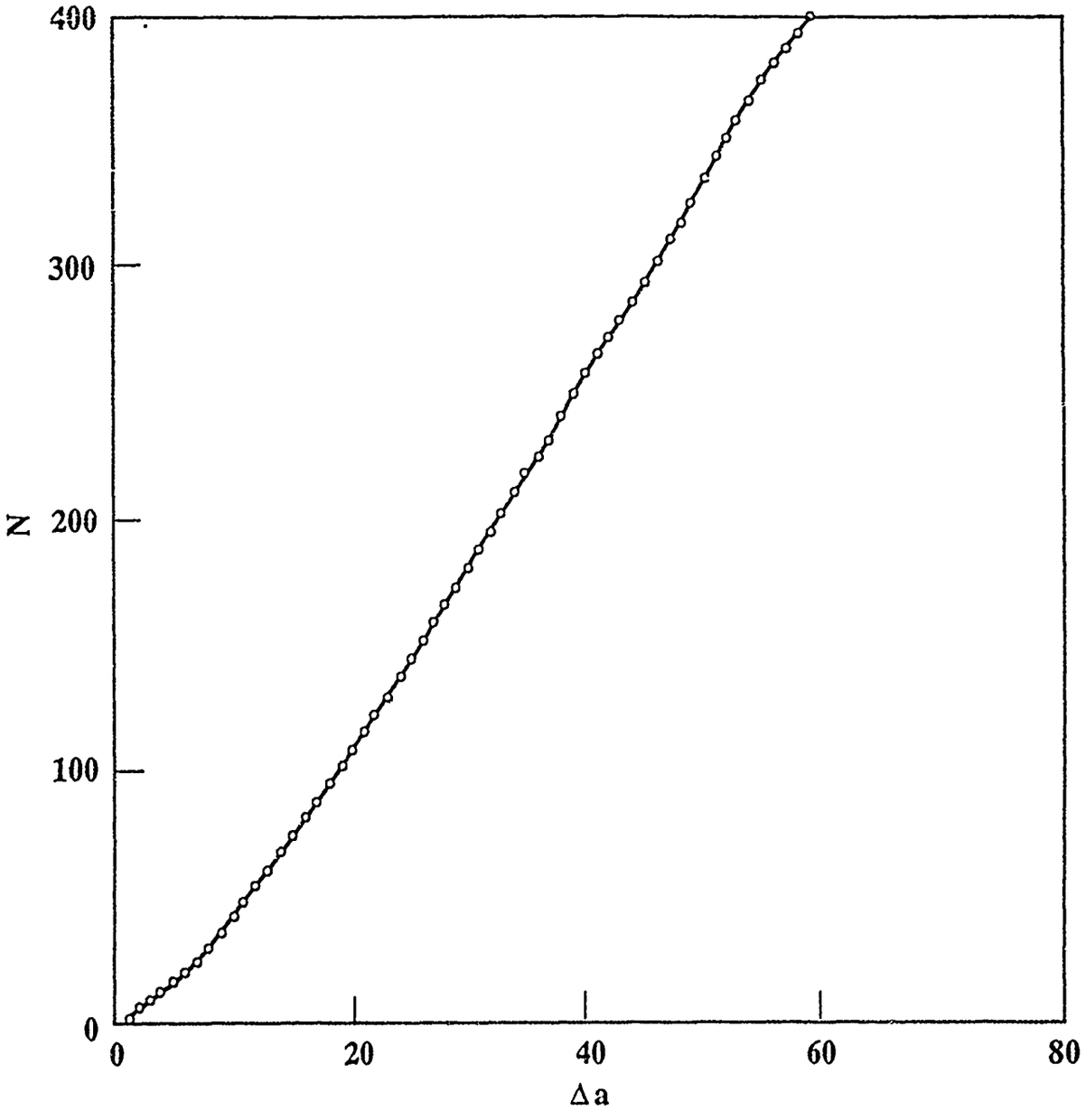

Fig. 6a

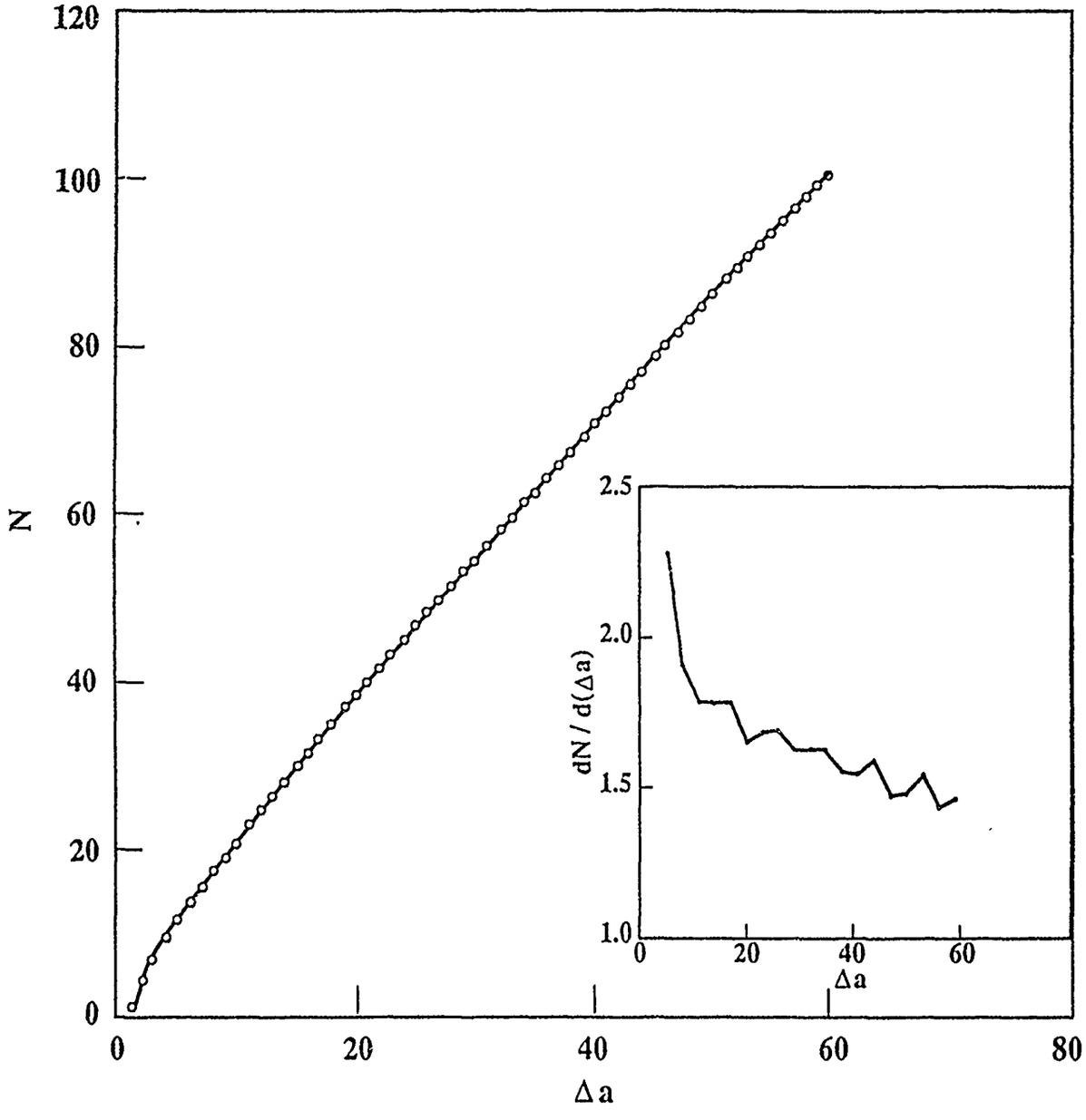

Fig. 6b

J. Phys.: Condens. Matter 3 (1991) 1019–1053. Printed in the UK

REVIEW ARTICLE

Fragments of matter from a maximum-entropy viewpoint

R Englman
Soreq Nuclear Research Centre, Yavne 70600, Israel

Received 30 July 1990

Abstract. After introducing the formalism of maximum entropy and reviewing alternative approaches for fragment size statistics, this paper derives a general distribution law (similar in form to the Bose–Einstein statistics) and applies it to distributions observed in rock mining, exploding metallic shells, shattered crystal pieces, droplets in spray, atomic or molecular clusters, space debris and fragmented nuclei. Variations of fragment number with size that are power-law-like (fractal), humped or exponential can lead to physically significant conclusions regarding the fracturing mechanism. Theoretical aspects of the maximum-entropy method in the derivation of the distribution law (including some inherent difficulties) are discussed.

1. Introduction

The pieces of a broken object are among the most common examples of randomness and disorder (Zurek 1989, section V). There may be psychological reasons for associating disorder with broken pieces, perhaps due to our dismay at seeing a nicely designed object shattered and to the need to clean up the resulting mess, but it is a fact that it has been found difficult to read some regularity into fragments. The regularity that we can hope to get is a law describing the *distribution* of fragments, especially with respect to their sizes but also regarding shapes and internal parameters. The prediction of distribution has in many cases practical advantages, relevant to scientific and technological issues. A few instances taken from physics will be given later (section 6); at this point I shall describe the industrial importance of oil-shale fragment size distribution since it was through this that I became involved in fragmentation.

In a standard mode of operation (called 'bench blasting') the bituminous rock (oil shale) is explosively mined to produce the debris containing fragments. The large specimens are then comminuted mechanically to bring them down to a size such that retorting (or extraction of oil by partial burning) can be carried out. Since comminution takes time and money, large fragments (exceeding about 50 cm in diameter) are undesirable, and so are small pieces (less than 0.5 cm) since these clog up the retort. The mining has to be planned accordingly and, while one rarely has control over the geomechanical properties (faults, cracks, etc) of the rock, one can still vary some parameters of the mining, namely, location of explosion boreholes, temporal sequence of their activation and type of explosive. By correct choice of these one can hope to obtain a fragment size distribution with the desired properties of not having too many pieces

0953-8984/91/091019 + 35 $03.50

outside the lower and upper limits. The task at hand is thus the derivation of a fragment size distribution in the context of a physical process (the passage of detonation stress waves) and in a given geometric setting (some borehole pattern and major fault structure in the rock) (Jaeger *et al* 1986b). At the same time, several physical factors will remain unknown, like subsurface joints and cracks, leaving the theoretician with an underdefined assignment.

It would appear that the maximum-entropy method (MEM) is an ideal tool to handle this situation and others in which we wish to predict fragment distributions. Reasons both favouring and opposing this expectation are outlined in the next section and in appendix 1, where we return to a discussion on the claims of MEM.

Fracture of solids as a physical process is the subject of appendix 2.

2. The method of entropy maximization

Let us denote by j the events that we wish to predict (like the event of finding n fragments of a given size in a debris heap) and by p_j the corresponding probabilities. We then assert that the MEM gives the most conservative probability distribution p_j subject to the available knowledge, which enters the formalism as 'constraints'. The maximum-entropy solution is that which maximizes the information entropy (also called 'missing information')

$$S = -\sum_j p_j \log p_j \tag{1}$$

(Shannon 1948) subject to the constraints. The constraints are assured mathematically by Lagrange multipliers (appendix 1).

The meaning of 'most conservative' in the assertion of the last paragraph is twofold. First, the MEM probabilities p_j are about the smoothest, flattest functions of the events j (suitably ordered) consistent with the constraints; secondly, the predictions p_j make do with just the constraints explicitly imposed and not with any other constraints perhaps tacitly implied (in obtaining non-MEM p_j). The latter meaning provides a simple, heuristic proof of the assertion. It can be shown that imposing any additional constraints reduces S, i.e. it reduces the 'missing information'. If our choice for the probabilities p_j is non-MEM, this choice will reduce S below its maximum value and will imply some extra constraint. Therefore the MEM solution is the only one consistent with the explicitly stated knowledge.

More impressive claims have also been made for the MEM as a predictive method (Jaynes 1983, Skilling 1984, Rosenblatt-Roth 1987, 1988). In the context of fragmentation, one can show that, if N independent fragmentation experiments are performed, the mean of the size distributions will tend, asymptotically as $N \to \infty$, to the MEM value of p_j.

A consistency criterion was enunciated by Tikochinsky *et al* (1984) in the following sense: the distribution of MEM is the only one that will be confirmed by successive repetition of experiments.

In view of the existence of several time-honoured and practised predictive procedures (like maximum-likelihood, least-squares fitting, Bayesian predictions), the preceding claim is bound to have raised opposition (Titterington 1984). To answer this, Skilling (1984) writes: 'I find the arguments for using maximum entropy to be deeply compelling. [MEM] stands in splendid isolation, on fundamental grounds.'

But even this is not all, since according to Jaynes (1983), MEM predictions *cannot* be mistaken: if they are not supported by experiment, they must be regarded as disclosing (the need for or existence of) additional informational constraints. Jaynes is to be credited with the use of information entropy as a predictive tool in physics and this review does perhaps no more than describe the implementation of this programme for fragmentation. In his works (collected in Jaynes (1983)) thermodynamic entropy is represented as a measure of the insufficiency in our knowledge of a physical system. In an opposite view (Denbigh and Denbigh 1985) thermodynamic entropy is regarded as an objective attribute of the system. In a compromise approach (Zurek 1989) the thermodynamic entropy is a sum of contributions of physical randomness and of the observer's ignorance.

Without taking sides in this controversy, we wish to demonstrate here that the maximum-entropy solution p_j with energy $\hat{E}$ given is formally identical to the minimum-energy solution P_j with entropy $\hat{S}$ given. With the introduction of Lagrange multipliers, denoted by β, ν and T, μ (respectively) for the two problems, the quantities (henceforth called Lagrangians) to be extremized are

$$L = S - \beta(E - \hat{E}) = -\sum_j p_j \log p_j - \beta\left(\sum_j \varepsilon_j p_j - \hat{E}\right) - \nu\left(\sum_i p_i - 1\right) \tag{2}$$

and

$$-\Lambda = E - T(S - \hat{S}) = \sum_j \varepsilon_j P_j \div T\left(\sum_j P_j \log P_j \div \hat{S}\right) - \mu\left(\sum_j P_j - 1\right). \tag{3}$$

The sets of equations $\partial L/\partial p_j = 0$ and $\partial \Lambda/\partial P_j = 0$ have evidently formally the same solutions. These become equal,

$$p_j = P_j = \exp(-\varepsilon_j/T) \Big/ \sum_i \exp(-\varepsilon_i/T) \tag{4}$$

if one supposes the relations

$$T = \beta^{-1} = \hat{E}/\hat{S}. \tag{5}$$

Clearly equation (4) is also the solution obtained by minimizing the free-energy expression (for temperature T given). The maximum-entropy procedure would thus appear to be beyond doubt, but questions remain whether the system (especially a classical one) is truly ergodic over the events j.

3. Distribution of fragments

3.1. Exponential distributions based on MEM

Apparently the earliest use of MEM for fragment size distribution is due to Griffith (1943). He supposed that:

(i) a given quantity of energy is converted to fragmentation (this quantity depending on the nature and intensity of the fracturing process);
(ii) the energy goes entirely into the creation of free surfaces; and
(iii) each molecule in the solid competes for the available energy on equal footing.

If N_s denotes the number of molecules belonging to s-sized fragments, N_s/s is the number of s-sized fragments. The energy invested in each fragment is $\gamma s^{2/3} g$, where γ is the surface energy density and g a geometrical factor. The constraint is

$$\hat{E} = \gamma g \sum_s s^{2/3} N_s/s = \gamma g \sum_s s^{-1/3} N_s \tag{6}$$

so that identifying ε_j in equation (2) with $\gamma g s^{-1/3}$ and regarding the solutions in equation (4) one derives

$$N_s \propto \exp(-\lambda/s^{1/3}) \tag{7}$$

where λ is a constant to be evaluated from equation (6). In practice, in the break-up of solids, the number of fragments N_s/s decreases with size much faster than that given by equation (7), indicating that assumption (iii) places too much weight on large fragments and that sinks of energy other than the surface energy (involved in assumption (ii)) are also present. Moreover, molecules in the middle of the fragment do not feel the fracture process in the same way as do molecules on the surface. We shall see that when fragments are formed by accretion of molecules, assumption (iii) has an empirical basis (section 6.4).

In a discussion of the size distributions of exploding shells and of other two-dimensional objects, Grady and Kipp (1985) used only a geometrical constraint, namely

$$A = g \sum_s n_s s \tag{8}$$

meaning that the number n_s of plane fragments of size s times their area gs (where g is again a geometrical factor) sums up to the total area A. The MEM soution is clearly

$$n_s \propto \exp(-gs/A). \tag{9}$$

This is to be contrasted with the semiempirical distribution due to Mott (1947) (see also Mott and Linfoot 1943) in which the cumulative distribution arising from n_s is an exponential function of the *linear* size, namely $s^{1/2}$ in two dimensions and $s^{1/3}$ in three dimensions. Data on metallic shells have been accounted for by Mott's distribution (Sternberg 1973), though discrepancies appear, which are treated in greater detail in section 6.1. Deviations from Mott's law have been found in fragmented rock data and in a numerical simulation (Englman *et al* 1984).

3.2. Fragmentation by a fast, sudden process

Fracture by fast energy input, such as occurs in explosions, projectile or laser impact, a shattering event, explosive expansion or a sharp temperature change, has been the subject of dynamic theories (Mott 1947, Grady 1982, Grady *et al* 1985, Glenn and Chudnovsky 1986, Glenn *et al* 1986, Curran *et al* 1987).

These theories are incorporated in the probabilistic prediction of fragmentation that we describe now. Characteristic of fast processes is that fracture events take place at different points of the solid independent of one another. This is because newly created fractures have no time to communicate with each other, except that the energy invested in the fracture cannot exceed the total energy available for fracture and that the fragmented volumes are also bounded by the original volume. Following Grady (1982), we suppose that all discontinuities formed by the stress wave (e.g. cracks, voids) immediately become faces of fragments. An alternative view, which remains to be explored, would

be to suppose that in the first place the fast process creates fractures that can then join up to enclose a fragment. The advantage of this second view is that unfinished fractures, called 'internal damage' (Jaeger *et al* 1986a, c, Yatom and Ruppin 1989) are also envisaged to be present as the result of stress.

Following a more detailed account in the original paper (Englman *et al* 1988b) we associate with each fragment of linear size a an energy $e(a)$ (see equation (10) below) which in essence contains all the physics entering the formation of fragments (figure 1). Summing $e(a)$ over all fragments, we equate the sum to the total energy input $\hat{E}$ for the fragmentation process: this provides the first constraint (equation (15) below). Implicit in this procedure is the assumption that at the instant of fragmentation all secondary features of the process (such as heat, noise, fragment motion) still reside in the fragments. Our way of invoking energy conservation differs from that of Glenn *et al* (1986), who balance the created surface energy against the kinetic and stored energies. The present approach appears justified (barring the role of expanding gases formed in an explosion) because it includes the physical state of the fragments immediately after fragmentation.

We assume fragments of linear size a and roughly spherical shape whose energy

$$e(a) = (2\pi/3)\rho u^2 a^3 + (2\pi/5)\rho\dot{\varepsilon}^2 a^5 + (4\pi/6K)\sigma^2 a^3 + 4\pi\gamma a^2(1 - a/R) \tag{10}$$

consists of the following terms: the kinetic energy (KE) of the fragment of mass density ρ moving as a rigid body with speed u (this term takes up the largest part of the energy); the internal KE about the centre of mass (expressed in terms of $\dot{\varepsilon}^2$, the volumetric dilatation rate squared, or the trace of the square of the stretching tensor); the stress energy stored in the fragments (Glenn *et al* 1986) including sound and elastic waves (σ being the stress and K the bulk modulus); and the surface formation energy (γ is the surface energy density and R is the radius of the spherical solid before fragmentation). Other terms depending on size a or on other variables (e.g. shape or chemical composition) may be added to equation (10).

The probability of having n_a fragments of size a is written

$$p(n_a, a) \qquad \text{with} \qquad \sum_{n_a} p(n_a, a) = 1 \tag{11}$$

and the most likely number of such fragments and their masses are, respectively,

$$\langle n_a \rangle = \sum_{n_a} n_a p(n_a, a) \tag{12}$$

and

$$w(a) = (4\pi/3)\rho a^3 \langle n_a \rangle. \tag{13}$$

Assuming that a fixed mass $\hat{W}$ of materials is being fragmented, we have the constraints

$$W = \sum_a w(a) = \hat{W} \tag{14}$$

and

$$E = \sum_a e(a)\langle n_a \rangle = \hat{E} \tag{15}$$

where the second constraint is due to energy conservation.

(In equation (11), we have chosen as the fundamental event whose probability $p(n_a, a)$ is sought the finding of n_a fragments of linear size a, rather than the event of finding

at random an a-sized fragment, whose relative frequency is $p(a)$. Our choice reflects the practice in mineral processing of the operation of sieving.)

In the sense of the MEM, the best distribution p subject to the constraints is obtained by maximizing

$$L = -\sum_a \sum_{n_a} p(n_a, a) \log p(n_a, a) - \beta(E - \hat{E}) - \mu(W - \hat{W}) \tag{16}$$

through variation of $p(n_a, a)$ and adjusting the Lagrange multipliers β and μ so that the constraints (13) and (14) are satisfied.

The solution is

$$p(n_a, a) = \exp(-n_a x_a) \Big/ \sum_{n_a} \exp(-n_a x_a) \tag{17}$$

where

$$x_a = \beta e(a) + \mu(4\pi/3)\rho a^3 \tag{18}$$

and

$$\langle n_a \rangle = (e^{x_a} - 1)^{-1} \tag{19}$$

$$\sim x_a^{-1} \tag{20}$$

for the majority of fragments, i.e. excluding large-sized fragments, for which $x_a > 1$, whose mean number decreases exponentially. In (18) the fragment mass and energy are both polynomials in a, with powers Θ ranging from 2 to 5 (equation (10)). In a size range where a single power law dominates in (18), the distribution of sizes will exhibit a power-law behaviour in the form

$$\int_a^\infty da \langle n_a \rangle \propto a^{-D} \tag{21}$$

with the 'fractal dimension' D being given in terms of the predominant values of Θ as $D = \Theta - 1$.

Turcotte (1986) has listed 21 objects whose fragment size distribution behaves according to (21), with D falling between 1.5 and 3.5, i.e. conforming to the theoretical values in equations (10), (18) and (20). Experiments on simulation of astroid impacts gave $D \sim 2.5$ (Capaccioni *et al* 1986).

To determine the parameters β and μ in the distribution $\langle n \rangle$ (equations (18)–(20)) from the constraints, we first combine (14) and (15) to write

$$I \equiv \beta\hat{E} + \mu\hat{W} = \sum_a x_a (e^{x_a} - 1)^{-1} \tag{22}$$

where the summation is over all sizes that are collected in discrete bins. Let the number of bins (or summands) be I_b, then

$$I < I_b \tag{23}$$

since the summand is less than unity. The dominant contribution to $e(a)$ and x_a is a term proportional to the fragment volume a^3. Thus, I is proportional to $\hat{W}$.

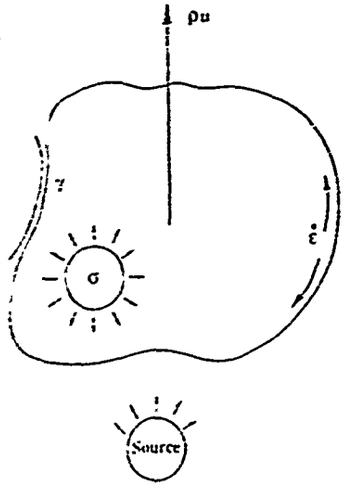

Figure 1. Forces acting on a fragment. The figure illustrates the body forces ρu (inertial) and σ (uniform stress), the surface energy density γ and the transverse dynamic strain $\dot{\varepsilon}$.

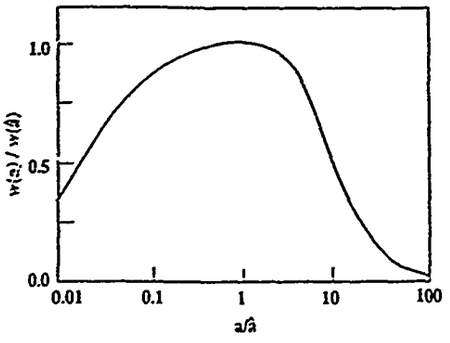

Figure 2. Weight distribution of fragments, equation (24). The weight $w(a)$ and the linear fragment size a are normalized to their values at $\hat{a}$ (equation (26)). Beyond $a/\hat{a} \sim 10^2$ the distribution drops off exponentially with a and equation (24), on which this figure is based, is not applicable. The parameter ν in equation (27) has the value 10^{-2}.

The weight distribution (13) for the majority of fragments (equation (10)) is expressed in a reduced form as

$$w(a) = \hat{W}I^{-1}/(2\nu s^{-1} + 1 + \nu s^2) \tag{24}$$

$$s = a/\hat{a}. \tag{25}$$

It has a maximum at $a = \hat{a}$, given by

$$\hat{a} = (5\gamma/\rho\dot{\varepsilon}^2)^{1/3} \tag{26}$$

which serves as a convenient scaling parameter for the fragments (Grady 1982). The other parameter ν in the distribution (24) contains the multipliers β and μ, which must be eliminated by calculating the mass (or weight) constraint (14). The result is

$$\nu = (\pi/3)(\hat{a}/Il)^2 \tag{27}$$

where l is the bin width, so that, as shown in equation (22), Il is the effective size range scanned by the sampling process. The saddle-point $\hat{a}$ must fall well inside the size range, so that

$$\nu \ll 1. \tag{28}$$

The weight distribution, shown in figure 2, has a maximum at $a = \hat{a}$, is broad, and is asymmetric. Thus, the maximum derived by MEM coincides with the characteristic fragment size of Grady (1982) and depends (through equation (26)) only on the dynamic fracture parameters γ and $\dot{\varepsilon}^2$. On the other hand, $\hat{a}$ is independent of either the centre-of-mass KE or of the stored stress σ, or indeed of any contribution to the energy that is

proportional to the fragment volume $4\pi a^3/3$. The mathematical explanation for this is that in the summand of (14),

$$w(a) \propto a^3 n_a \sim a^3 x_a^{-1} = [\beta e(a)/a^3 + \mu]^{-1}$$

all such contributions appear as an additive constant to the Lagrange multiplier μ, which is a parameter to be adjusted.

The empirical role of $\hat{a}$ is well documented in the fragmentation of oil shale (Grady 1982), brittle steel (Weiner and Rogers 1979) and rapidly heated water (Blink and Hoover 1985). Since we find that, in general, the mean size averaged over the distribution exceeds its maximum $\hat{a}$, a more careful determination of the average and a specification of the averaging procedure are called for.

In 'cratering' situations, where only part of the solid is fragmented, the constraint (14) on the total weight W does not apply and μ does not enter. Yet, remarkably, elimination of the parameter β leads to the same distribution (24) as in the fixed W situation. This was subject to test when fused alumina cement targets were partially (~30%) and almost fully (90%) fragmented by fast aluminium projectiles (Bianchi *et al* 1984). The fractal exponents were, respectively, $D = 2.76$ and 3.06, which do not support our result, though their magnitude is within the range predicted in equations (10), (18) and (20).

The weight $\hat{W}$ of the crater mass scales with the energy input $\hat{E}$ according to

$$\hat{W} = (2\pi\rho\hat{E}\hat{a}/9\gamma)(\hat{a}/Il)^2. \tag{29}$$

The threshold energy input E_t below which fragmentation cannot occur (the constraint equation (15) having no solution) is given by

$$E_t = 4\pi\gamma\hat{a}^2(\hat{a}/l). \tag{30}$$

A different threshold energy for fragmentation, resulting from a geometrical constraint, was obtained by Yatom and Ruppin (1989).

A striking result of the MEM distribution is the prediction of fractal distribution, equations (17)–(20), with fractal exponents in the range of the observed ones (Turcotte 1986). The result depends on two circumstances: first, on the property that the energy and volume terms, given by $e(a)$ and a^3, go to zero as the size a vanishes so that there is no contribution to the constraints from $a \to 0$, admitting of a 'Bose condensation'; secondly, on the absence of a constraint on the total number of fragments. Since the latter circumstance is tied to the non-atomistic description, it seems that fractal distributions might be the rule for classical objects. We emphasize though that fractal, inverse power-law behaviour is predicted only for the low size end; at large sizes an exponential decrease with size takes place. In our discussion of experimental distributions in the sequel, the question of power-law versus exponential form will come up frequently.

In summary of this section, an essentially simple, two-parameter ($\hat{a}$ and ν) distribution (equation (24)) has been derived, based on the broad principle of maximum entropy and incorporating the physics of fragmentation through the energy of fragments of size a (equation (10)). The typical Grady fragment size has been rigorously rederived and identified with the saddle-point $\hat{a}$ and the maximum of the distribution; $\hat{a}$ was found to be unaffected by mechanisms that are coextensive with the fragment volume.

3.3. Statistics of propagating fragmentation

In the previous section we have described a fragmentation process that is fast, sudden and happens in space uniformly. In contrast, 'propagating fragmentation' designates a

process wherein a medium gets fragmented over an extended duration of time and in an extended volume. The 'source term' driving the fragmentation is space- and time-dependent. By maximizing the information entropy density at all times and positions, subject to constraints involving the source term, we obtain fragment size distributions that are fully determined by the source term and the strain rate. We shall find that weak (or strong) sources result in a size distribution that is sharply (or broadly) peaked around the most likely fragment size.

This is the first instance in which the duration of the fragmentation process enters our consideration. We postpone a discussion of the temporal scale of fragmentation to a later section (section 4.2) where sequential fragmentation theories are reviewed; let us note though that MEM can bear extension to processes developing in time (Jaynes 1983, p 287, Levine 1985). The present approach keeps clear of intricate issues, such as the suggestions that a perturbed system will evolve by minimal rate of entropy production not far from equilibrium and by maximal rate of entropy increase when far from equilibrium (Prigogine 1978, Kaufman *et al* 1989).

We assume that the fragmented body can be subdivided into regions of unit volume that are sufficiently large for statistical considerations to be valid in each region and at the same time small enough that external forces or stresses can be regarded as uniform throughout the region. Regions are labelled by a convenient coordinate r and the time by t. Fragments formed in (t, r) are characterized by linear size $a = a(t, r)$ where a is a parameter specifying the fragment. More generally a might represent a set of fragment parameters (size, shape, composition, quality, etc), though we shall work with a as representing exclusively the linear size of the fragment. We seek by MEM the probability

$$p(n_a, t, r) \qquad \text{with} \qquad \sum_{n_a} p(n_a, t, r) = 1 \tag{31}$$

of finding n_a fragments in unit volume around position r and at time t having the dimension a. Under the conditions posited, the total entropy of information is the sum of the entropies of the regions

$$S(t) = \sum_r S(t, r) = -\sum_r \sum_a \sum_{n_a} p(n_a, t, r) \log p(n_a, t, r). \tag{32}$$

We maximize $S(t)$ for all times, subject to constraints described in the following, to obtain first the probabilities p and then the mean fragment number per unit volume for fragments of type a,

$$\bar{n}(a, t, r) \equiv \sum_{n_a} n_a p(n_a, t, r). \tag{33}$$

The expectation value of any quantity $Q(a)$ is given by

$$\langle Q \rangle \equiv \sum_a Q(a) \bar{n}(a, t, r). \tag{34}$$

The physical foundations of the method are some theoretical or empirical relationships between the parameter of fragmentation (a) and the parameters of the physical process that causes fracture. The relations are expected to have the form

$$F(\text{fragment parameters}) = \phi(\text{stress parameters}) \tag{35}$$

of which a particular case might be

$$\langle F(a, t) \rangle = \phi(\sigma(t'), t' \leqslant t) \tag{36}$$

where on the left we take an average over a function of fragment sizes a at time t and on

the right we have a function of the history of the stress pulse σ up to the time t. Numerous forms of the functions in (36) have been considered in the past (Curran *et al* 1987, Kachanov 1986).

We shall postulate an energy balance formulation (Tuler and Butcher 1968, Kachanov 1986) equating the energy residing in the fragments with the energy input invested up to time t by the source. As already written in (15)

$$\sum_a e(a)\bar{n}(a, t, r) = \hat{E}(t, r) \tag{37}$$

where

$$\hat{E} = W \times D \tag{38}$$

$$= W \times \left(A \int_0^t [\sigma(t') - \sigma_0]^n \, dt' \right). \tag{39}$$

On the left in equation (37) is the sum over the energy density functional for fragments of size a, while on the right appears a semiempirical relation for the energy input in unit volume required to create the fragments. In (39), $\sigma(t)$ is the stress at time t and position r, σ_0 is a threshold for fracture. (In a more realistic treatment one should use several thresholds for different kinds of stresses: compressive, tensile, shear.) W is the energy at full nominal damage that specifies the energy needed to produce the damage $D = D(t)$ defined by the large parentheses. A is another empirical constant that depends primarily on the properties of the medium: its mechanical strength and its state (e.g. the population of microcracks). The power n in the integral is commonly taken as 2.

The stress $\sigma(t)$ represents the external source of fragmentation. It is regarded in this study as an input parameter, being a function of the distance from the location of the energy deposition and of time. Theoretical and empirical estimates of $\sigma(t)$ take into account the intensity of the source (e.g. the powder factor of explosives), the stress input rate and the elastic constants of the medium. The stress σ decreases oscillatorily with both t and r, due to geometry and dissipation. In truth, the energy loss due to fragment formation itself reduces σ and it is necessary to use a σ that is self-consistent with both the energy loss and the degradation of the medium. For an inhomogeneous medium (e.g. with substantial variability in crack densities inside it) A and W will also have a distance- and time-dependent behaviour.

The energy functional $e(a)$ in (37) was given in (10); we rewrite it as

$$e(a)/2\pi = \tfrac{1}{3}\rho u^2 a^3 + \tfrac{1}{3}\sigma^2 a^3/K - 2\gamma a^3/R + \varepsilon_a/2\pi \tag{40}$$

where

$$\varepsilon_a = 2\pi\dot{\varepsilon}^2 a^5/5 + 4\pi\gamma a^2. \tag{41}$$

The separation of terms in (40) distinguishes between terms with a^3 dependence and the two terms in (41) with a different variation. Since by construction we partition the fragmented material into regions of unit volume, for which following constraint holds

$$\langle a^3 \rangle = 1 \tag{42}$$

having normalized for convenience to a cubic rather than spherical volume, the expectation values of the first three terms in (40) are constant. Physically this means that the energy input for fragmentation $\hat{E}$ is fully expended on ε_a in (41), whereas the first three terms consume energy in a way that is independent of the state of fragmentation.

Maximization of (32) subject to the constraints (37) and (42) leads to the following probabilities

$$p(n_a, t, r) = \exp[-n_a(\beta\varepsilon_a - \nu a^3)] \Big/ \sum_{m_a} \exp[-m_a(\beta\varepsilon_a - \nu a^3)] \tag{43}$$

where the Lagrange multipliers β and ν serve to satisfy (37) and (42). The expected number of fragments per unit volume is, according to (33),

$$n_a = [\exp(\beta\varepsilon_a - \nu a^3) - 1]^{-1}.$$

The constraint equations give, for each form of the energy functional $e(a)$, a universally valid solution as a function of $\hat{E}$ only, i.e. independent of t and r. The physical mechanism for fragmentation enters through the dependence of $\hat{E}$ on r and t (an example for which is the integral shown in (39)).

To describe the variation of the Lagrange parameters β and ν with E we find it convenient to transform them to dimensionless form,

$$\beta' = 2\pi\gamma\hat{a}^2\beta \tag{44}$$

$$\nu' = \hat{a}^3\nu \tag{45}$$

where

$$\hat{a} = (5\gamma/\rho\dot{\varepsilon}^2)^{1/3} \tag{46}$$

is a length characteristic of fragment size (Grady 1982) shown in equation (26). With the choice of (46) for the length unit the equations determining β' and ν' are

$$1 = \langle s^3 \rangle = \sum_s s^3 n(s) \tag{47}$$

$$E' = E/2\pi\gamma a^2 = \sum_s (2s^2 + s^5) n(s) \tag{48}$$

$$n(s) = \{\exp[\beta'(2s^2 + s^5) - \nu' s^3] - 1\}^{-1}. \tag{49}$$

In these units the ratio of ε_a to a^3 is

$$\varepsilon'(s)/s^3 = 2s^{-1} + s^2. \tag{50}$$

As shown in figure 3, for $E' \to \infty$, ν' tends to the value -1.0534, while β' varies exponentially as $\exp(-1/2|\nu'|E')$. As the energy input decreases, β' increases and ν' changes sign. In the limit β' approaches infinity and ν' approaches $3\beta'$ from below. However, the limiting value of the energy E' where this occurs is not zero, but 3+, or for the physical energy in (48)

$$E \to E_{\text{lim}} = 6\pi\gamma\hat{a}^2. \tag{51}$$

This remarkable result of an energy threshold dictated by statistical requirements, and additional to the crack-mechanical threshold implied by σ_0 in (39), will now be interpreted on the basis of equations (47)–(49). In the simplest terms, for the mean energy to be large, n has to be large, and this is tantamount to the exponent in (49) being small. Therefore β' decreases steadily with increase of energy input, as seen in figure 3. However, the increase of n has to be kept in check, since the expectation value of the volume is constant (equation (42)), and this is ensured by the other Lagrange multiplier ν' having the tendency to counterbalance the decrease of β'. More illuminating is the

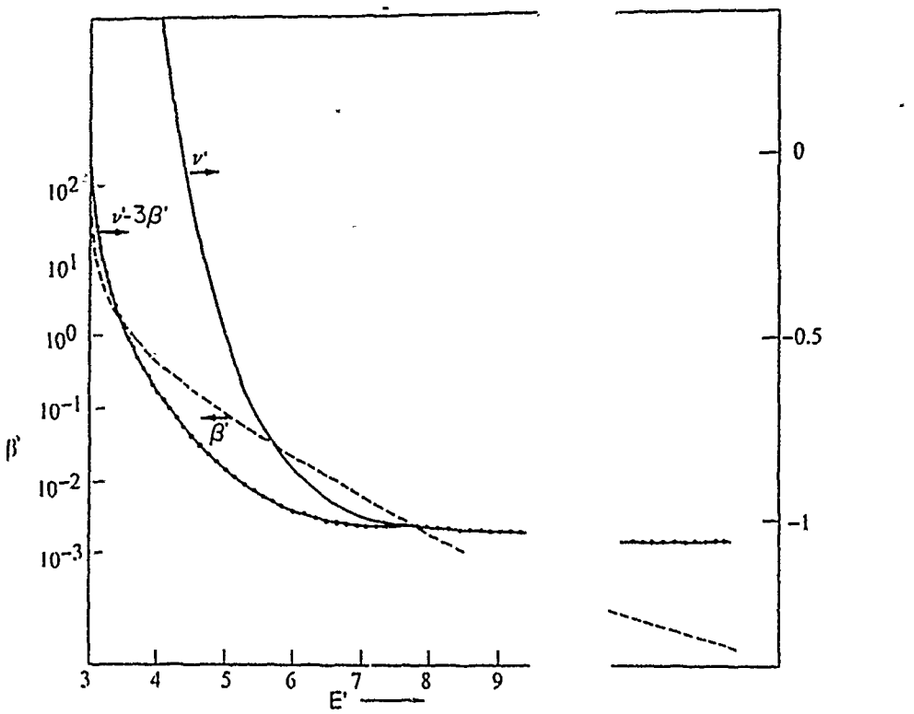

Figure 3. Lagrange multiplier parameters in the distribution as a function of the energy input E' responsible for the fragmentation. The energy multiplier β' (left-hand vertical scale) and the volume multiplier ν' and $\nu' - 3\beta'$ (right-hand scale) are shown, all in dimensionless units (equations (44), (45) and (48)). The asymptotic behaviours of β' and ν' are shown on the far right.

behaviour of the distributions (shown in figures 4(*a*)–(*c*)) as the energy E' varies. We note that the energy functional $\varepsilon(s)$ goes as s^2 and s^5, while the volume varies as s^3. Thus $\varepsilon(s)$ dominates for both large and small sizes, while the volume may do so at intermediate ones. (The ratio of the two quantities, equation (50), is minimum at $s = 1$.) Therefore the distribution is broad for large energy inputs and sharpens towards the value $s = 1$ for small E' (see figure 4). At its extreme sharpest, the volume or energy distribution acts as a delta function and the ratio of the energy and volume expectations is given by 3 (equation (40) at $s = 1$), which represents the threshold for energy input per volume a^3. For smaller energy input a maximum-entropy solution does not exist and the distribution is likely to be an irregular, haphazard one.

The general trend of our results, including the interesting sharpening of the distribution at small energy inputs, holds for energy functionals different from that in (40) and (41), provided the energy/volume minimum occurs at finite sizes. This permits the generalization of our results to include a term

$$Cs^z \tag{52}$$

where C is a constant and $z \simeq 4.5$, which represents the energy expenditure in creating internal damage (i.e. cracks that do not join up to form fragments) (Jaeger *et al* 1986a, Aharony *et al* 1986).

The distribution in (49) allows, formally, fragments of size larger than the unit volume, into which the medium was subdivided. To lighten the paradox, one must

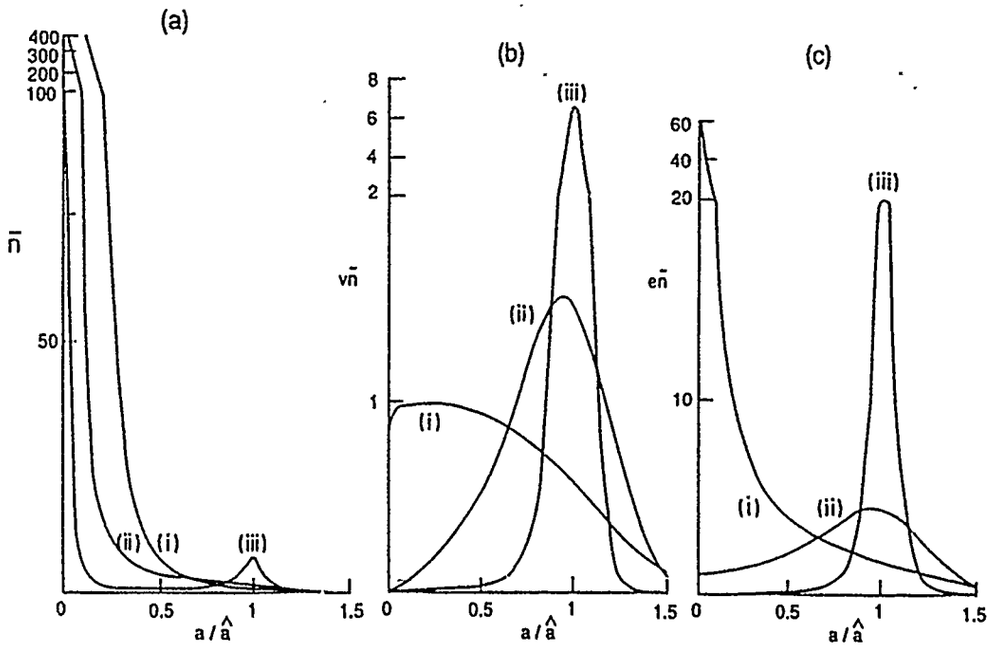

Figure 4. Distributions as a function of the reduced fragment size $a/\hat{a}$ or s; $\hat{a}$ is shown in equation (46). Plotted are: (*a*) $\bar{n}$, the expected number of fragments per unit volume (equation (49)); (*b*) $a^3\bar{n}$, the expected volume (in units of $\hat{a}^3$); and (*c*) $\varepsilon_a\bar{n}$, the expected energy (in units of $2\pi\gamma\hat{a}^2$). In the figures: (i) is for a strong source of fragmentation, $E' = 7.26$, $\beta' = 0.001$, $\nu' = -1.03$; (ii) is for an intermediate strength source, $E' = 3.62$, $\beta' = 1$, $\nu' = 2.48$; (iii) holds for a weak energy input source, $E' = 3.06$, $\beta' = 10$, $\nu' = 29.85$. The distributions sharpen as the energy input decreases. Note the changes in the vertical scales.

regard the distribution as referring to an *ensemble* of fragmenting bodies, in which the occurrence of a fragment larger than a unit adds to the weight of distributions in neigbouring regions.

4. Alternative theories of fragment distributions

Several theories give n_s, the distribution function of fragments of size s (n_s is the number of fragments of size s (s-fragments)). We describe some of these. Summaries from differing viewpoints are due to Dehn (1981), Grady and Kipp (1985) and Campi (1989).

4.1. Geometrical methods

4.1.1. Poisson statistics. The linear, 1D distribution is easily derived and will turn out to be of interest also in higher dimensions (in connection with the so-called Mott distributions). To avoid boundary effects we consider a ring of perimeter length L which is broken up into P pieces by randomly placed cuts (figure 5). The probability of obtaining a piece having a size between s and $s + ds$, anywhere, is equal to the product of probabilities of placing one cut anywhere (=1), of placing a second cut in the interval $(s, s + ds)$ measured from the position of the first cut (probability = ds/L), of not having

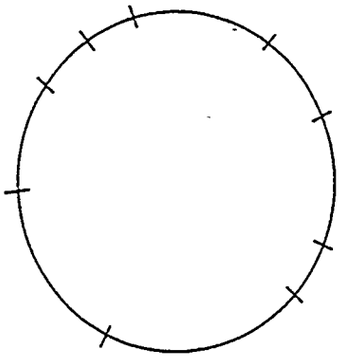

Figure 5. One-dimensional Poisson process. A ring is broken up into n (here 9) segments by n randomly placed cuts.

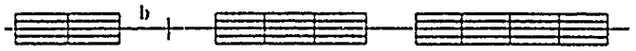

Figure 6. Percolation construction of fragments. Elementary segments of size b are chosen randomly with a probability p, resulting in compound fragments of sizes $2b$, $3b$ and $4b$. An equivalent approach is to choose fragment voids with probability $(1-p)$.

any of the remaining $P-2$ cuts falling in the interval (probability $= [(L-s)/L]^{P-2}$) and multiplied by the number of cuts ($= P-1$) following the first. Altogether

$$\mathrm{d}s\, n_s(P) = 1\,\frac{\mathrm{d}s}{L}\left(\frac{L-s}{L}\right)^{P-1}(P-1). \tag{53}$$

In the limit of L/s and P being large numbers, this reduces to

$$n_s = (1/\bar{s})\exp(-s/\bar{s}) \tag{54}$$

where $\bar{s} = L/P$ is the mean size.

In units where $\bar{s} = 1$ and definition of a new variate z through changes of mean, scale and exponent according to

$$s = [(z - z_0)/\mu]^{1/q}$$

one obtains the Weibull distribution

$$n_z = \frac{1}{\mu q}\left(\frac{z-z_0}{\mu}\right)^{1/q-1}\exp\left[-\left(\frac{z-z_0}{\mu}\right)^{1/q}\right] \tag{55}$$

where $1/q$ is called the shape parameter.

4.1.2. Percolation statistics. In a 1D discrete network consisting of L cells of length b (as shown in figure 6) the 'elementary' segment sizes (cells) are fixed (b). Larger fragments of size sb can form by joining s contiguous fragments, separated from neighbouring ones by the presence of the edges of empty cells whose probability of occurrence on each cell is $(1-p)$. The number of s-fragments is

$$n_s(p) = Lp^{s-1}(1-p)^2. \tag{56}$$

For more details on percolation in one, two, three and higher dimensions, see Stauffer (1979, 1985), Deutscher *et al* (1983) and Zallen (1983).

Table 1. What is fixed and what varies in Poisson and percolation statistics (Campi 1988).

	Poisson	Percolation
Fixed	Number of cuts (P)	Probability of segment (p)
Variable	Probability of segment	Number of fragments

Table 1 sets out the relation between percolation and Poisson statistics. It can be shown (Campi 1988) that the mean or expectation number of fragments of all sizes, namely

$$\sum_{s=1}^{\infty} n_s(p)$$

equals $L(1-p)$ so that in percolation

$$p = 1 - \sum_s n/L = 1 - P/L \tag{57}$$

where we have replaced Σn by P, the number of cuts featuring in the Poisson statistics. Inserting this result in (56) we obtain

$$n_s(p) = \exp[-(P/L)s](L/P)$$

which agrees with the result for Poisson statistics. Size distribution of fragments (or, to use the more common term, of clusters) near the percolation limit $p \to p_c$ can be shown to be derivable from maximum-entropy principles (section 5). It has also been shown that when the cells are identified with crack positions, fragmentation of a three-dimensional object occurs, within the percolation description, as a sudden transition with a crack concentration $p = p_{cII}$ (Aharony *et al* 1986). This is higher than the usual critical concentration for percolation $p_c(\equiv p_{cI})$. The reason is that at p_{cI} one gets a continuous structure of cracks in the solid without the solid breaking up into pieces. This (namely, fragmentation) occurs only at a higher crack concentration, for $p = p_{cII}$ or higher. Computed fragment statistics are shown in figure 7 and are compared with an experimental distribution (Englman *et al* 1984).

4.1.3. Tessellation. Cutting up a plane with lines or a solid with planes, or, alternatively, forming Voronoi polygons or polyhedra, are further ways of constructing fragments. The essential difference from the physical standpoint is whether one allows lines or planes to cut across each other. (As a rule, true cracks do not intersect except when their propagation velocity is high.) Extensive simulations with random lines in two dimensions by Grady and Kipp (1985) have indicated fragment numbers that decrease exponentially either with the linear dimension ('Mott distribution') or with the area of fragments. In simulations by Sprecher (Jaeger *et al* 1986a, c) the internal structure of fragments was also studied. We mention these, not only to correct the imbalance in this review, which deals almost exclusively with fragment *sizes* whereas other parameters of fragments are also susceptible to statistical treatments, but also to stress the importance of unfinished cracks within the fragment ('internal damage'), which can take up a substantial part of the energy available for fracture.

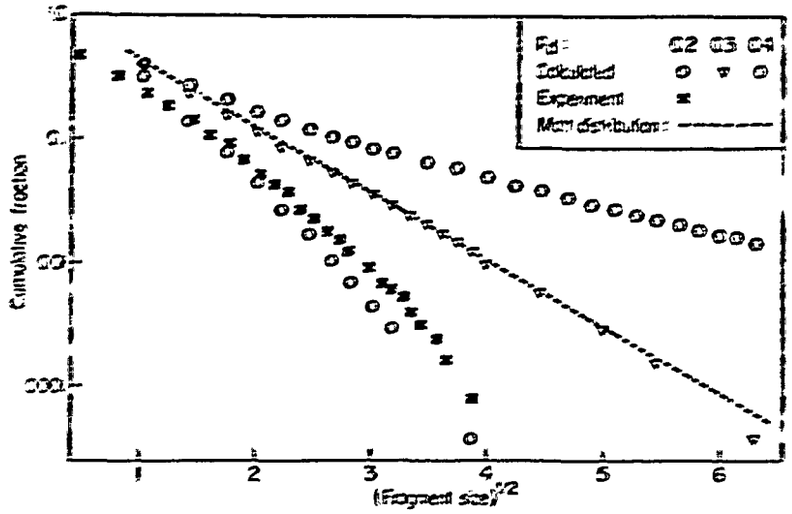

Figure 7. Cumulative fractions (the fraction of two-dimensional fragments being larger than size s) plotted logarithmically against $s^{1/2}$ for intermediate s. Three calculated data sets are shown (open symbols) for the dual lattice percolation probabilities $p_d = 0.2, 0.3, 0.4$ (so that the crack occupation probabilities are $p = 0.8, 0.7, 0.6$) and data points (full squares) for fragments larger than 1 grain, obtained from the explosion of a metal cylindrical shell 0.63 cm thick filled with 47 3DX/31 TNT/22 Al (Sternberg 1973). The line designated 'Mott distribution' represents equation (58).

Leaving aside the question of physical justification for intersecting cracks we can provide a heuristic proof for the Mott distribution generalized to higher dimensions d (>1), namely

$$n_s \propto \exp[-(s/\mu)^{1/d}]. \tag{58}$$

The proof assumes a high density of interesting randomly thrown cracks, such that most fragments have the minimum number of sides, i.e. triangles in a plane and tetrahedra in space. A d-sided object is not yet a fragment, but must await the arrival of another side (the $(d+1)$th crack) to become one. This will fall on the d-sided object at a distance from the opposite apex that follows a Poisson distribution: hence the distribution law in (58), which is Poisson-like in the linear dimension.

4.2. Kinetic distribution

We now describe theories in which a sequence of fragmentation stages is considered, such that each stage retains the memory of the preceding one only by the size of the fragments that are present, not through their state of stress (McGrady and Ziff 1987; Cheng and Redner 1988, Derrida and Flyvbjerg 1987). The results appear to be independent of the physical causes of fracture, yet there is a prediction of 'shattering transitions' in which the numbers of small fragments multiply to infinity as the size of the fragments decreases.

The following integro-differential equation gives the number of fragments $N(s, t)$ of size s at time t in terms of the rate $\nu(s)$ of s-fragments breaking up and the channelling ratio $K(s', s)$ (this quantity gives the fraction of s'-fragments ($s' < s$) created out of the

original s-fragments)

$$\dot{N}(s,t) = -\nu(s)N(s,t) + \int_s^\infty \nu(s')N(s',t)K(s,s')\,ds'. \tag{59}$$

Constraints include mass conservation

$$\int_0^s s'K(s',s)\,ds' = s$$

and a postulated mean number $\bar{n}$ of fragments created at each step (e.g. 2 upon cutting) given by

$$\int_0^s K(s',s)\,ds' = \bar{n}. \tag{60}$$

A problem that can be solved exactly is

$$\nu(s) \propto s^\lambda$$

(e.g. $\lambda = 1$ for random cutting)

$$K(s,s') = b(s/s')/s' \tag{61}$$

(e.g. $b = 2$ for random cutting when $\bar{n} = 2$ in (60)).

The initial condition $N(s, 0) = \delta(s - L)$ for a single piece has the solution

$$N(s,t) = e^{-st}[\delta(s-L) + 2t + t^2(L-s)].$$

The form in (61)

$$b(s/s') = (s/s')^m$$

gives $\bar{n} = (m+2)/(m+1)$. For negative m the number of small fragments rises leading to a 'shattering transition', in which an increasing number of tiny fragments is generated (Ziff and McGrady 1986, McGrady and Ziff 1987).

4.3. Physics-based theories

To my knowledge, apart from the MEM, which forms the subject of this review, there exist no theories of fragment size distribution that are rooted in detailed physical mechanisms. This situation is probably due to the difficulty of disentangling the stochastic and the deterministic aspects of fracture (Grady and Kipp 1989, Jaeger and Englman 1991).

There are indeed physical theories of *fracture*, of which Mott's is perhaps the most notable (Mott 1947, Kipp and Grady 1985, Grady and Kipp 1989). These give, as a rule, mean fragment sizes, but not distributions.

Furthermore there are also models of fracture (mainly in brittle media) and of failure (like yield in ductile solids (Tate 1967, 1969)). Some of these are in the form of extensive computer codes, starting in the early 1970s with the one developed at Stanford (McHugh 1983, Seaman *et al* 1984, Shockey *et al* 1985, Curran *et al* 1987) and simultaneously at Sandia (Davison and Stevens 1972, Davison *et al* 1977), and continuing with several others (Rice 1975, Ravid and Bodner 1983, Ravid *et al* 1987, Kipp *et al* 1980, Taylor *et al* 1985, Kuszmaul 1986, Brandon 1988). However, the quantitative measures

of fracture, failure or damage that are given by the codes, frequently by mapping them onto the interior of the disintegrating body, are not immediately translatable into fragment formation and into a distribution of fragment sizes.

5. Maximum-entropy method and percolation theory

It is of some theoretical interest to establish a link between percolation theory and MEM, though most results are more easily obtained from numerical generation of percolation clusters than by using MEM with the constraints imposed that are in any case the outcome of simulations. In an early effort Kikuchi (1970) used a mean-field treatment to derive critical percolation probabilities by entropy maximization. The agreement with correct values was poor.

The events j in equation (1) for the probabilities p_j are taken to represent the finding of n_s clusters of size s per lattice site

$$p_j \equiv p(n_s, s).$$

We note that in percolation a cluster arises as a connected entity of bonds (or sites) each of which is realized with a fixed probability p. The mean number of s-clusters is

$$\langle n_s \rangle = \sum_{n_s=0}^{\infty} p(n_s, s) n_s.$$

The constraints are, as before,

$$\sum_{n_s} p(n_s, s) = 1$$

for each s and the following relations are given by Stauffer (1981) to define critical indices α, β, γ and δ:

$$\left(\sum_{s=1,\ldots} \langle n_s \rangle \right)_{\text{sing}} \propto \varepsilon^{2-\alpha} \tag{62}$$

$$\left(\sum_{s} s \langle n_s \rangle \right)_{\text{sing}} \propto \varepsilon^{\beta} \tag{63}$$

$$\sum_{s} s^2 \langle n_s \rangle \propto \varepsilon^{-\gamma} \tag{64}$$

$$\sum_{h \to 0, s} s(1 - \mathrm{e}^{-hs}) n_s(p \to p_c) \propto h^{1/\delta}. \tag{65}$$

In these relations $\varepsilon \equiv |p - p_c|$, where p_c is the critical occupation probability for percolation, and the subscript 'sing' represents the leading singular part of the sum which remains finite at $p = p_c$.

The MEM solution for the cluster size distribution is

$$p(n_s, s) = L^{-d} \exp(-n_s x_s - \lambda^1)$$

where

$$\begin{aligned} x_s &\equiv_{h \to 0} A + Bs + Cs^2 + Ds(1 - \mathrm{e}^{-hs}) \\ \langle n_s \rangle &= L^{-d} (\mathrm{e}^{x_s} - 1)^{-1} \end{aligned} \tag{66}$$

and λ' is a normalizing constant independent of the size L. The coefficients $A, \ldots, D$

are fitted to satisfy the constraints (62)–(65). The fitting is not easy to carry out since several limiting processes are involved, namely $\varepsilon \to 0$, $h \to 0$, L (size of lattice) $\to \infty$; however, it is clear that for s in some region (s large, yet smaller than L^d) the terms

$$Cs^2 + Ds(1 - e^{-hs})$$

will dominate the expression (66) for x_s. Rewriting this for the given range of s as

$$x_s \simeq C's^2 + D's^3 + O(h) \tag{67}$$

and noting that, for $x_s \ll 1$,

$$\langle n_s \rangle = L^{-d} x_s^{-1} \tag{68}$$

we conclude that the mean number of clusters of size s will show an effective power-law dependence of the form

$$\langle n_s \rangle \propto s^{-\tau} \tag{69}$$

where $2 < \tau < 3$.

For another, heuristic derivation of this result see Zallen (1983). Numerical estimation of cluster numbers near $p = p_c$ gives in three dimensions $\tau = 2.2$, whereas more generally (with $p \neq p_c$) the relationship in (69) becomes modified by a smooth bell-like function of s (Stauffer 1979). However, outsize cluster numbers decrease with size exponentially.

The relation between fragment sizes and percolation clusters appears to have been determined in the first instance by Englman *et al* (1984). A fragment is formed when a piece of material is fully surrounded by linear cracks (in two dimensions) or by crack plaquettes (in three dimensions). The size of fragments is given by the cluster size in the *dual* lattice, defined by placing a bond across a face where a plaquette is missing (or across a line where a crack is missing, in two dimensions) and removing a bond where a crack plaquette is present. The corresponding occupation probabilities in the two lattices are related by

$$p_{\text{dual}} = 1 - p_{\text{crack}}. \tag{70}$$

Fragment distributions for $p_{\text{crack}} > p_c$ (= the critical crack concentration) were obtained by a two-dimensional simulation and followed a modified Mott distribution law, with positive or negative deviations at very large sizes (Englman *et al* 1984) (figure 7).

Let it be remarked that mechanical failure of the solid occurs at $p_{\text{crack}} = p_{\text{cII}}$, so that the condition $p_{\text{crack}} > p_{\text{cII}}$ will be achieved in practice through continued stress loading of the solid, while it is being held together artificially: either by confinement or inertially. In an impact loading (by projectiles, fragments or laser light) the confinement would not be expected to occur and the fragmentation would take place as soon as $p_{\text{crack}} = p_{\text{cII}}$ obtains (Blackman and Goldsmith 1978, MacAulay 1987). Then one would expect to see the relation (69) in effect.

6. Experimental distributions in relation to MEM predictions

6.1. Exploding cylindrical shells

Cylinders made of Armco iron or of heat-treated steel were filled with explosives and

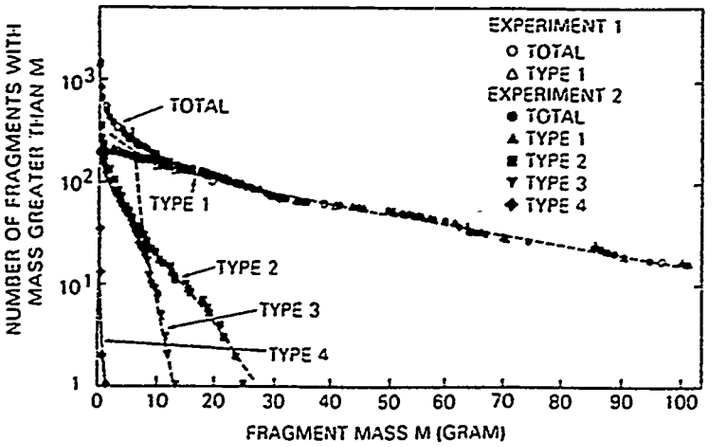

Figure 8. Cumulative fragment distributions from two tests by Mock and Holt (1983) on metal cylinders. Total distributions are shown together with partial distributions for types 1–4, classified according to fragment shapes and origin. The broken curves are theoretical fits in which the contribution of the strain energy term (equation (10)) changes with the type number as follows: $1 \ll 2 \ll 3$. The full curve for type 4 guides the eye.

the resulting fragment size distributions analysed by Mock and Holt (1983) (figure 8). The cylinder walls were about 2 cm thick and the mean diameter about 20 cm, which makes it questionable whether to apply two-dimensional (shell-like) or three-dimensional modelling. However, the authors separated the fragments in accordance with a characterization scheme based on the nature (brittle or shear) of the fracture surfaces. Different fragment types (labelled type 1–4 in figure 8) had different mean mass per fragment. The type with the largest mean mass (type 1 in figure 8) followed a roughly exponential cumulative distribution, except for small sizes, as a function of the fragment mass M. However, the types with smaller mean masses (types 2–4) showed a decrease with mass that was faster than that. The explanation is straightforward in terms of the formulae (10), (18) and (19). The small mean mass is indicative, by (26), of larger strain rate $\dot{\varepsilon}$. In formula (10) for the exponent in the distribution $\langle n_a \rangle$, equation (19), the strain-rate term goes as a^5, or the 5/3 power of mass, to be compared with the inertial term going as the mass, which is expected to be dominant for the smaller strain-rate, type 1, fragments.

A large number of fragment distributions arising from explosively shattered cylindrical shells were obtained by Sternberg (1973) with variations in the shell composition and treatment and in the explosive. A simple exponential (Mott-type) distribution failed to account for the data over the whole mass range and consequently a distribution was synthesized from three separate exponentials, appropriate to small, medium and large sizes. The MEM distribution in two dimensions is given as a function of linear dimension a by equation (19), where x_a takes the form analogous to equations (10) and (18)

$$x_a \propto Aa + Ba^2 + Ca^3. \tag{71}$$

With suitable choice of the parameters A, B and C the MEM fits quite well the results of Sternberg (1973) for two combinations of steel and explosive (figures 9(a) and (b)).

Exploding mild-steel tubes with wall thickness/diameter ratios ranging from 0.05 to 0.17 were investigated by Stronge *et al* (1989), regarding the dependence of the fragment size distribution on the fracturing mechanism. This was varied through changing the explosive (charge) mass/metal mass (C/M) ratio over a 10-fold range. A two-dimen-

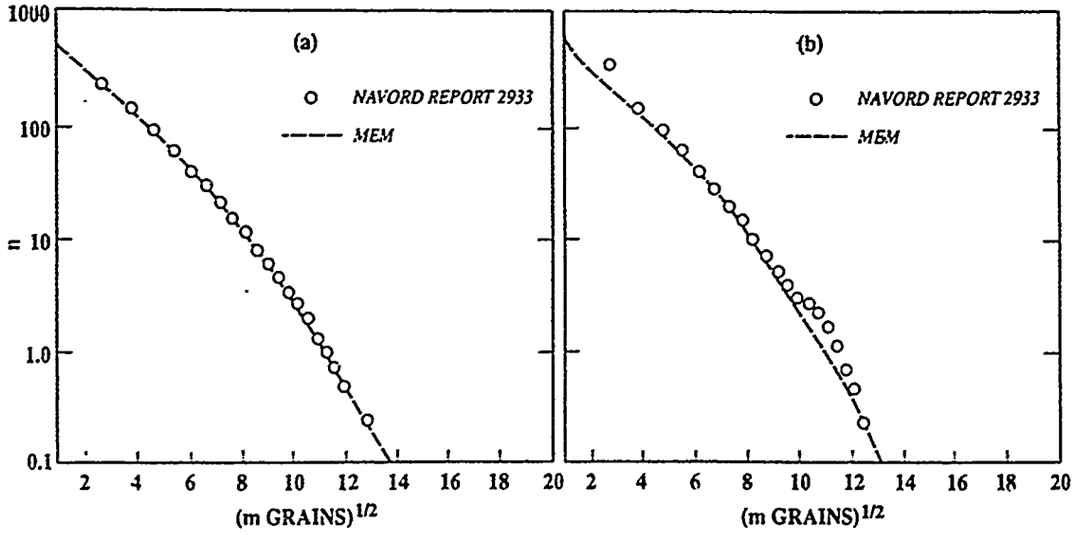

Figure 9. Distributions of fragments from an exploding metal shell versus the square root of the fragment mass (Sternberg 1973). The broken curves show two-dimensional MEM distributions, equation (71), in which a^2 represents the fragment mass and the parameters take the following values (in mass units of milligrains): (*a*) $A = 0.22$, $B = 0.05$, $C = 0.05$; (*b*) $A = 0.22$, $B = 0.05$, $C = 0.0625$.

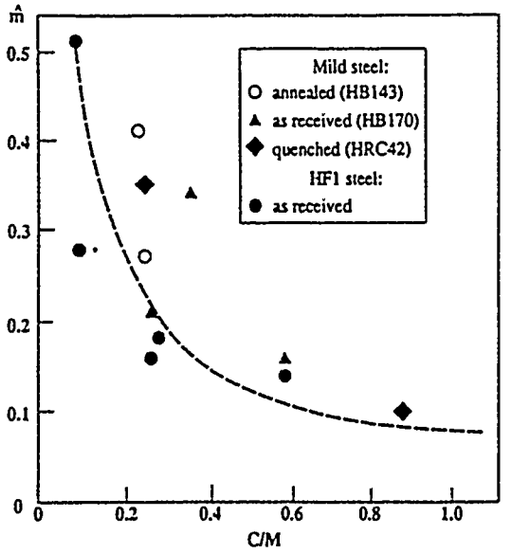

Figure 10. Mean mass $\hat{m}$ of mild-steel fragments versus the charge/metal mass C/M ratio (Stronge *et al* 1989). The broken curve shows the theoretical result of equation (73).

sional Mott distribution was assumed without obvious evidence. The mean mass decreased with C/M as seen in figure 10.

In the theory the most likely mass $\hat{m}$ ($\propto a^3$) varies with the strain rate as

$$\hat{m} \propto \dot{\varepsilon}^{-2}. \tag{72}$$

We can relate the explosive/metal mass ratio to the strain rate by using the Gurney relation (Jones *et al* 1980):

$$v_0 = [2G/(0.5 + M/C)]^{1/2} \tag{73}$$

where v_0 is the velocity with which the outer part of the cylinder moves and G is the

energy release by the explosive per unit mass. We associate the strain rate with v_0/inner cylinder radius and obtain from (72) and the expression for v_0

$$\hat{m} \propto 0.5 + (M/C). \tag{74}$$

The broken curve in figure 10 indicates quite reasonable agreement with the experimental data points.

On the basis of a large number of fragmentation experiments with exploding cylinders, Lin *et al* (1989) proposed a numerical fit for the number of fragments N_{tot} as a function of the dimension, hardness and composition of the cylinder and of C/M, the charge/metal mass ratio:

$$N_{tot} = 177t + 107CP - 0.39H + (C/M)(-3250 + 10462CP - 2.52H) + 34.5$$

where t is the thickness of the cylinder (cm), H its (Vickers) hardness and CP the carbon content percentage. (It is appropriate to remark here that Mott's involvement in the mechanism of fracture arose during the Second World War from his investigation into the difference between N_{tot} in Allied and German shells. Eventually it was all traced to CP, which increased the metal brittleness) (Mott 1984, private communication).)

6.2. Fragments in mining operations

It might be thought that a distribution with three free parameters, such as given by equations (10) and (19), is bound to agree with practically any experimental curve, especially when the cumulative distribution is plotted (on a logarithmic scale). The following example shows that this is not the case and that when sufficiently accurate data are plotted for a wide enough fragment size range the MEM distribution postulated in equation (10) can be discredited and, instead, another MEM distribution with different constraints appears to operate. Unfortunately, the latter constraints do not have any simple physical meaning.

Boreholes of 3.2 cm diameter were filled with Donarite and exploded in an underground site of the Rotem (Negev, Israel) oil-shale fields of the PaMA company (Jaeger *et al* 1986b). Post-explosion fragments were kept in place by chicken wire, collected from several locations and layers around the original boreholes, the pieces individually weighed and their distributions determined for each location. The derived distributions differed significantly, according to the distance of the locations from the centre and somewhat on their orientations (the terrain was anisotropic due to major faults). However, (quite remarkably) all distributions could be brought into coincidence by scaling the sizes at each location with a scale factor $\lambda(R)$ that increased monotonically with the distance R of the location from the borehole as $R^{1.75\pm0.3}$ (figure 11).

We have not found it possible to fit the collapsed distribution with any set of Lagrangian parameters appearing in equation (19). A least-squares fit of the parameters was not done, but the intuitively 'best' fits shown in the figure as broken curves are evidently inadequate to reproduce the results over the four decades of linear size variation. A MEM distribution of the form

$$n_a = \{\exp[(a/a_1) + b\log(a/a_0)] - 1\}^{-1} \tag{75}$$

was found to fit the observed cumulative weight distribution

$$\int_{a_0}^{a} \rho \dot{a}^3 n_a \, da$$

reasonably well, with the choice and interpretation of the parameters as follows:

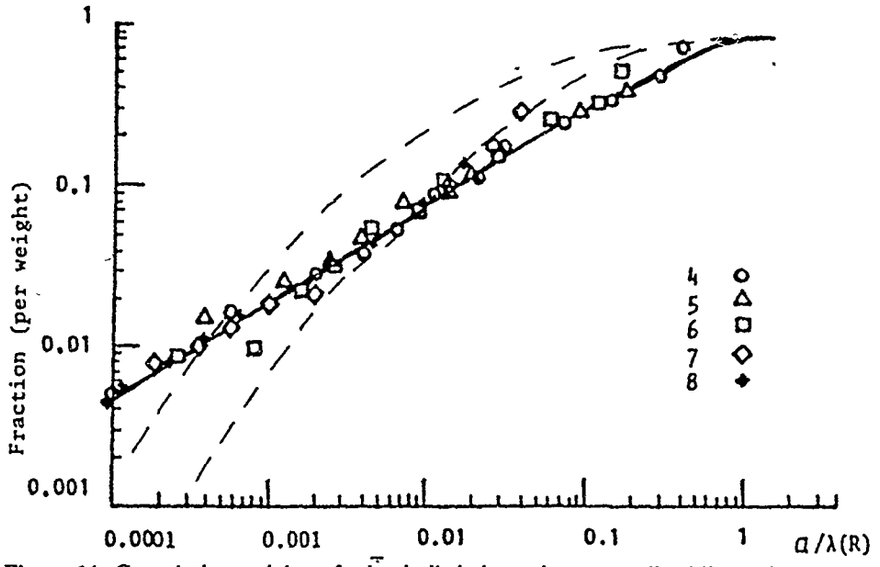

Figure 11. Cumulative weights of mined oil shale against normalized linear fragment size (Jaeger *et al* 1986b). Results from five regions, numbered according to increasing distance from the borehole, lie on the same curve when a length scale parameter $\lambda(R)$ is adjusted. The broken curves are based on equations (18) and (19), and are plainly inadequate. The full curve is obtained using equation (75) with parameters given in the text.

a_1 (upper cut-off of size) $= 2\lambda(R)$

a_0 (lower cut-off of size) $= 8 \times 10^{-5}\lambda(R)$

b (effective inverse power of distribution) $= 3.43$.

The two functions in n_a (a and $\log a$) indicate the existence of physical constraints (appendix 1) on the distribution. The constraint on a can be accorded some physical meaning in terms of dense cracks (along the lines of the discussion in section 4.1.3); however, the constraint related to $\log a$ is obscure.

In a similar type of experiment, though on a much smaller scale, Curran *et al* (1977) collected the ejecta from the crater formed by high explosives in contact with the surface of fine-grained quartzite rock. The number of fragments per unit fragment radius a, n_a, follows (for about five decades of variation in n_a) remarkably well the power-law relationship

$$n_a \propto a^{-2.1} \tag{76}$$

indicating the importance of the surface energy term (proportional to a^2) in equation (1). (Figure 4.10 in Curran *et al* (1987) shows the cumulative number of fragments. The theoretical fit in the figure suffers from identification of fragment and crack size distributions in their equation (4.6).) The surface term is indeed expected to dominate for small fragments ($a \ll \hat{a}$) and for such fragments we anticipate a power-law behaviour, like that in (76).

6.3. Distribution of space debris

Man-made debris in space exceeds the number of natural meteoroids and represents a danger to spacecraft (Kessler 1985, Rajendran and Elfer 1989). The fragments arise from defunct space vehicles that have broken up, exploded or become involved in collisions. Added to this are solid fuel particles. Three distributions are given as a function of the mass m (Johnson and McKnight 1987) or of the size s.

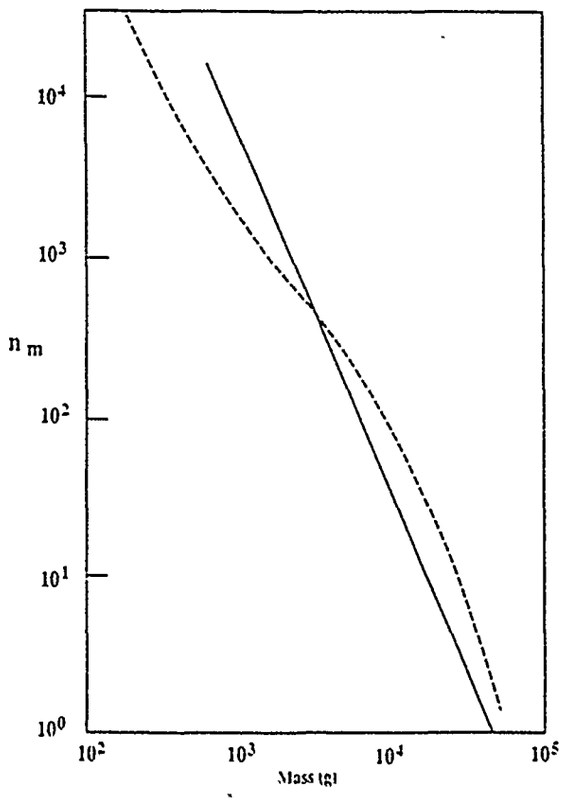

Figure 12. Distribution of masses in space due to defunct, broken-up satellites. Broken curve: observation (described in the text). Full curve: fit by a power law based on percolation theory.

Small fragments due to collisions have a power-law (fractal-like) distribution.

$$n_s = C_1 s^{-1.75}. \tag{77}$$

Larger fragments, but not exceeding 1960 g, follow the distribution

$$n_s = C_2 m^{-1/2} \exp(-0.0575 m^{1/2}) \tag{78}$$

with m in grams. For even larger fragments, caused mainly by explosions, one finds

$$n_s = C_3 m^{-1/2} \exp(-0.0205 m^{1/2}). \tag{79}$$

The coefficients C_1, C_2 and C_3 depend on the total masses included in the distribution and are not relevant to the expected distribution from a single event. In figure 12 we have combined the three distributions in one smooth curve and compared the resultant with the percolation result $n_s \propto s^{-2.2}$.

The experimental distribution drops slower than this prediction for small sizes and faster for larger fragments. In some sense, the prediction represents a simple averaging over the full range.

6.4. Charged atomic clusters

Clusters consisting of 10–10^2 atoms or molecules are of interest theoretically (as transition species between molecules and solids) and experimentally (e.g. as potential catalysts). A review of early results was given by Phillips (1986). Clusters can be formed from the gaseous phase by accretion or condensation after passing through a jet (Levinger *et al* 1988, Rayane *et al* 1989) or from an impacted solid by sputtering (Weiland *et al* 1989). The distribution of cluster masses can be obtained by time-of-flight mass spectrometry and depends on the conditions under which clusters form (e.g. the ambient

gas pressure). The distributions are frequently peaked (as in rare-gas clusters Ar_m^+) at magic numbers associated with favourable conditions for packing or with bunching of electronic (binding) energies (Knight *et al* 1984, Stephens and King 1981). The broad envelopes of mass distribution, which are our concern here, generally possess a maximum, though exceptions from this situation do exist. Thus, counts of positively charged uranyl acetate clusters decrease monotonically for cluster sizes of up to 50 units, while the negatively charged clusters show a maximum. Charged clusters are easier to observe in experiments than neutral ones.

Writing the MEM distribution as a function of the mass m in the form appearing in equation (19), namely

$$n_m = (e^{x(m)} - 1)^{-1} \tag{80}$$

where

$$x(m) = \sum_r a_r m^r \tag{81}$$

(cf equation (19)), we note that, for n_m to have a maximum at a non-zero mass, at least some of the exponents in the above sum must be negative. We recall that the energy equipartition constraint of Griffith (1943) described in section 3.1 led to a negative exponent $r = -1/3$.

This arose from supposing that the available energy was first distributed equally between all atoms or molecules, so that each atom absorbs a part of the order m^{-1} and then expends this on the surface energy (which is proportional to $m^{2/3}$). In addition, one can suppose that the absorbed energy is also expended on creating a transverse dynamic tension (analogous to the strain energy term in (10)) proportional to $m^{5/3}$. Then in the sum (81) one also has a term with exponent $r = 2/3$.

A fitting of expressions (80) and (81) to the mass distribution data of Levinger *et al* (1988) for Ar_m^+ was made, with the choice of the coefficients in (81), given (in Ar mass units) by

$$a_{-1/3} = 8.5 \qquad a_{2/3} = 15$$

(figure 13). Fits of similar goodness were achieved to other data obtained by the above authors for Ar_m^+ and by Rayane *et al* (1989) for positively charged indium and lead clusters, by choice of slightly different coefficients. The formation of small ions ($m < 5$) is probably due to factors not included in the energy constraint and for these the misfit is excusable. It is notable that the skewness of the experimental distribution is reproduced by the theory. To end this section, we wish to stress this adaptation of the MEM to fragment formation by growth, rather than by disintegration, as in the rest of this article.

6.5. Droplets

The distribution of droplets in a spray is important for the operation of fuel injection engines, for painting and elsewhere. The liquid column or sheet is unstable due to fluctuations and breaks into droplets that are subject to several forces (inertial, nozzle pressure, aerodynamic drag by the ambient gas). Studies have been made of droplet sizes and velocities as a function of pressure and distance along the flow and perpendicular to it. Experimental investigations use phase/Doppler techniques (Bachalo *et al* 1988, Sellens 1989). For a description of the subject, including an introduction to size distribution results, the book of Lefebvre (1989) is of use. MEM were applied to obtain the

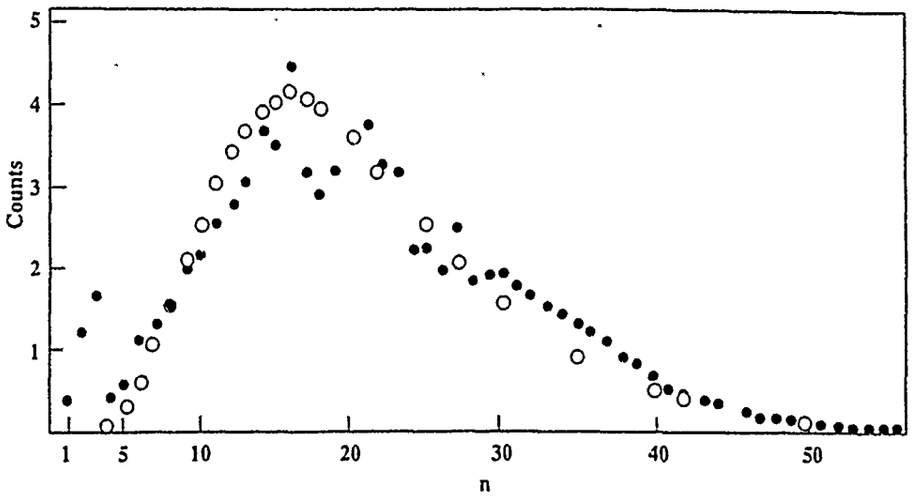

Figure 13. Counts of charged argon clusters against argon mass number n. Full circles: experimental data obtained by time of flight (Levinger *et al* 1988). Open circles: theoretical results (equations (80) and (81) with parameters shown in text).

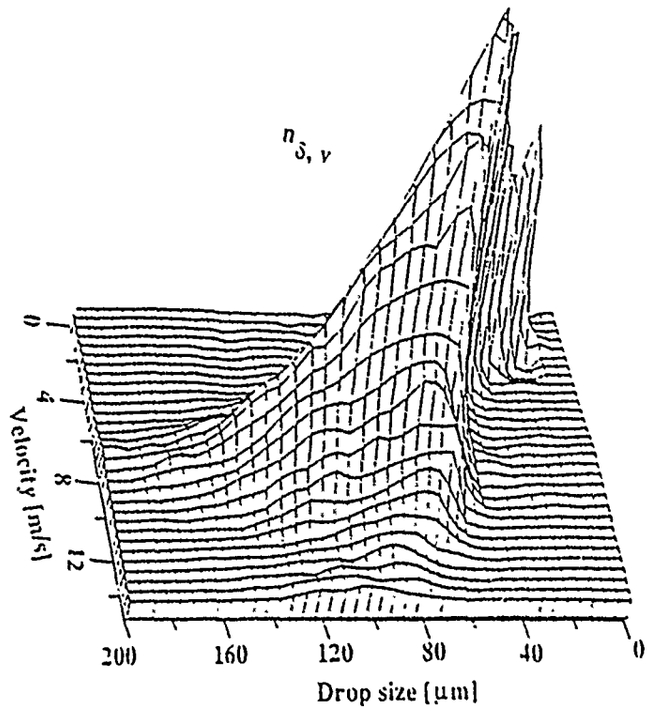

Figure 14. A typical surface of droplet distributions as a function of linear size and downstream velocity. (After Sellens (1989).)

joint, velocity size distribution function, employing constraints on the total mass, the surface energy, kinetic energy and total momentum (Sellens and Brzustowski 1986, Sellens 1989). It is, however, stated that 'it is simpler to measure the resulting spray, rather than the input conditions' (Sellens 1989). An example of the experimentally determined joint distribution is shown in figure 14 as a function of the droplet size δ (typically $10^2\,\mu$m) and velocity v. The theoretical distribution has the form shown in equation (A1.3), where ϕ are functions of δ and v entering the constraint expressions.

The marginal size distribution reproduces the observations satisfactorily, but in the v–δ correlations there are discrepancies. The use of correlations in MEM has been described (Englman *et al* 1988b). In the experiments the mean velocity decreases with droplet size, due to the aerodynamic drag being more effective for small droplets, while the prediction shows constancy (since the drag is not formulated as a constraint). This situation differs from that typical for fragmentation of solids, where smaller-sized fragments fly off faster than larger ones (Grady *et al* 1985). The latter result can in fact be regarded as a direct consequence of the momentum and kinetic energy constraints, which introduce the functions

$$\phi = v\delta^3 \qquad \text{and} \qquad v^2\delta^3$$

in the exponential in (A1.3), so that (the Lagrange multiplier λ^r being presumed positive) smaller sizes lead to higher speeds.

In a related subject, although many orders of sizes away, the condensation of interstellar clouds by fluctuations was considered (Kiguchi *et al* 1988, Narita *et al* 1988, Stahler 1983). Blobs, stars of 10^{-3}–10^{-1} solar masses, materialize by collapse and fragmentation, and so do rings of up to 10^2 solar masses from rotating clouds.

Returning to Earth, we note the exponential distributions with a low size cut-off in one-dimensional composite fibres (Wagner and Eitan 1990).

6.6. *Nuclear disintegration*

A percolational critical point has been shown to operate in nuclear disintegration (Campi 1988, Gross 1990). High-velocity gold ions impinging on emulsion produced a distribution of fragments with charges between 1 and 79 (= the number of charges on Au), observed by Waddington and Freier (1985). Campi (1988) has found correlations between the second, first and zeroth moments of the size distribution that strongly resembled the correlations in a percolative system near $p = p_c$. (Use was made of the relation (57) originally noted by him.)

The largest fragment in disintegration can be associated with the cluster that tends to percolate (i.e. extend throughout the media) at critical concentration p_c and whose mass density is known as the fractal dimension (Zallen 1983). In a finite-sized nucleus the largest fragment size is related to the total mass of the nucleus by finite size scaling (Stauffer 1979). By proper identification of the largest fragments and of p_c in the experimental data of several atoms, Campi (1989) has found a fractal dimension that agrees with that for the percolating cluster. In the same paper Campi proposed a valuable hypothesis, elaborated by Gross (1990), for the ergodicity of the percolation model, which is also pertinent to the ergodic behaviour underlying the use of MEM. According to this, the sudden fracturing event leaves the incipient fragments in an excited state, which probes all distributions in an ergodic fashion. At a later stage, a relaxation occurs in which mass distributions do not change any more.

7. Conclusions

Fragment distributions based on maximum entropy not only have theoretical soundness (alas, not universally acknowledged), but they also possess the merits of containing both probabilistic and physical components and of accommodating naturally exponential and inverse power behaviours (as a function of particle size). Various experimental

distributions have been well reproduced by MEM, though other *ad hoc* laws can do this too, except in the extremities of very small and large fragments. Some characteristics of empirical distributions (like fractal nature or possession of a hump) have their signature in MEM, leading (with some measure of certainty) to physically significant conclusions as to the breaking mechanism.

Concerning useful extensions of the subject, one envisages future uses of maximum entropy for non-equilibrium phenomena, like rates of catalytic reactions involving particulates or fluid flow in fragmented media.

Acknowledgments

I gladly affirm the strong supporting role of Zeev Jaeger in the preparation of this article and the value of advice received from Rafi D Levine. This work was supported in part by the US Air Force Office of Scientific Research, Air Force Systems Command, USAF, under Grant No. 83-0374. The US Government is authorized to reproduce and distribute reprints for Governmental purposes notwithstanding any copyright notation therein.

Appendix 1. On maximum entropy

A1.1. Basics

In the basic formulation of the maximum-entropy method (MEM) one maximizes the information entropy S with respect to the probabilities p_j of events j, subject to the R observational inputs or constraints written as:

$$\langle \phi^r \rangle = \sum_j p_j \phi^r(j) = \int p(j)\phi^r(j)\,\mathrm{d}_j \qquad r = 1, 2, \ldots, R. \tag{A1.1}$$

Summation or integration (for continuous variates) is over the range of variation.

Formally, and in practice, one maximizes the following function of probabilities, named Lagrangian (Rivier *et al* 1989):

$$L(\{p\}) = -\sum_j p_j \log p_j - \lambda^1\left(\sum_j p_j\phi^1(j) - \langle\phi^1\rangle\right) - \ldots - \lambda^R\left(\sum_j p_j\phi^R(j) - \langle\phi^R\rangle\right) \tag{A1.2}$$

obtaining for the MEM probabilities

$$p_j = \exp[-\lambda^1\phi^1(j) - \ldots - \lambda^R\phi^R(j)] \tag{A1.3}$$

in which the Lagrange multipliers are fitted to satisfy the constraints (A1.1). As already noted in the introduction, the MEM solution is characterized by a smooth behaviour as a function of j.

Examples of constraints are first, the normalization condition on the probabilities,

$$1 = \sum_j p_j = \int p(j)\,\mathrm{d}j \tag{A1.4}$$

and observed averages like

$$\langle j \rangle = \sum_j p_j j \qquad \text{and} \qquad \langle j^2 \rangle = \sum_j p_j j^2$$

etc. Acceptable constraints are also observed frequencies of events, in the form

$$\langle \delta_{jj_0} \rangle = \sum_j p_j \delta_{jj_0}. \tag{A1.5}$$

Because of the presence of the singular function δ_{jj_0} or $\delta(j - j_0)$ in the exponent of p_j in (A1.3), the MEM solution is in general no longer smooth, but is probably still more conservative than alternative non-MEM solutions.

In fact, the range of the variate j can also be written as a constraint, in the sense of zero frequency of occurrence outside the range.

A1.2. Priors $\Pi(j)$

These are introduced as generalizations of the summations over the events in (A1.2), with the purpose of weighting each event by a factor $\Pi(j)$, so that the entropy becomes

$$S_\Pi = -\sum_j \Pi(j) p_j \log p_j \tag{A1.6}$$

and a typical constraint

$$\langle \phi \rangle_\Pi = \sum \Pi(j) p_j \phi(j). \tag{A1.7}$$

The priors are weights ascribed *a priori* (that is, without regard to observations) to each event and correspond to 'measure' in set theory. Skilling (1989) writes about them thus: 'Π is the Lebesgue measure associated with [the variable], which must be given before an integral can be defined.' A possible probabilistic interpretation identifies the priors with subjective beliefs or reliance attached to the events. Physically, priors may be related to instrumental effects. An example of this is the photofragmentation studies of Ar_n^+ cluster ions (section 6.4). In making a statistic of the number of detached ions as a result of photoabsorption, the data must be weighted by the dependence of the photoabsorption cross section on the size (n) of the cluster ion (Levinger *et al* 1988).

If the priors are known or postulated there is no difficulty since one can proceed as follows. Let the weighted probabilities of events be denoted by

$$P_j = \Pi(j) p_j. \tag{A1.8}$$

Then we rewrite (A1.6) and (A1.7) as

$$S_\Pi = -\sum_j P_j \log P_j/\Pi(j) \qquad \text{and} \qquad \langle \phi \rangle_\Pi = \sum P_j \phi(j). \tag{A1.9}$$

We maximize the Lagrangian with respect to P_j. Equation (A1.8) is the solution, with p_j given in (A1.3). The functional form of the exponential part, i.e. the dependence

on $\phi^1, \phi^2, \ldots, \phi^R$, is not affected by the introduction of the prior, but the pre-exponential part is, and so are the numerical values of the Lagrangian multipliers, λ^1 to λ^R. This follows since these are given by the implicit equations

$$\langle \phi^r \rangle = \sum_j \phi^r(j) \Pi(j) \exp[-\lambda^1 \phi^1(j) - \ldots - \lambda^R \phi^R(j)] \tag{A1.10}$$

which contain Π. In the use of MEM as a pure predictive tool for natural phenomena, the dependence of the solution on the priors raises the question: 'Which is the best prior?' (Jeffreys 1961, Jaynes 1983, Englman *et al* 1988a). It seems that no satisfactory answer exists at this stage, except perhaps to say that the MEM solution is unique as far as its asymptotic exponential dependence is concerned but not regarding the prefactor.

The following, related problem appears to have been solved (Rivier *et al* 1989). Suppose that there exist a number K of possible priors (e.g. K alternative beliefs or hypotheses), given by

$$\Pi^k(i) \qquad k = 1, \ldots, K. \tag{A1.11}$$

What linear combination

$$\Pi(j) = \sum_{k=1}^{K} p^k \Pi^k(j) \tag{A1.12}$$

gives the best prior? 'Best' is to be considered in terms of incoming information, since before that information we suppose (democratically) that all priors have the same weight. The proposed solution relies on maximizing the following generalized functional of the event probabilities and of the weights p^k:

$$\mathcal{L}(\{P_j\}, \{p^k\}) = -\sum_j p_j \log P_j/\Pi(j) - \sum_r \lambda^r \left(\sum_j P_j \phi^r(j) - \langle \phi^r \rangle \right) - \nu \sum_{k=1}^{K} p^k \log p^k \tag{A1.13}$$

where Π is defined in (A1.12) and ν quantifies the credit accorded to the diversity of views relative to factual evidence. (Rivier *et al* (1989) assumed $\nu = 1$, which is as good a starting point as any.) The MEM weights are

$$p^k = \exp(X_k/\nu) \Big/ \sum_k \exp(X_k/\nu) \tag{A1.14}$$

where

$$X_k = \sum_j \Pi^k(j) \exp\left(-\sum_r \lambda^r \phi^r(j) \right) \tag{A1.15}$$

is the overlap between the prior Π^k and the exponential part of the MEM probability. The dependence of the weights p^k on the incoming evidence is through the expectation values $\langle \phi^r \rangle$ and the resulting values of λ^r.

It is interesting to compare this result with the Bayesian rule (Jaynes 1985, Jeffreys 1961, Skilling 1989)

$$P(k|\langle \phi \rangle) = P(k) P(\langle \phi \rangle | k) / P(\langle \phi \rangle) \tag{A1.16}$$

whose meaning in the present context is the following. The probability $P(k|\langle \phi \rangle)$ for the hypothesis (or prior) k, given that the mean has the observed value $\langle \phi \rangle$, is equal to the probability $P(k)$ of the same hypothesis, irrespective of the observation on $\langle \phi \rangle$,

multiplied by the probability $P(\{\phi\}|k)$ of obtaining $\{\phi\}$ on the basis of the k hypothesis and divided by the probability $P(\{\phi\})$ of obtaining the observation $\{\phi\}$ on the mean. The Bayesian interpretation of the result in (A1.14) and (A1.15) is then, in an obvious notation,

$$P(\{\phi\}|k) = \exp[X_k(\{\phi\})/\nu] \Big/ \sum_{\{\phi\}} \exp[X_k(\{\phi\})/\nu] \tag{A1.17}$$

$$P(\{\phi\}) = \sum_k P(\{\phi\})|k) \tag{A1.18}$$

$$P(k) = \sum_{\{\phi\}} \exp[X_k(\{\phi\})/\nu] \Big/ \sum_k \sum_{\{\phi\}} \exp[X_k(\{\phi\})/\nu]. \tag{A1.19}$$

We now recognize the merit of MEM as providing a systematic method for differentiation between alternative hypotheses (beliefs, physical mechanisms) on the basis of incoming evidence. The shortcoming of MEM is that much of our knowledge, understanding and 'feeling' for the behaviour of the physical system that is not phrased explicitly in the form of constraints receives no expression in the predictions.

Appendix 2. Fracture diversity

A2.1. Causes of fracture

Mechanical fracture is frequently the physical process that precedes and causes fragmentation, though such is not the case in droplet formation (section 6.5), photofragmentation, nuclear events (section 6.6), desorption, etc.

At the root of the fracture of solids is the breakage of atomic or molecular bonds. Simulations of the fracture process on this fundamental level have been numerous (Esterling 1979, Latanision and Pickens 1983, Paskin *et al* 1983, Thomson 1986, Thomson and Fuller 1982). There are three considerations that render this approach of limited scope or excessive difficulty. ('Clearly, for the near term, there is not likely to be a first-principles calculation of a crack tip' (Thomson 1986).)

(i) Subsequent to fracture there is a large-scale relaxation, i.e. shift of particle positions, in the solid surrounding the created discontinuity (or bond breakage) (Mai and Lawn 1987). Thus a presumed single-particle scission is in truth a many-particle effect. Owing to this and other causes, nominal atomic surface energy densities (the energy input needed to cut atomic bonds over a unit surface) exceed observed surface energy densities (the quantity that enters Griffith's expression for the fracture strength (Griffith 1920)) by two or three orders of magnitudes (Sih 1983).

(ii) The region in the vicinity of the crack tip shows (even in brittle solids) plastic behaviour. Such behaviour is difficult to model with elastic strings (obeying Hooke's law, at least up to a range, as is frequent practice in atomistic simulations) or to formulate fracture in the context of ordinary thermodynamics.

(iii) The applied stress that brings about breakage does so not by initiating and opening up a single void, but by giving birth to a number of microcracks (or microvoids, in ductile materials), which then interact and ultimately merge to propagate the macrocrack (Curran *et al* 1987). This viewpoint is becoming increasingly more firmly established as better observational techniques on the microevent length scale ($<1\ \mu$m) and fast timescales ($<10^{-9}$ s) are available (Bowling *et al* 1987, Faber *et al* 1988). In

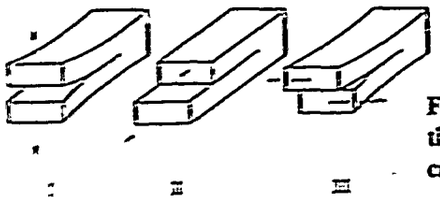

Figure 15. The three modes of fracture, showing the direction of the stresses with reference to the crack about to be opened.

fast processes (which cause most of the fragmentations treated in this review) the proliferation of microcracks is particularly decisive. This can be understood by the following argument.

Two events taking place in the solid at a separation of Δl develop independently of each other, provided the ratio propagation velocity/Δl is smaller than the relative strain rate $\dot{\varepsilon}/\varepsilon$ due to an externally applied force. With propagation or sound velocities of the order of $10^3\,\mathrm{m\,s^{-1}}$, strains $\varepsilon \sim 10^{-1}$ and strain rates $\dot{\varepsilon} > 10^6\,\mathrm{s^{-1}}$ (appropriate to explosive breakage), two cracks at distances larger than

$$\Delta l = 10^{-4}\,\mathrm{m} \tag{A2.1}$$

prefer to develop independently, rather than let stress release operate by the growth of one crack (presumably the larger one). Likely, the true distances are smaller than that in (A2.1).

A2.2. Fracture in real-life situations

Modalities of fracture in real-life situations are so multifarious that either an all-embracing treatment or one that is based on a single viewpoint is likely to court failure. Therefore, in the following brief essay we emphasize just the different varieties of modes and forms that fracture can take, as seen by several leading workers in the field. The putative moral from this exercise is that in view of the wide spectra of manifestations one is inevitably thrown back to a stochastic description, like that provided by MEM.

The three modes of external stress with respect to the fracture plane, shown in figure 15 and traditionally known as modes I, II and III, are perhaps the least relevant subdivision of fracture-causing processes, since in most of the fragmentation situations discussed in this review the imposed stress appears in mixed modes. This claim is supported by recent observation of crack types in indented ceramics where also the variety of observed cracking sequences has defied systematization in terms of the nature of the applied load (Cook and Pharr 1990). In talking about the initiation of microdefects, one should perhaps temper the claim for an excessive variety in the following sense. Theories of microvoid nucleation, pioneered by Raj and Ashby (1975) in the context of polycrystalline metals, apparently lead to the same, exponential microflaw size distribution (as a function of the linear flaw dimension), no matter what are the details of the flaw-producing mechanism (Curran *et al* 1987).

An important differentiation is between ductile and brittle fracture, the former being characteristic of most metals, metallic alloys and also of high temperatures and low strain rates, whereas the latter operates in rocks, ceramics, etc, at low temperatures and in fast processes (ubiquitously). Typical flaws are, respectively, voids and cracks. A seminal contribution to fracture processes in a metal ring was made by Mott (1947), who used momentum conservation to calculate the time that stress unloading requires to propagate away from the point of fracture until completion of

failure. For elaboration of this theory we refer to Kipp and Grady (1985). For brittle fracture the corresponding advances are due to Griffith (1920) and Irwin (1957), who formulated an energy-balance-based criterion for the run-away motion of cracks. This will happen when the release of stress energy around a growing crack (regarded as a free surface) exceeds the energy expenditure involved in the crack extension.

Using considerations similar to those given in the previous section regarding the rate dependence of defect activation, Grady and Kipp (1989) distinguished between fracture processes that are dominated by the input stress energy and those by the defect population density. In the former the rate of fracturing depends on the loading intensity; in the latter strengthening the load does not enhance fracture, since the number of microdefects is insufficient to respond to the added load and the energy gets diverted into other channels (like mass motion or heat). As a rule, high strain rates ($\dot{\varepsilon}$) ensure the creation of sufficiently dense defect population so that fracturing rate becomes energy-dominated, while low $\dot{\varepsilon}$ creates defect bottlenecks.

Experimentally observed crack-tip shapes fall into three broad categories that link the fracture process both to the brittle–ductile material characterization and to the emission of dislocations from and around the growing crack (Thomson 1986). Sharp knife-edged cracks cleave, have brittle characteristics and displace, but do not generate, dislocations as they advance; wedge-shaped cracks emit new distinctly oriented dislocations that advance to a free surface as the crack grows; finally, blunt or rounded crack tips emit a mixture of dislocations, typical of plastic behaviour. The implication of dislocations in crack motion is well recognized (it is akin to the molecular basis of gas thermodynamics), and the dislocation-based approach has had its successes in relating metal hardness to granularity (Hirth 1972). However, difficulties of treatment have so far prevented a broadly significant contribution to crack growth and fracture. Perhaps recent advances in lattice gauge theories might point to new directions, though at this stage this clearly seems a remote subject on which to pin our expectations (Kleinert 1989).

References

Aharony A, Levi A, Englman R and Jaeger Z 1986 *Ann. Isr. Phys. Soc.* 8 112

Bachalo W D, Rudoff R C and Brena de la Rosa A 1988 *AIAA 26th Aerospace Sciences Meeting (Reno, NA)*

Bianchi R, Capaccioni F, Cerroni P, Coradini M, Flamini E, Martelli G and Smith P N 1984 *Astron. Astrophys.* 139 1

Blackman M E and Goldsmith W 1978 *Int. J. Eng. Sci.* 16 1-99

Blink J A and Hoover W G 1985 *Phys. Rev.* A 32 1027

Bowling G D, Faber K T and Hoagland R G 1987 *J. Am. Ceram. Soc.* 70 849

Brandon D G 1988 *Materials at High Strain Rates* ed T Z Blazynski (London: Elsevier) pp 187–217

Campi X 1988 *Phys. Lett.* 208 351

—— 1989 *J. Physique Coll.* 50 CR-183

Capaccioni F, Cerroni P, Coradini M, di Martino M, Farinella P, Flamini B, Martelli G, Paolicchi P, Smith P N, Woodward A and Zappola V 1986 *Icarus* 66 4871

Cheng Z and Redner S 1988 *Phys. Rev. Lett.* 60 2450

Cook R F and Pharr G M 1990 *J. Am. Ceram. Soc.* 73 787

Curran D R, Seaman L and Shockey D A 1987 *Phys. Rep.* 147 1

Curran D R, Shockey D A, Seaman L and Austin M 1977 *Proc. Symp. on Planetary Cratering Mechanics—Impact and Explosion Cratering* ed D I Roddy, R O Pepin and R B Merrill (Oxford: Pergamon) p 1057

Davison L and Stevens A L 1972 *J. Appl. Phys.* 44 668

Davison L, Stevens A L and Kipp M E 1977 *J. Mech. Phys. Solids* 25 11
Dehn J 1981 *Aberdeen Proving Ground, Maryland, Report No.* ARBBL-TR-02332
Denbigh G and Denbigh J S 1985 *Entropy in Relation to Incomplete Knowledge* (Cambridge: Cambridge University Press)
Derrida B and Flyvbjerg H 1987 *J. Phys. A: Math. Gen.* 20 5273
Deutscher G, Zallen R and Adler J (ed) 1983 *Percolation structure and processes; Ann. Isr. Phys. Soc.* 5
Englman R, Jaeger Z and Levi A 1984 *Phil. Mag.* B 50 307
Englman R, Rivier N and Jaeger Z 1988a *Nucl. Phys.* B (Proc. Suppl.) 5A 345
—— 1988b *Phil. Mag.* B 56 751
Esterling D 1979 *Comments Solid State Phys.* 9 105
Faber K, Iwagoshi T and Ghosh A 1988 *J. Am. Ceram. Soc.* 71 C-399
Glenn L A and Chudnovsky A 1986 *J. Appl. Phys.* 59 379
Glenn L A, Gommerstadt B Y and Chudnovsky A 1986 *J. Appl. Phys.* 60 1224
Grady D E 1982 *J. Appl. Phys.* 53 322
Grady D E, Bergstresser T K and Taylor J M 1985 *Sandia Report No.* 85-1545
Grady D E and Kipp M E 1985 *J. Appl. Phys.* 58 1210
—— 1989 *Structural Failure* ed T Wierzbicki (New York: Wiley) ch 1
Griffith A A 1920 *Phil. Trans. R. Soc.* A 221 163
Griffith L 1943 *Can. J. Res.* 21 57
Gross D H E 1990 *Rep. Prog. Phys.* 53 605
Hirth J P 1972 *Metall. Trans.* 3 3047
Irwin G R 1957 *J. Appl. Mech.* 24 361
Jaeger Z and Englman R 1991 *Trans. ASME* No 1 at press
Jaeger Z, Englman R, Gur Y and Sprecher A 1986a *J. Mater. Sci. Lett.* 5 5
Jaeger Z, Englman R and Slotky D 1986b *Ann. Isr. Phys. Soc.* 8 517
Jaeger Z, Englman R and Sprecher A 1986c *J. Appl. Phys.* 59 40
Jaynes E T 1983 *Papers on Probabilities, Statistics and Statistical Physics* ed R D Rosenkrantz (Dordrecht: Reidel)
—— 1985 *Highly Informative Priors in Bayesian Statistics 2* ed J M Bernard *et al* (New York: Elsevier) pp 329–60
Jeffreys H 1961 *The Theory of Probability* 3rd edn (Oxford: Oxford University Press) ch III
Johnson N L and McKnight D S 1987 *Artificial Space Debris* (FL: Orbit) pp 35 and 73
Jones G E, Kennedy J E and Bertholf L D 1980 *Am. J. Phys.* 48 264
Kachanov L M 1986 *Introduction to Continuum Damage Mechanics* (Dordrecht: Martinus Nijhoff)
Kaufman J H, Melroy O R and Dimino G M 1989 *Phys. Rev.* A 39 1420–8
Kessler D J 1985 *Adv. Space Res.* 5 3
Kiguchi M, Narita S, Miyama S M and Hayashi C 1988 *Prog. Theor. Phys.* (Suppl.) 96 63
Kikuchi R 1970 *J. Chem. Phys.* 53 2713
Kipp M E and Grady D E 1985 *J. Mech. Phys. Solids* 33 399
Kipp M E, Grady D E and Chen E P 1980 *Int. J. Fract.* 16 471
Kleinert H 1989 *Gauge Field Theories in Condensed Matter* (Singapore: World Scientific)
Knight W D, Clemenger K, De Heer W, Saunders W, Chou M and Cohen M 1984 *Phys. Rev. Lett.* 52 2141
Kuszmaul J S 1986 *Sandia Report No.* 86-2427C
Latanision R and Pickens J (ed) 1983 *Atomistics of Fracture* (New York: Plenum)
Lefebvre A H 1989 *Atomization and Sprays* (New York: Hemisphere)
Levine R D 1985 *Theory of Chemical Reaction Dynamics* vol 4, ed M Baer (Boca Raton, FL: CRC) p 1
Levinger N E, Ray D, Alexander M L and Lineberger W C 1988 *J. Chem. Phys.* 89 5654
Lin X, Wei H-Z, Zhu H-S and Yu Q 1989 *Proc. 11th Int. Symp. on Ballistics (Brussels, May 1989)* vol 2, pp 569–75
MacAulay M A 1987 *Introduction to Impact Engineering* (London: Chapman and Hall)
Mai Y W and Lawn B R 1987 *J. Am. Ceram. Soc.* 70 289
McGrady E D and Ziff M 1987 *Phys. Rev. Lett.* 58 892
McHugh S 1983 *Proc. 1st Int. Symp. on Rock Fragmentation by Blasting (Lulea, Sweden)* vol 1, ed R Holmberg and A Rustan, pp 407–18
Mock W Jr and Holt W M 1983 *J. Appl. Phys.* 54 2344
Mott N F 1947 *Proc. R. Soc.* 189 A 300
Mott N F and Linfoot E H 1943 *Ministry of Supply (GB) Report* AC 3348
Narita S, Miyama S M, Kiguchi M and Hayashi C 1988 *Prog. Theor. Phys.* (Suppl.) 96 50

Paskin A, Som D K and Dienes G J 1983 *Acta Metall.* **31** 1253, 1841
Phillips J C 1986 *Chem. Rev.* **86** 619
Prigogine I 1978 *Science* **201** 777
Raj R and Ashby M F 1975 *Acta Metall.* **23** 653
Rajendran A M and Elfer N 1989 *Structural Failure* ed T Wierzbicki and N Jones (New York: Wiley) p 4
Ravid M and Bodner S R 1983 *Int. J. Eng. Sci.* **21** 577
Ravid M, Bodner S R and Holcman I 1987 *Int. J. Eng. Sci.* **25** 473
Rayane D, Melinon P, Cabaud B, Hoareau A, Tribollet B and Broyer M 1989 *J. Chem. Phys.* **90** 3295
Rice I 1975 *Constitutive Equations in Plasticity* ed A S Argon (Cambridge, MA: MIT Press) p 23
Rivier N, Englman R and Levine R D 1990 *Maximum Entropy and Bayesian Methods* ed P F Fougère (Dordrecht: Kluwer) pp 233–42
Rosenblatt-Roth M 1987 *C.R. Acad. Sci., Paris* **304** 343
—— 1988 *C.R. Acad. Sci., Paris* **306** 283
Seaman L, Gran J and Curran D R 1984 *Application of Fracture Mechanics to Cementitous Composites* ed S P Shah (NATO-ARW, Northwestern University, Evanston, IL)
Sellens R W 1989 *Part. Part. Syst. Charact.* **6** 17
Sellens R W and Brzustowski T A 1986 *Combust. Flame* **65** 273
Shannon C E 1948 *Bell Syst. Technol. J.* **27** 379
Shockey D A, Seaman L and Curran D R 1985 *Int. J. Fracture* **27** 145
Sih G C 1983 *Can. Fracture Conf.* **10** 65
Skilling J 1984 *Nature* **312** 382
—— 1989 *Maximum Entropy and Bayesian Methods* ed J Skilling (Dordrecht: Kluwer) pp 45–62
Stahler S W 1983 *Astrophys. J.* **268** 115
Stauffer D 1979 *Phys. Rep.* **54** 1
—— 1981 *Scaling Properties of Percolation Clusters (Lecture Notes in Physics 149)* (Heidelberg: Springer) pp 9–25
—— 1985 *Introduction to Percolation Theory* (London: Taylor and Francis)
Stephens P W and King J G 1981 *Phys. Rev. Lett.* **51** 1538
Sternberg H M 1973 *NOLTR Report 73-83* (INTIS, Springfield, VA)
Stronge W I, Xiaoing M and Lanting Z 1989 *Int. J. Mech. Sci.* **31** 811
Tate A 1967 *J. Mech. Phys. Solids* **15** 387
—— 1969 *J. Mech. Phys. Solids* **17** 141
Taylor L M, Kuszmaul J S and Chen E P 1985 *ASCE/ASME Mechanics Conf. (Albuquerque, NM, June 1985)* AMD vol 69, p 95
Thomson R 1986 *Physics of Fracture (Solid State Physics 39)* ed H Ehrenreich and D Turnbull (Orlando: Academic) pp 2–129
Thomson R and Fuller E 1982 *Fracture Mechanics in Ceramics* ed R C Bradt, D P H Hasselman and E F Lange (New York: Plenum)
Tikochinsky Y, Tishby N Z and Levine R D 1984 *Phys. Rev. Lett.* **52** 1357
Titterington D M 1984 *Nature* **312** 381
Tuler F R and Butcher B M 1968 *Int. J. Fracture Mech.* **4** 431
Turcotte D L 1986 *J. Geophys. Res.* **91** 1921
Waddington C J and Freier P S 1985 *Phys. Rev.* C **31** 888
Wagner H D and Eitan A 1990 *Appl. Phys. Lett.* **56** 1965
Weiland P, Wien K, Della-Negra S, Depaw J, Joret H and Le Beyec Y 1989 *J. Physique Coll.* **50** C2 141
Weiner R J and Rogers H C 1979 *J. Appl. Phys.* **50** 8025
Yatom H and Ruppin R 1989 *J. Appl. Phys.* **65** 112
Zallen R 1983 *The Physics of Amorphous Solids* (New York: Wiley)
Ziff R M and McGrady E D 1986 *Macromolecules* **19** 2513
Zurek W H 1989 *Phys. Rev.* A **40** 4731

PCS—MS 974 MB-8/5/91

J. Phys. Chem. Solids Vol. 00, No. 0, pp. 000–000, 1991
Printed in Great Britain.

GRÜNEISEN PARAMETERS OF A CRACKED SOLID

R. RUPPIN
Soreq Nuclear Research Center, Yavne 70600, Israel

(*Received* 6 *August* 1990; *Accepted* 13 *March* 1991)

Abstract—A method for calculating the dependence of the Grüneisen parameters of a cracked solid on crack density is presented. The method utilizes the effective elastic moduli, for which two alternative theories are employed, the self-consistent scheme and the differential scheme. Numerical calculations indicate that the Grüneisen parameters decrease with increasing crack density, the rate of decrease being higher for the self-consistent scheme.

Keywords: Grüneisen parameter, cracks, Debye model, effective elastic constants.

1. INTRODUCTION

The purpose of the present work is to calculate the Grüneisen parameter of an elastic body containing many disordered micro-cracks. Since cracked solids may be viewed as a particular subset of composite materials, we first recall what is known about the Grüneisen parameter of the latter. Budiansky [1] has presented a theory for evaluating the Grüneisen parameter γ of composites consisting of a random mixture of a number of constituents, with roughly spherical particles. His method was a natural extension of previous self-consistent calculations of the elastic constants of a composite medium [2]. However, his formula for γ contains parameters which are not easily related to experimentally measurable quantities.

Many methods for calculating the effective elastic moduli of cracked solids have been presented in the literature [3–9], but none of these seems to have been extended for the purpose of evaluating γ. We present here a simple scheme for extending any given theory for the effective elastic moduli, so as to enable the calculation of the dependence of γ on crack density. The only experimental parameters that are required are the elastic moduli of the uncracked solid and their pressure derivatives. We apply this procedure to two effective elastic moduli theories, the self-consistent scheme (SCS) [4] and the differential scheme (DS) [7, 9], and present examples of calculations of γ as a function of crack density.

2. EFFECTIVE ELASTIC MODULI AND THEIR PRESSURE DERIVATIVES

We consider an elastic and isotropic solid which is permeated by many flat cracks. The distributions of the sizes, locations and orientations of the cracks are assumed to be random, so that the cracked body is macroscopically isotropic and homogeneous. The proposed method for evaluating γ utilizes the effective elastic moduli and their pressure derivatives. From the many available methods for calculating the effective moduli we employ here two representative ones, one of the SCS type and one of the DS type. While in both theories the effective elastic moduli decrease with increasing crack density, the most obvious difference between the two schemes is that in SCS the effective moduli vanish at a finite value of the crack density [4], whereas in the DS they vanish only asymptotically with increasing crack density [9]. It is not our purpose here to discuss the merits and disadvantages of the two methods, but simply to point out that each of them can be employed as a basis for the evaluation of the dependence of γ on crack density.

(*a*) *Self-consistent scheme*

We employ the well-known version of Budiansky and O'Connell [4]. For a solid containing flat circular cracks the effective bulk modulus $\bar{K}$ is related to the bulk modulus K of the undamaged solid by

$$\frac{\bar{K}}{K} = 1 - \frac{16}{9}\left(\frac{1-\nu\bar{\nu}^2}{1-2\nu\bar{\nu}}\right)\epsilon. \tag{1}$$

Here $\bar{\nu}$ is the effective Poisson ratio and ϵ is the crack density parameter. For circular cracks $\epsilon = N\langle a^3\rangle$, where N is the number of cracks per unit volume, a is the crack radius and the angular brackets denote an average. The effective shear modulus $\bar{G}$ is related to G by

$$\frac{\bar{G}}{G} = 1 - \frac{32}{45}\frac{(1-\bar{\nu})(5-\bar{\nu})}{(2-\bar{\nu})}\epsilon \tag{2}$$

and the dependence of $\bar{\nu}$ on ϵ is given by

$$\epsilon = \frac{45}{16}\frac{(\nu-\bar{\nu})(2-\bar{\nu})}{(1-\bar{\nu}^2)[10\nu-\bar{\nu}(1+3\nu)]}. \tag{3}$$

Differentiating (1)–(3) with respect to pressure we obtain

$$\frac{\partial \bar{K}}{\partial P} = \frac{\bar{K}}{K}\frac{\partial K}{\partial P} + \frac{32\epsilon}{9}\bar{K}\frac{\bar{\nu}-1-\bar{\nu}^2}{(1-2\bar{\nu})^2}\frac{\partial \bar{\nu}}{\partial P} \tag{4}$$

$$\frac{\partial \bar{G}}{\partial P} = \frac{\bar{G}}{G}\frac{\partial G}{\partial P} + \frac{32\epsilon}{45}G\frac{(2-\bar{\nu})(6-\nu-\bar{\nu})-(1-\nu)(5-\bar{\nu})}{(2-\bar{\nu})^2}\frac{\partial \bar{\nu}}{\partial P}. \tag{5}$$

$$\frac{\partial \bar{\nu}}{\partial P} = \frac{(1-\bar{\nu}^2)(2-\bar{\nu})[(\nu-\bar{\nu})(10-3\bar{\nu})-10\nu+\bar{\nu}(1+3\nu)]}{(1-\nu^2)[10\nu-\bar{\nu}(1+3\nu)](2\bar{\nu}-2-\nu)-(\nu-\bar{\nu})(2-\bar{\nu})[(1+3\nu)(7\bar{\nu}^2-1)-20\nu\bar{\nu}]}\frac{\partial \nu}{\partial P}. \tag{6}$$

No pressure derivative of ϵ appears in these equations because $\partial\epsilon/\partial P = 0$. The long dimensions of a crack are unaffected by hydrostatic pressure applied to the surrounding medium [10] and the crack density parameter does not depend on the width of the small opening between opposite crack faces. Equations (1)–(6) enable us to calculate the effective elastic moduli and their pressure derivatives, using the corresponding parameters of the uncracked solid.

(b) *Differential scheme*

We employ the DS results for a body containing penny-shaped cracks [7, 9]. The effective moduli are given by

$$\frac{\bar{K}}{K} = \left(\frac{1-2\nu}{1-2\bar{\nu}}\right)\left(\frac{\bar{\nu}}{\nu}\right)^{16/9}\left(\frac{3-\nu}{3-\bar{\nu}}\right)^{1/9} \tag{7}$$

$$\frac{\bar{G}}{G} = \left(\frac{1+\nu}{1+\bar{\nu}}\right)\left(\frac{\bar{\nu}}{\nu}\right)^{16/9}\left(\frac{3-\nu}{3-\bar{\nu}}\right)^{1/9} \tag{8}$$

$$\epsilon = \frac{5}{128}\ln\left(\frac{3-\bar{\nu}}{3-\nu}\right) + \frac{15}{64}\ln\left(\frac{1-\bar{\nu}}{1-\nu}\right) + \frac{45}{128}\ln\left(\frac{1+\bar{\nu}}{1+\nu}\right) - \frac{5}{8}\ln\frac{\bar{\nu}}{\nu} \tag{9}$$

Differentiating (7)–(9), again using $\partial\epsilon/\partial P = 0$, we obtain

$$\frac{\partial \bar{K}}{\partial P} = \bar{K}\left\{\frac{1}{K}\frac{\partial K}{\partial P} - \frac{\partial \nu}{\partial P}\left[\frac{2}{1-2\nu}+\frac{1}{9(3-\nu)}+\frac{10}{9\nu}\right] + \frac{\partial \bar{\nu}}{\partial P}\left[\frac{2}{1-2\bar{\nu}}+\frac{1}{9(3-\bar{\nu})}+\frac{10}{9\bar{\nu}}\right]\right\} \tag{10}$$

$$\frac{\partial \bar{G}}{\partial P} = \bar{G}\left\{\frac{1}{G}\frac{\partial G}{\partial P} + \frac{\partial \nu}{\partial P}\left[\frac{1}{1+\nu}-\frac{10}{9\nu}-\frac{1}{9(3-\nu)}\right] - \frac{\partial \bar{\nu}}{\partial P}\left[\frac{1}{1+\bar{\nu}}-\frac{10}{9\bar{\nu}}-\frac{1}{9(3-\bar{\nu})}\right]\right\} \tag{11}$$

$$\frac{\partial \bar{\nu}}{\partial P} = \frac{F(\nu)}{F(\bar{\nu})}\frac{\partial \nu}{\partial P} \tag{12}$$

$$F(x) = \frac{1}{x}+\frac{3}{8(1-x)}-\frac{9}{16(1+x)}+\frac{1}{16(3-x)}. \tag{13}$$

Equations 7–13 again provide a scheme for calculating the effective elastic moduli and their pressure derivatives.

3. GRÜNEISEN PARAMETERS

We first recall some properties of the Grüneisen parameter of perfect, uncracked solids. The Grüneisen parameter γ, which appears in the Mie–Grüneisen equation of state, can be expressed in the form [11]

$$\gamma = \frac{\alpha K}{C_v \rho}, \tag{14}$$

where α is the volume coefficient of thermal expansion, C_v is the specific heat at constant volume and ρ is the density. Equation (14) is convenient for evaluating γ from parameters for which experimental data are usually available. For our purpose of calculating the dependence of γ on crack density we find it more expedient to start from the more basic relation [11]

$$\gamma = \sum_i c_i\gamma_i \Big/ \sum_i c_i, \tag{15}$$

which expresses γ in terms of the microscopic γ_i of the lattice vibrational modes. The mode Grüneisen parameters are defined by

$$\gamma_i = -\frac{\partial \ln \nu_i}{\partial \ln V}. \tag{16}$$

where ν_i is the frequency and c_i the Einstein heat capacity of the i-th normal mode. The summations in (15) are taken over all the normal modes of the lattice. Calculations of γ_i for all acoustic and optical modes have been performed for some solids using detailed lattice dynamical models [12–19]. For cracked solids such an approach will be impracticable and we therefore resort to a Debye type approximation, in which the summations are taken only over the three acoustic branches, which are assumed to be non-dispersive. For an acoustic mode characterized by an elastic constant C_i the mode Grüneisen parameter is given by the Smith formula [20]

$$\gamma_i = -\frac{1}{6}+\frac{K}{2C_i}\frac{\partial C_i}{\partial P}. \tag{17}$$

For an isotropic solid there are only two sound velocities, the shear velocity v_s, given by $\rho v_s^2 = G$, and the compressional velocity v_p, given by $\rho v_p^2 = K + 4G/3$. The corresponding Grüneisen parameters are given by:

$$\gamma_s = -\frac{1}{6} + \frac{K}{2G}\frac{\partial G}{\partial P} \tag{18}$$

$$\gamma_p = -\frac{1}{6} + \frac{K}{2\left(K + \frac{4G}{3}\right)}\frac{\partial\left(K + \frac{4G}{3}\right)}{\partial P}. \tag{19}$$

At very low temperatures only the non-dispersive acoustic modes are excited and the specific heat weighting in eqn (15) may be replaces by a v^{-3} weighting, where v is the wave velocity. The low temperature limit, γ_L, of the Grüneisen parameter is therefore given by

$$\gamma_L = \frac{1}{2+\alpha}(\alpha^3\gamma_p + 2\gamma_s), \tag{20}$$

where $\alpha = v_s/v_p$. For the high temperature Grüneisen parameter γ_H the Debye model yields the simple average

$$\gamma_H = \tfrac{1}{3}(\gamma_p + 2\gamma_s). \tag{21}$$

While expression (20) for γ_L is exact, eqn (21) for γ_H is an approximation. Nevertheless, for a number of materials γ_H lies close to the room temperature value of γ, as determined experimentally from (14).

So far we have discussed the Grüneisen parameters of the perfect solid ($\epsilon = 0$). The dependence of the Grüneisen parameters on crack density is obtained by replacing $K, G, \partial K/\partial P$ and $\partial G/\partial P$ in all the formulae of this section by $\bar{K}$, $\bar{G}$, $\partial\bar{K}/\partial P$ and $\partial\bar{G}/\partial P$, respectively. The latter quantities are calculated by the methods described in section 2.

4. NUMERICAL RESULTS AND DISCUSSION

We present the results of calculations of the dependence of the Grüneisen parameters on crack density for the minerals periclase and lime. They were chosen as examples because for $\epsilon = 0$ their calculated high temperature Grüneisen parameters γ_H agree well with the experimental room temperature values obtained from (14) [21]. Thus, we may expect γ_H to provide a good estimate of γ also for the cracked solid. For the uncracked solid elastic moduli and their pressure derivatives the data compiled by Anderson *et al.* [21] have been employed. For each material both SCS and DS calculations were performed. The calculated

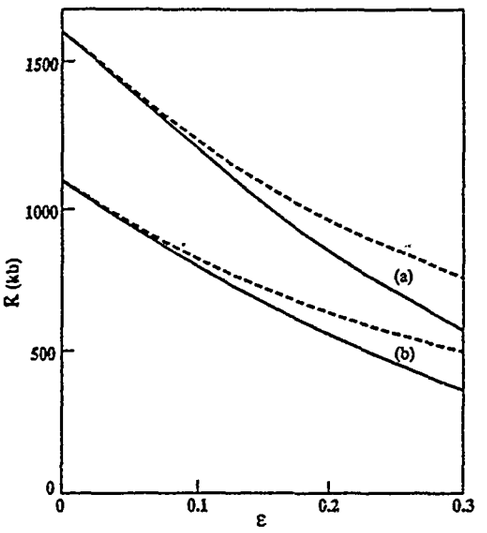

Fig. 1. Calculated dependence of the effective bulk modulus on crack density for: (a) periclase; (b) lime. Full curves—SCS; dashed curves—DS.

dependence of the effective moduli $\bar{K}$ and $\bar{G}$ on crack density is shown in Figs 1 and 2, respectively. The Grüneisen parameters are shown in Figs 3–6. We find that the Grüneisen parameters decrease with increasing crack density. The rate of decrease is higher in the SCS than in the DS. In this respect the qualitative benaviour is similar to that of the effective elastic moduli (Figs 1 and 2), which also decrease faster in the SCS.

Acknowledgements—This work was sponsored in part by U.S. Air Force Systems Command, USAF under Grant No. 89-0374.

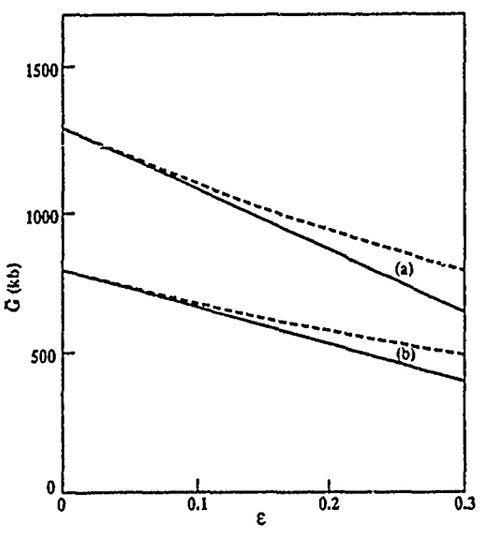

Fig. 2. Calculated dependence of the effective shear modulus on crack density for: (a) periclase; (b) lime. Full curves—SCS; dashed curves—DS.

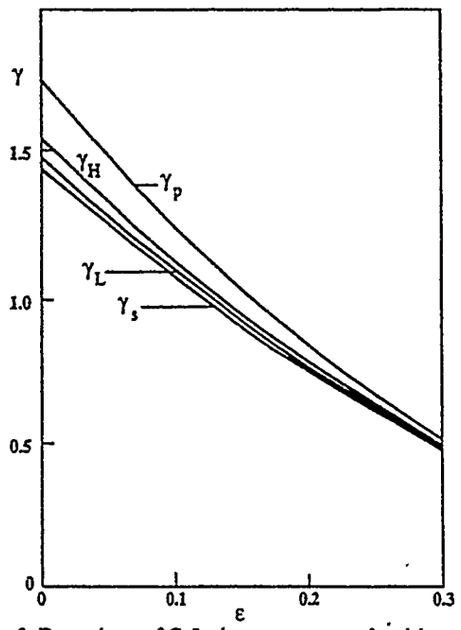

Fig. 3. Dependence of Grüneisen parameters of periclase on crack density, as calculated from the SCS.

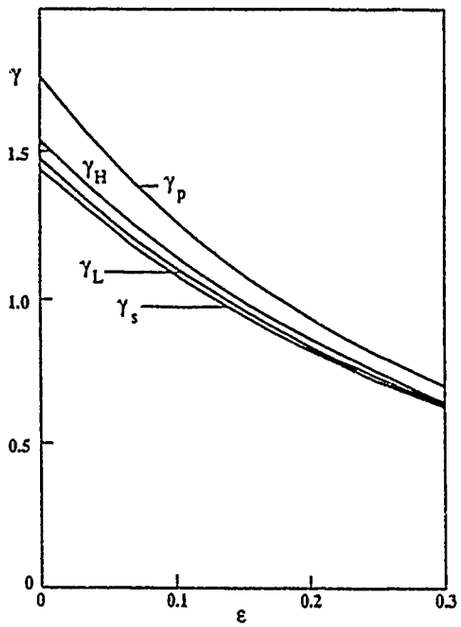

Fig. 4. Dependence of Grüneisen parameters of periclase on crack density, as calculated from the DS.

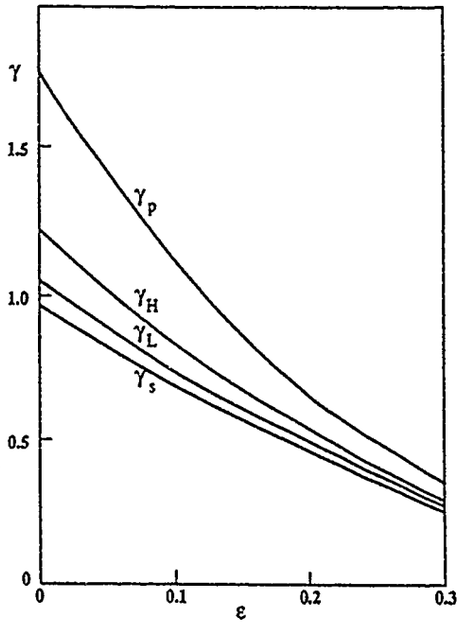

Fig. 5. Dependence of Grüneisen parameters of lime on crack density, as calculated from the SCS.

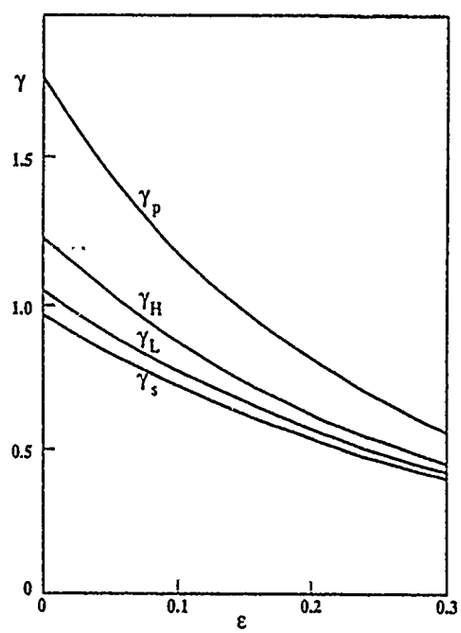

Fig. 6. Dependence of Grüneisen parameters of lime on crack density, as calculated from the DS.

REFERENCES

1. Budiansky B., *J. Comp. Mater.* 4, 286 (1970).
2. Budiansky B., *J. Mech. Phys. Solids* 13, 223 (1965).
3. Walsh J. B., *J. geophys. Res.* 70, 381 (1965).
4. Budiansky B. and O'Connell R. J., *Int. J. Solids Struc.* 12, 81 (1976).
5. Christensin R. M., *Mechanics of Composite Materials.* Wiley, New York (1979).
6. Walsh J. B. and Grosenbaugh M. R., *J. geophys. Res.* 84, 3532 (1979).
7. Zimmerman R. W., Ph.D. Thesis, University of California, Berkely (1984).
8. Laws N. and Brockenbrough J. R., *Int. J. Solids Struct.* 23, 1247 (1987).
9. Hashin Z., *J. Mech. Phys. Solids* 36, 719 (1988).
10. Berg C. A., *J. geophys. Res.* 70, 3447 (1965).
11. Slater J. C., *Introduction to Chemical Physics.* McGraw Hill, New York (1939).
12. Barsch G. R. and Achar B. N. N., *Phys. Stat. Sol.* 35, 881 (1969).
13. Vetelino J. F., Namjoshi K. V. and Mitra S. S., *J. appl. Phys.* 41, 5141 (1970).

14. Vetelino J. F., Mitra S. S. and Namjoshi K. V., *Phys. Rev.* B2, 2167 (1970).
15. Ruppin R. and Roberts R. W., *Phys. Rev.* B3, 1406 (1971).
16. Achar B. N. N. and Barsch G. R., *Phys. Rev.* B3, 4352 (1971).
17. Ruppin R., *J. Phys. Chem. Solids* 33, 83 (1972).
18. Ruppin R., *J. Phys. Chem. Solids* 33, 945 (1972).
19. Hardy R. J. and Karo A. M., *Phys. Rev.* B7, 4696 (1973).
20. Schedule D. E. and Smith C. S., *J. Phys. Chem. Solids* 25, 801 (1964).
21. Anderson O. L., Schreiber E., Liebermann R. C. and Soga N., *Rev. Geophys.* 6, 491 (1968).

PART 7

R. Englman:

"Statistical Models for the Fracture of Disordered Media" Edited by H.J. Herrmann and S. Roux (North Holland, Amsterdam, 1990)

A Review for J. Statistical Physics.

The book divides easily into three parts: An introductory one, an experimental part (or, more accurately, a material science part) and, finally, the detailed description of several theoretical models.
Most of the introductory chapters are written by the editors and are a joy to read: especially for being shown how engineering concepts are moulded into physical thinking or language (like thermodynamic energy, duals, localization, renormalization, scaling, etc.)
The experimental sections focus on the dependencies of material properties on parameters like temperature, composition, morphology, manufacture, treatment, changes in microstructure, process rates.

When one reaches the theoretical papers one is confronted with the realization that these hardly ever address the real problems and the questions that occupy practitioners. (In essence, these questions add up to one: how to produce materials that have improved material properties. In the ceramic - fish diagram on page 44 each scale stands for a real-life problem that awaits solution. Needless to say that scaling-laws do not provide this. An exception is the article on fragmentation, which is geared to communition processes, though only in a qualitative fashion.However, in another article (on randomness) one experimental figure, about twenty years old, is all that is presented in "support" of 25 pages of results from models.

It is clear that fracture is a difficult subject whose complexities have defied 70 years of research. The approach in this book (and the uniformity of the articles bemuses the reader) breaks away from the traditional, for reasons that (I would hazard) are rooted in the shine and lure of modern

has so few experimental facts for its support, a more balanced choice of the articles would have been justified in a book of this title. Both "Statistical models" and "Disorder" are also present in the approaches of Atkins, Evans, Kachanov, Lawn, Mai, Rice, where disorder enters in the form of microcracks, voids, stress distributions either before or after the application of external stresses.

In many of the simulations described in the book there are springs or beams (that oppose fracture or bending on a basic level), and it is not clear how these relate to the primary bonds that characterize the material The question is not pedantic, since it is these primary bonds that the material scientist aims at changing (by introduction of new constituents, additives or reinforcements) to meet his ends. Similarly, it is not evident how the primary length unit in the simulation is chosen (in cases other than granular solids, in which the grain may, but not necessarily does, define a fundamental length scale). One supposes that an averaging of some material property over some domain in the medium is implied and that the size of this domain defines the basic length scale. But this is not discussed and one wonders in view of instability of some cracks whether the length unit ought not to depend on stress or on some other parameter.

A quotation from page 150 in the book well summarizes the situation: "The authors have presented their belief of what the Truth is, but the reader should keep in mind that there are other competing Truths around."

PART 8

Fracture in granular materials with geometrical disorder

(Work performed by M. Lemanska, Z. Jaeger and R. Englman)

A two dimensional model of solids consisting of polygonal grains has been constructed by Voronoi-tessellation. This means that (up to 2000) points were chosen randomly in a plane and, by joining up the perpendicular bisectors that link neighboring points, the plane was divided into polygons of different sizes and shapes (Figure 1). The average number of sides in the polygons is 6. For a theory of side distribution in 2D and in 3D see Ref. 1. The present, Voronoi-tessellation is a reasonable approximation to disordered multiphase structures containing irregular grains. More precisely, it is deemed superior to alternative models in which disorder enters through randomness of bond strengths in a geometrically regular (e.g. square or triangular) lattice.

Fracture is simulated by applying either a fixed stress or a fixed elongation (constant strain) at two parallel edges and calculating the elongation in each bond for a harmonic, central force model of springs.

One or more bonds break when their calculated extensions or relative extension, (defined as the ratio of the extension to the original bond length) exceed a certain value. Then the stress or strain is reapplied or is raised until newer bonds breaks (and in fact they do so with greater facility since the broken bonds no longer support the stress). The procedure is repeated until one gets a continuous domain of broken bonds cutting across the sample, which is then considered fractured.

Several parameters of the fracture process are computed, such as:

(a) the least stress or strain which causes fracture (the fracture stress or strain),

(b) The number of bonds that are broken at each stage of the fracture process,

(c) the location of the broken bonds (Fig. 2)

(d) the distribution of broken bonds as function of their length (Fig. 3).

(e) the number of bonds broken at rupture as function of sample size (Fig. 4) and of other parameters.

The work is still in progress, with a view of gaining insight into the connection between microproperties and breakdown strength. Still, one can already derive from Fig. 4. an important connection between the present Voronoi model and the numerically much more extensively studied regular lattice models with strength disorder:

In the latter at breakdown, the number of fractured bonds n_f is found to be related to the linear size L of the system by:

$n_f \propto L^{7/4}$ (Ref. (3))

The slope of 1.85 in Fig. 4 is quite close to this, showing the similarity in the breakdown behavior of solids that are elastically and geometrically disordered.

(1) N. Rivier, J. de Physique, Colloque C9, 43, C9 (1982).

(2) P.M. Duxbury, "Breakdown of diluted and hierarchical systems" in "Statistical Models for the Fracture of Disordered Media", H.J. Herrmann and S. Roux, Editors (Elsevier - North Holland, Amsterdam 1990).

(3) L. de Arcangelis, A. Hansen, H.J. Herrmann and S. Roux, Phys. Rev. B 40, 877 (1989).

Figure Captions

Fig. 1. Voronoi-tessellation
A relatively small number of points (70, numbered 1–70) are placed randomly in the plane and the area sub-divided into polygons (as described in the text).

Fig. 2. Fracture in a disordered structure.
In the last of three steps (achieved by successively reapplying the strain) the structure is ruptured by intragranular cracking. Full lines are normal to intact intragranular surface. Broken lines represent cracked surfaces normal to the lines.

Fig. 3. Histogram of broken bonds as function of the original bond length at fracture. The data represent averaging over several runs. The criterion for bond rupture is that the relative elongation δ of bonds exceeds 0.2. The distribution of original lengths is also shown by broken lines and the percentage of bonds broken by dotted lines. In our model short bonds have a preference for being broken.

Fig. 4. Log-log plot of the number of broken bonds (at rupture of the sample) versus the square root of the number of Voronoi polygons (essentially, the linear size of the system)
The slope of the line is about 1.85.

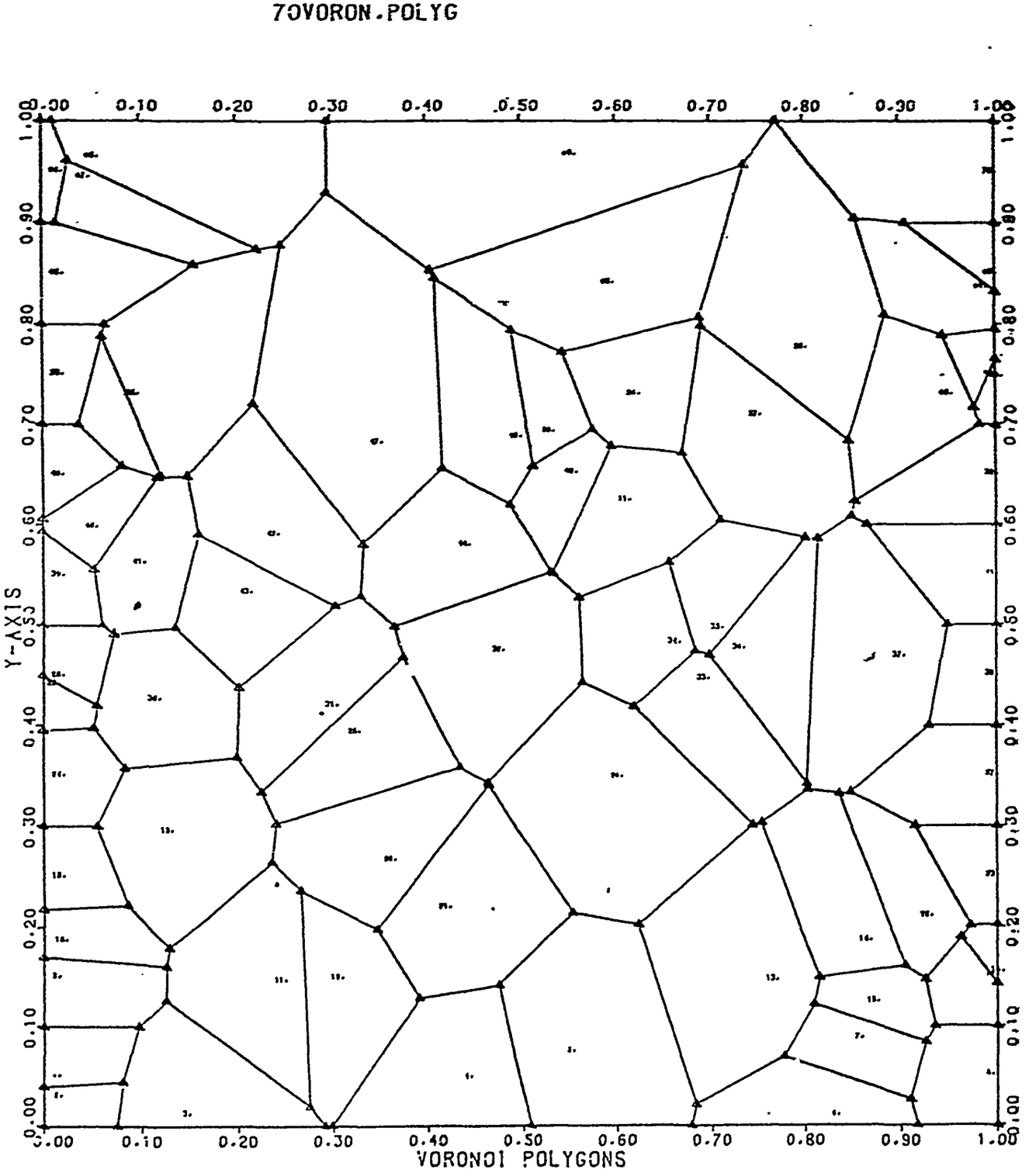
VOVORON.POLYG
0.00
0.10
0.20
0.30
0.40
0.50
0.60
0.70
0.80
0.90
1.00
Y-AXIS
VORONOI POLYGONS

Fig. 1

70 VORON POLYG.

STEP 1

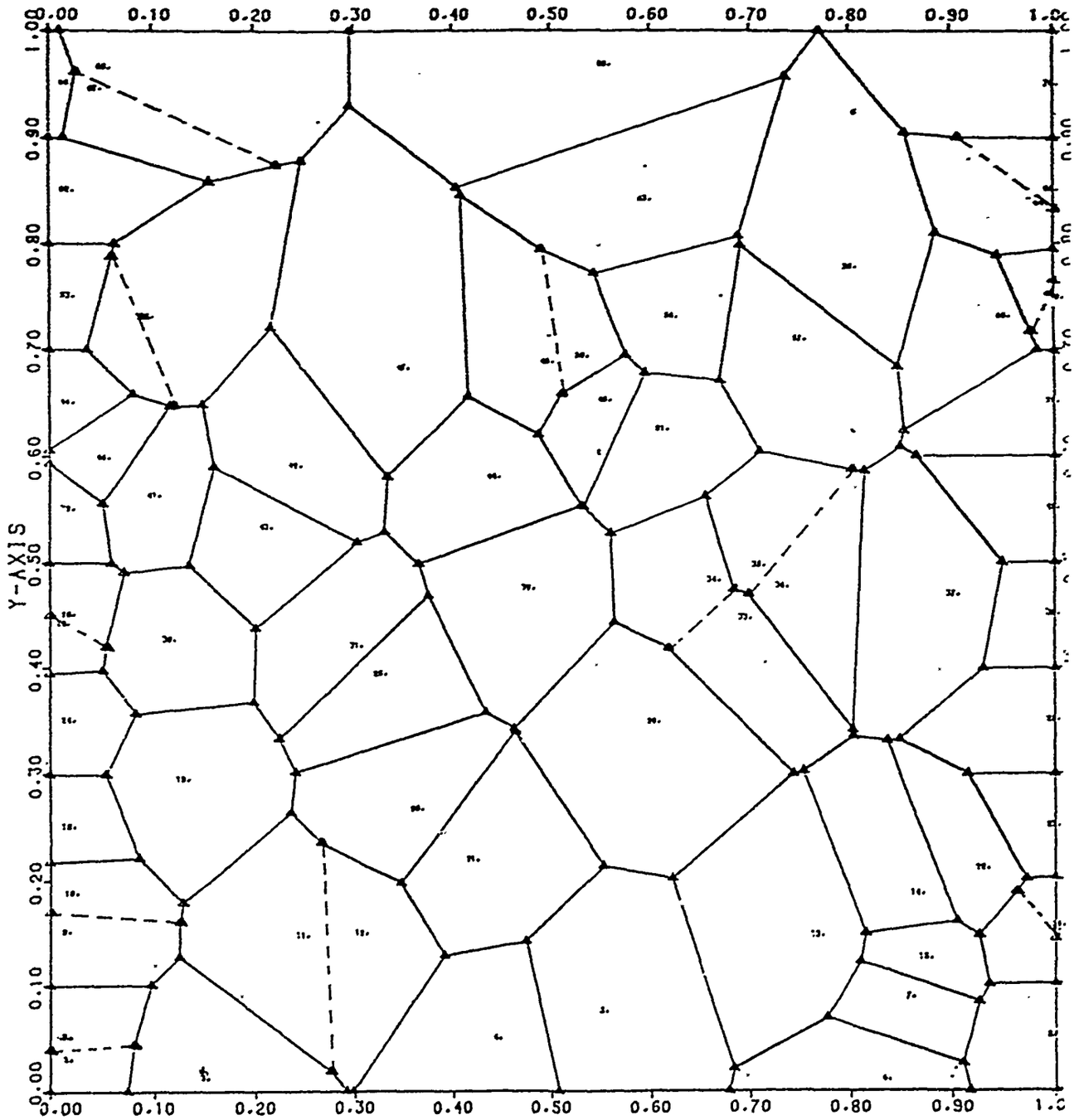

Fig. 2 I

70 VORON POLYG.

STEP 2

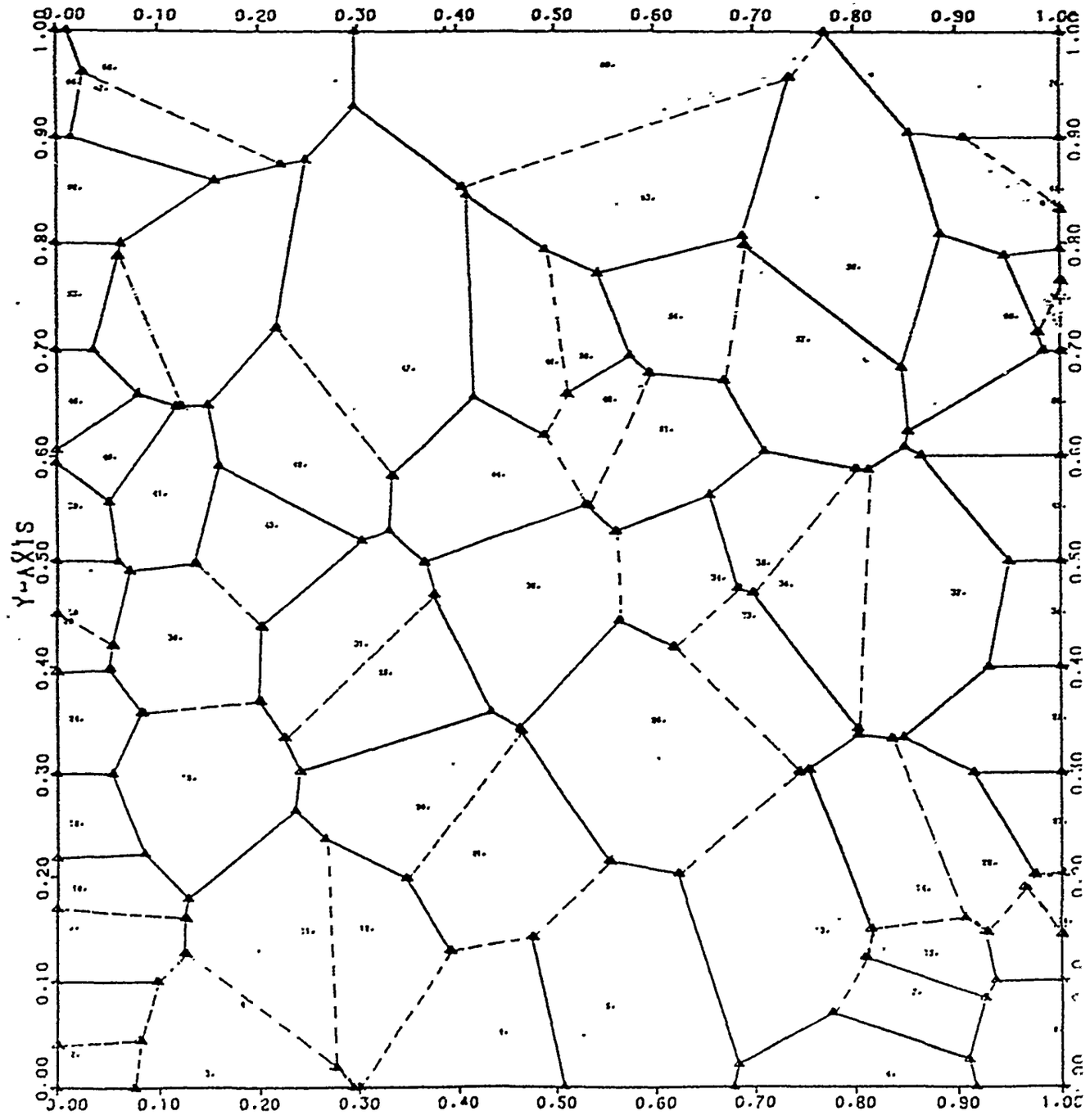

Fig. 2 II

70 VORON POLYG.

STEP 3

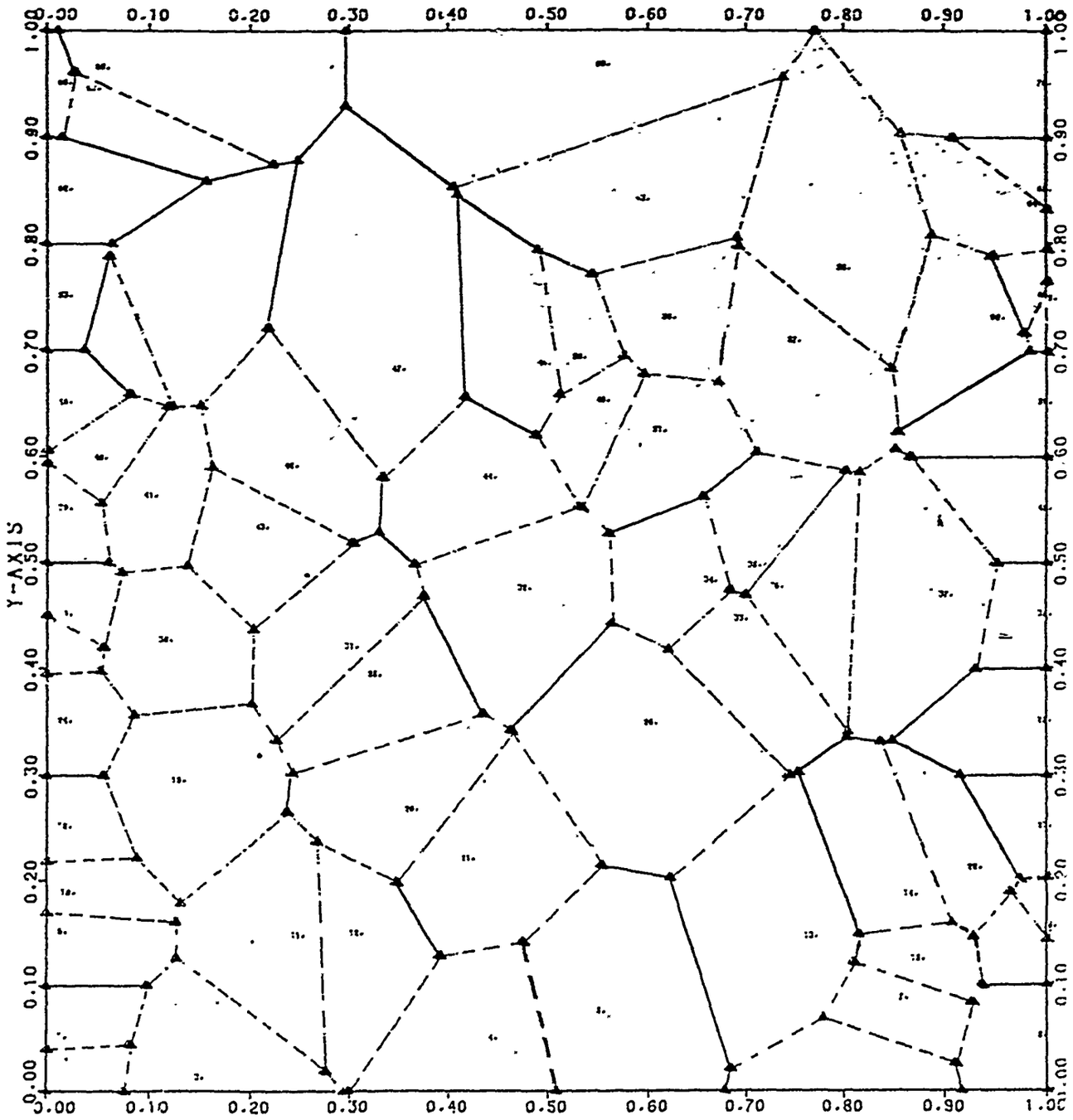

Fig.2 III

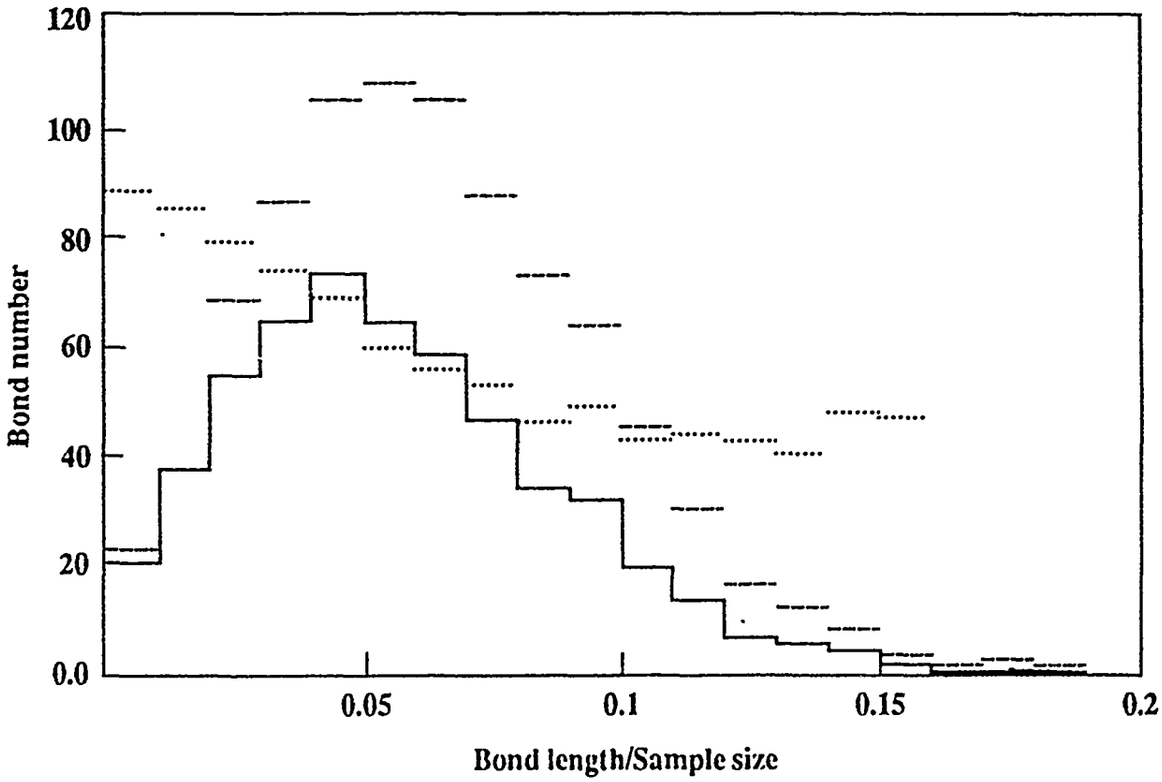
120
100
80
60
40
20
0.0
Bond number
0.05
0.1
0.15
0.2
Bond length/Sample size

Fig. 3

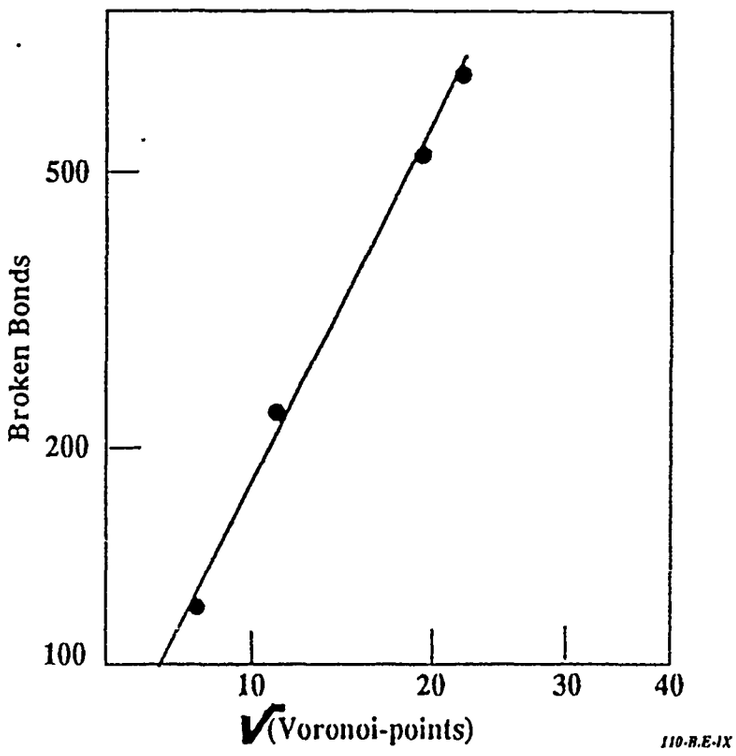

Fig. 4

PART 9

Experimental Validation

Extensive tests of fracture and fragmentation behaviors of reinforced concrete slabs have been performed by Vargas, Hokanson and Rindner(1). Since their test results are readily interpretable in terms of our percolation approach (especially through their employment of variable length scales for reinforced bar spacing and slab thickness), we describe the experimental arrangement at some length.

Concrete walls with dimensions (in cm length units) of about 50 x 50 x (5-8) were subjected to detonations at close quarters from several types of charges. The walls were reinforced by tightly locking horizontal and vertical wires in the concrete matrix, with spacing that varied from 2.5 to 5 cm. The debris was collected and its distribution determined as function of mass, velocity, range and, in a less precise manner, of shape and provenance. The present section treats only the mass distributions, as being most closely related to the theories laid out in the preceding parts; the analysis of the other distribution requires more detailed considerations of the dynamics of the fragmentation process, which has not yet been given.

In summary it can be stated that, though the experimental data are subject to a great deal of scatter, there are strong indications of a percolation-like process occurring causing the fragmentation.

Following the authors of the report[1], we quantify the external forces that bring about the fragment by the specific impulse factor IF which is defined as "the total impulse [imparted by the exploding charge to the slab] divided by the square root of the effective [slab] thickness". Without undertaking a deep analysis of IF, we can appreciate that it affects both the strength of the stresses in the fragmenting slab and the strain rate in it.

The geometrical parameters are the reinforced-bar ("rebar" spacing (R_s) and the slab thickness T. The effect of the former on fragmentation is much more marked than that of the latter (as will be shown shortly). This leads us to the supposition (which actually has some far-reaching practical implications), that the rebars divide up the slab into smaller panels of size R_s x R_s. The different panels fragment independently of each other; in other words: the effective lateral dimension of the solid is R_s (rather than

the slab size). Furthermore, there are indications from the data that the slab (or the panels) behaves as a two-dimensional solid (more precisely, the effective dimensionality of the slab is nearer to 2D than to 3D, as will be seen later.) Since the rebars lie in two horizontal planes that are 0.6 cm from the exterior planes and 4-6 cm from each other, it is not clear a priori why the rebars should have such a strong effect on the fragmentation process. If a future investigation should find the answer to this question, this could improve the use of rebars in concrete (and also of whiskers and fibers in ceramics, etc.).

In a more recent work on explosion effects on aircraft shelters (ACS), fragment distributions (adding up to 40 tons) were obtained[2] (for a graphical representation of the results see (3)). Though the test results available in (3) were fewer than in the smaller structures (slabs) of (1), we have also included these in our percolation theory analysis.

Results

I. Cummulative mass distributions

Percolation theory[4] predicts the following density n_m of fragments (no. per unit mass) as function of the fragment mass.

$$n_m \propto m^{-\tau}$$

where $\tau = 2.05$ in two dimensions (2D)
$= 2.2$ in three dimensions (3D)

The cumulative distribution N_c will threfore have exponents $-(\tau - 1)$ and will appear on a log N_c - log m plot as a straight line. About 14 of the 39 test results in the slab test[1] have a linear section in the higher mass range; in 25 no linear section was discerned. Examples of the linear section are seen in Fig. 1. The slopes [identified with $-(\tau - 1)$] differ from case to case. The cummulative distribution of the 14 slopes is shown in Fig. 2. Though a significant scatter is evident among the test events, the slopes fall quite close to the percolation theory values: 1.05 (two dim.) and 1.2 (three dim.), showing better agreement with the former. We have also included the two slopes from ACS results[2,3], which also lie near the percolation - theory slopes.

Let it be remarked that the linearity in the long-log plot by itself is a strong vindication of the percolation model, since most of the other distributions are exponential[5]. The curving (non-linearity) of the distributions in the smaller mass range is an indication of some intrinsic length scale, like some structure or granularity of the material.

II. Impulse dependence of fragments

The authors of the slab tests[1] counsel a more detailed statistical investigation. This was undertaken by us for both the observed total fragment number N and mean fragment mass m collected as functions of the impulse factor IF. Following Ref. (1) we have made a fit with linear regression of the form:

$$N = A(IF) + B$$

$$m = C(IF) + D$$

separately for four combinations of the geometrical parameters slab thickness T and rebar spacing R_s. The results are shown in Table 1. The regressions were examined for statistical significance by Student's t-test[6]. The obtained t-values (shown in columns 7 & 12 of the table) are much higher (better) than those (2-4) needed for assuring significance. At this stage the regression analysis does not warrant the drawing of physical conclusions - except from the mean mass $\bar{m}$ (last column in the table).

Table 1. Statistical Analysis of Impulse Dependence for Fragment Number and Size (in cm). (Mass in grams).

Geometry		# Event	Regression coefficients and significance									
T	R_s	n	A	B	σ	t	N	C	D	σ	t	$\bar{m}$
5	2.5	9	12.5	123	.09	25.5	167	-5	31	.13	18	13
5	5	8	36	36	.05	47	180	-1.8	45	.17	13	3
7.5	2.5	9	2.7	88	.14	16	100	-1.4	21	.12	14	15
7.5	5	9	35	-6	.09	25	146	-19	-37	.08	20	45

III. **Finite size scaling of mean mass**.

The entries for $\bar{m}$ show that the mean mass scales strongly with rebar spacing

$$\bar{m} \propto R_s^{1.63}$$

and weakly with slab thickness

$$\bar{m} \propto T^{0.42}$$

(Fig. 3)

Regarding the thickness as constant, the upper relation can be rewritten in terms of the volume V of the panel, since $V = R_s^2 T$,

$$\bar{m} \propto V^{0.815} \qquad \text{(T constant)}$$

Now the mean mass of percolating clusters at the critical crack density ($p = p_c$) scales with the finite size of the sample as

$$\bar{m} \propto V^{(2D_f - d)/d}$$

where D_f is the fractal dimension of the crack cluster and d is the Eucledian dimension. (Table II).

Table II. Percolation Exponents

Dimension d	2	3
Fractal dim. D_f	1.9	2.5
$2D_f/d - 1$	.9	.66
Experiment	.815	

From the table one notes that the experimental exponent lies between the percolation exponents in two and three dimension, favoring (as in the earlier instance) a two dimensional crack framework. The observed exponents differ significantly from

$$\tau - 1 = .67$$

which is known from the Gaudin - Schuhmann distribution(7,8). This characterizes several mineralogical fragments in the low mass range, while our power law is for the heavier masses .

Visual (microphotographic), as well as quantitative, support for the percolation concept is obtained from creep in several structural ceramics. Wiederhorn and coworkers have discerned cavity-coalescence induced failure in some of their materials (like Coors SCRB210) and have similarly interpreted results by others[9]. The percolation process observed in void-coalescence is highly correlated, anisotropic and has a position dependence in terms of the distance from the main crack. All these ramifications are present in our general thermo-dynamic theory and in some of the computations presented in this report. However, for a quantitative comparison with available creep studies and the derivation of general laws further work is needed.

References

1. L.M. Vargas, J.C. Hokansen and R.M. Rindner "Explosive Fragmentation of Dividing Walls", Final Report AD - A104 - 348, July 1981.

2. J.M. Ward, N.M. Swisdak, P.J. Peckham, W.G. Soper, R.A. Lorenz, "Modeling of Debris and Airblast Effects from Explosions inside Scaled Hardened Aircraft Shelters". NSWC TR 85-470, 1985.

3. M. Held in Proc. V. International Symp. on the Interaction of Conventional Munitions with Protective Structures, Mannheim, Germany. (April 1991) pp. 346 - 354 (in German). (Bundesakademie fur W. and W., Seckenheimer Landstr. 8-10, D-6800 Mannheim 25, Germany).

4. D. Stauffer, "Introduction to Percolation Theory" (Taylor & Francis, London, 1985).

5. R. Englman, J. Phys. Condensed Matter. 3, 1019 (1991).

6. H.L. Adler and E.B. Roessler, Introduction to Probability and Statistics (Freeman, San Francisco, Ca., 1960).

7. A.M. Gaudin and T.P. Meloy, Trans. AIME - SME 223, 40, 43 (1962).

8. R. Schuhmann, Jr., Trans. AIME - SME 217, 22 (1960).

9. S.M. Wiederhorn, B.J. Hockey and T.J. Chang, "Creep and Creep Structure in Structural Ceramics", Paper presented at NATO Workshop "Toughening Mechanisms in Quasi-brittle Materials (Evanston, Ill., July 1990).

Figure Captions

Fig. 1. Cumulative mass distribution in concrete slab tests[1]. The double logarithmic plot shows in the higher mass range a linear portion, indicating an inverse power law relation.

Fig. 2. Distribution of mass exponents. The cumulative number of the observed mass exponents is shown by full lines for the slab tests[1] and by thickened lines for the aircraft shelter (ACS) tests. Experimental results show a scatter around (and not far) from the percolation theory predictions (broken line in three dimensions, chained line in two dimensions).

Fig. 3. The average masses m against the slab thickness T and the rebar spacing R_s on a log-log plot.

Full squares $\bar{m}$ vs R_s
Open circles $\bar{m}$ vs T

The full line gives the exponent 1.63 of R_s, and the two broken lines both fit an exponent of 0.42 for T.

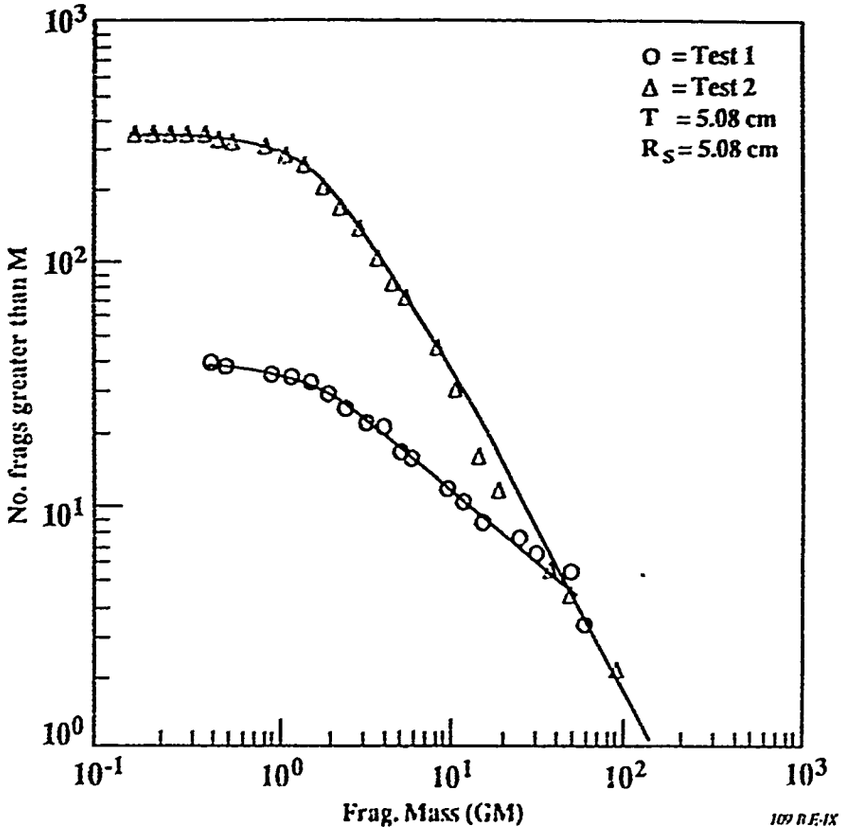
O = Test 1
Δ = Test 2
T = 5.08 cm
R_S = 5.08 cm
No. frags greater than M
10^3
10^2
10^1
10^0
10^{-1}
10^0
10^1
10^2
10^3
Frag. Mass (GM)
109 R.E.IX

Fig. 1

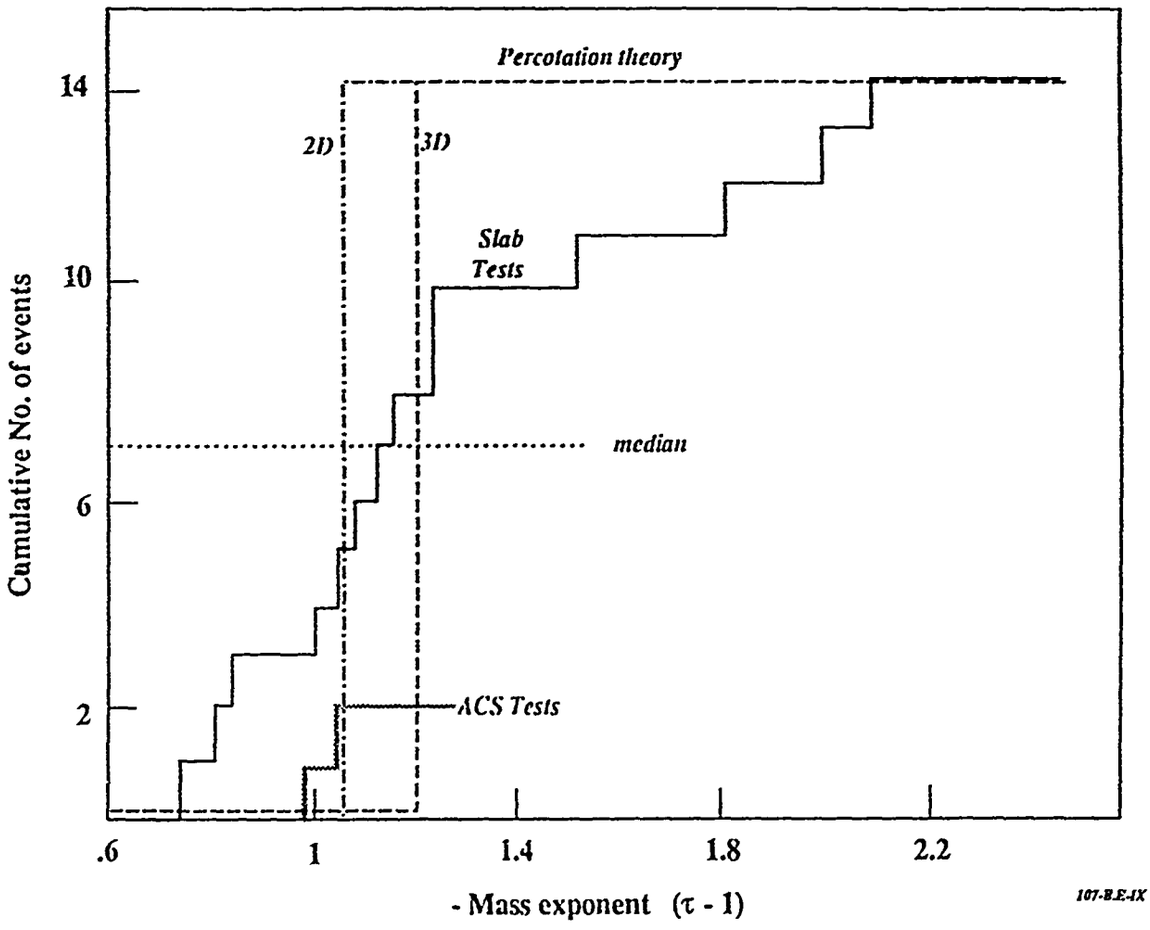
Percolation theory
2D
3D
Slab
Tests
median
ACS Tests
14
10
6
2
Cumulative No. of events
.6
1
1.4
1.8
2.2
- Mass exponent (τ - 1)
107-B.E-IX

Fig. 2

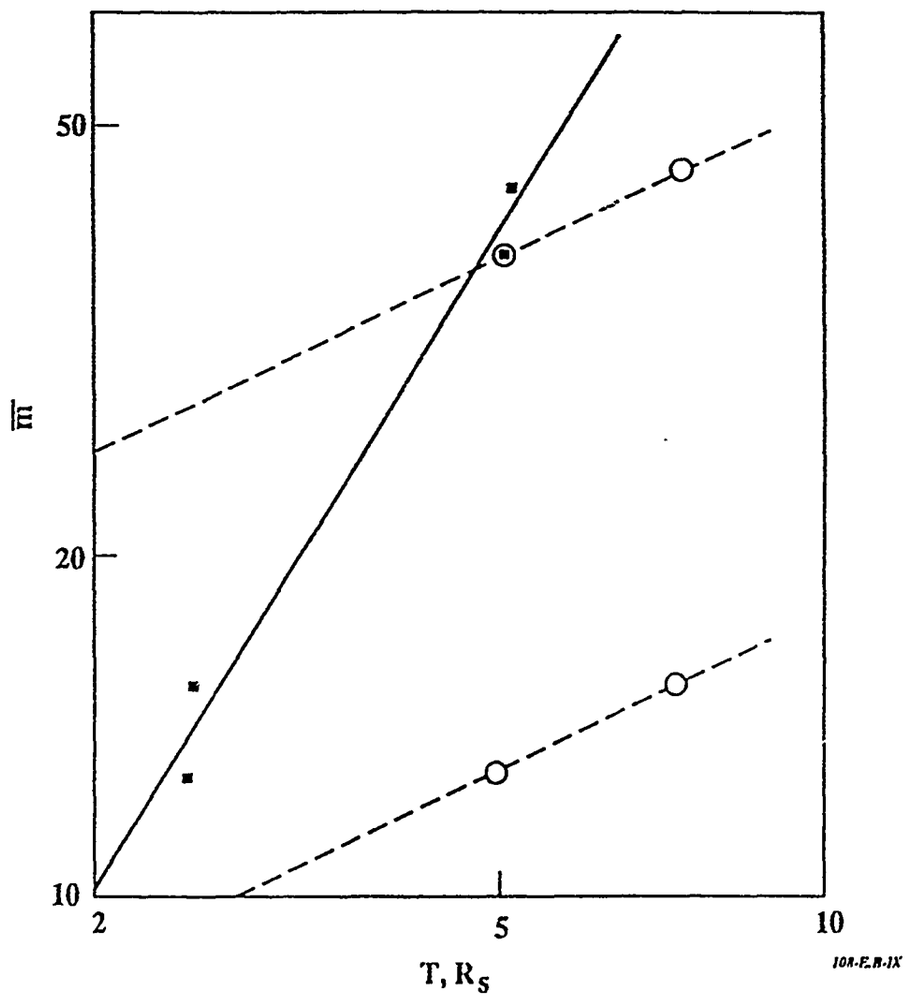

Fig. 3

This page is left intentionally blank.